

**DESIGN OF MUON DETECTOR BASED ON
PLASTIC SCINTILLATOR FOR THE COSINE-100
DARK MATTER EXPERIMENT**

DISSERTATION

**In partial fulfillment of the requirements
for the degree of Doctor from
Institut Teknologi Bandung**

By

HAFIZH PRIHTIADI

NIM: 30214010

(Doctoral Program in Physics)



INSTITUT TEKNOLOGI BANDUNG
August 2019

ABSTRACT

DESIGN OF MUON DETECTOR BASED ON PLASTIC SCINTILLATOR FOR THE COSINE-100 DARK MATTER EXPERIMENT

By

Hafizh Prihtiadi

NIM : 30214010

Doctoral Program in Physics

Number of astronomical observations suggest that the dominant matter in the universe is non-baryonic dark matter. However, the searches for dark matter has been one of the most challenging research topics in physics. Weakly Interacting Massive Particles (WIMPs) are promising candidates of dark matter, supporting by many astronomical considerations and theoretical predictions. Many of direct dark matter experiments are looking for WIMP dark matter by using various detection techniques and technologies. But one exceptional, DAMA group reported over 20 years of annual modulation signal using NaI(Tl) crystal scintillation detectors. They claim that this signal is WIMP-like signal in their detectors. However, no experiments can prove the signal with set limits which are incompatible with DAMA result. An experiment is needed with same target material detector to resolve both result without conflict. COSINE-100 is a joint effort experiment by the KIMS-NaI (Korean Invisible Mass Search) and the DM-Ice with a goal to reproduce or refute the annual modulation signature reported by DAMA group using Sodium Iodide crystal scintillations. COSINE-100 experiment is operating and located at the Yangyang Underground Laboratory (Y2L) in South Korea. The construction and assembly process was completed in the Summer of 2016 and the detector is currently collecting physics data. During the operation, several things needed to be considered are backgrounds level including from the cosmic-ray showers. In rare event searches, cosmic-ray muons can produce seasonal modulation of event which can mimic weakly interacting massive particle (WIMP) signal in nuclear recoils. To tag the muon-events and study the correlations between muon and crystal-events, COSINE-100 has installed the muon detectors in the outside shielding structure. An array of 3-cm thick plastic scintillator panels surrounds

the crystal detector in all sides. This work focuses on the design, construction and assembly process, data analysis of the COSINE-100 detector, with particular emphasis on muon-modulation. Muons, identified by a selection criteria, are developed with a coincidence technique and time difference between two panels. A coincidence and threshold are used to remove γ -backgrounds at low energy and showed the muon-like events in high energy region. The threshold is set to be different for each side detector. A time difference cut has been developed to reduce fake-event in signal area. The muon coincident signal should be in close time-range of the gap. The time correlation observed for the muon candidate events, a signal range of $-100\text{ns} \leq \Delta T \leq -115\text{ns}$. Considering the background distribution, the background contamination in the signal region is calculated to be 0.3%. Furthermore, the muon selection efficiency was estimated to be $99.9 \pm 0.1\%$ when the charge threshold cuts are applied. A similar muon selection technique is applied for all pairs of different sides to tag muon candidate events. Muon events were found with direct or prompt energy deposition $\geq 4\text{MeV}$. Muons can also induce low energy phosphorescence event in crystals which can mimic WIMP signal with a confined modulation signature. A event selection for crystal study has been used by rejecting 30ms from a muon hit in plastic scintillator. It gives approximately 0.1 % dead-time in the detector. This rejection is used in crystal analysis to prevent large number of accidental events. With 2 years of physics data, an annual modulation behaviour has been observed with an amplitude of $(0.51 \pm 0.24)\%$ and a phase of $(182 \pm 25)\text{d}$ corresponding to a maximum on the 30st of June. Using the atmospheric temperature data, we studied the correlation between muon and temperature modulation with a positive correlation. With an effective coefficient $\alpha_T = 0.815 \pm 0.097$. This result represents the study of the muon flux modulation for Y2L site and is in good agreement with theoretically expectations.

Key words: cosine-100 experiment, dark matter searches, plastic scintillator detector

ABSTRAK

PERANCANGAN MUON DETEKTOR BERBASIS PLASTIK SINTILATOR UNTUK EKSPERIMEN COSINE-100 MATERI GELAP

Oleh

Hafizh Prihtiadi

NIM : 30214010

Program Studi Doktor Fisika

Sejumlah pengamatan astronomi menunjukkan bahwa penyusun materi di Semesta didominasi oleh materi gelap *non-baryonic*. Namun, pencarian materi gelap telah menjadi salah satu topik penelitian paling menantang dalam fisika. *Weakly Interacting Massive Particles (WIMPs)* telah menjadi kandidat materi gelap yang menjanjikan, didukung oleh banyak pertimbangan dari para astronom dan prediksi teoritis. Banyak eksperimen berusaha mengungkap misteri dari materi gelap dengan berupaya mengoperasikan pencarian langsung materi gelap dengan berbagai teknik dan teknologi deteksi. Tapi hal yang luar biasa, kelompok DAMA melaporkan lebih dari 20 tahun sinyal modulasi tahunan (*annual modulation effect*) yang teramati oleh detektor mereka menggunakan bahan target NaI(Tl) *Sodium-Iodide* seperti yang diharapkan dari kandidat materi gelap bernama *weakly interacting massive particle (WIMP)*. Namun, tidak ada percobaan lain yang dapat membuktikan sinyal dengan batas sensitivitas yang ditetapkan tidak sesuai dengan hasil DAMA. Eksperimen sejenis mutlak diperlukan dengan detektor bahan target yang sama untuk menyelesaikan kedua hasil tanpa konflik. COSINE-100 adalah eksperimen bersama oleh KIMS-NaI (*Korea Invisible Mass Search*) dan DM-Ice dengan tujuan untuk mereproduksi atau menyangkal adanya modulasi tahunan yang dilaporkan oleh kelompok DAMA menggunakan kristal *Sodium Iodide*. COSINE-100 eksperimen beroperasi dan berlokasi di *Yangyang Underground Laboratory (Y2L)* di Korea Selatan. Proses konstruksi dan perakitan selesai pada musim panas 2016 dan detektor saat ini sedang mengumpulkan data fisika. Selama operasi, beberapa hal yang perlu dipertimbangkan diantaranya adalah tingkat *background* dari sinar kosmik. Dalam pencarian materi gelap, muon sinar kosmik dapat menghasilkan modulasi tahunan yang dapat meniru sinyal seperti

partikel masif (WIMP) yang berinteraksi lemah dalam recoil nuklir. Untuk menandai kejadian muon dan mempelajari korelasi antara muon dan *crystal-event*, COSINE-100 telah memasang detektor muon dalam struktur pelindung luar. Susunan panel plastik sintilator setebal 3 cm mengelilingi detektor di semua sisi. Penelitian ini berfokus pada proses desain, konstruksi, dan perakitan, analisis data detektor COSINE-100, dengan penekanan khusus pada modulasi muon. Muon dapat diidentifikasi oleh kriteria seleksi, dikembangkan dengan *coincidence technique* dan perbedaan waktu antara dua panel. Sebuah *coincidence technique* dan ambang batas (*threshold*) digunakan untuk mengurangi γ -backgrounds pada energi rendah dan dapat menunjukkan sinyal muon pada wilayah energi tinggi. Ambang batas yang berbeda diterapkan untuk setiap sisi detektor. Sebuah *timing cut* telah dikembangkan untuk mengurangi adanya *fake-events* pada daerah sinyal. Muon harus berada dalam jeda waktu yang dekat. Korelasi waktu diamati untuk mencari kandidat muon, daerah sinyal $-100\text{ns} \leq \Delta T \leq -115\text{ns}$. Mempertimbangkan distribusi *backgrounds*, kontaminasi dari *backgrounds* di wilayah ambang batas sinyal dihitung 0.3%. Selain itu, efisiensi seleksi muon dihitung sebesar $99.9 \pm 0.1\%$ ketika ambang batas diterapkan. Teknik pemilihan muon yang serupa diterapkan untuk semua panel dari sisi yang berbeda untuk menandai kandidat muon. *Muon-events* pada kristal detektor dengan energi deposisi $\geq 4\text{MeV}$. Muon juga dapat menginduksi *low energy phosphorescence event* pada kristal yang dapat meniru bentuk dari sinyal WIMP. Sebuah teknik seleksi event pada studi kristal telah digunakan dengan meniadakan 30ms dari sinyal muon pertama pada plastik sintilator. Hal ini memberikan efek dengan perkiraan 0.1% *deadtime* pada detektor. Teknik ini digunakan untuk menghindari jumlah besar dari *accidental events*. Dengan 2 tahun dari data, muon menunjukkan perilaku modulasi tahunan dengan amplitudo sebesar $(0.51 \pm 0.24)\%$ dan sebuah fase (182 ± 25) d sesuai dengan maksimum pada 30st Juni. Dengan menggunakan data atmosfer temperature, kami melakukan studi korelasi antara modulasi muon dan temperatur yang menunjukkan positif korelasi. Dengan nilai koefisien efektif $\alpha_T = 0.815 \pm 0.097$. Hasil ini menunjukkan studi modulasi muon dan temperature pada Y2L dan menunjukkan hasil sesuai prediksi teoritis dan ekspektasi.

Kata kunci: eksperimen cosine-100, pencarian materi gelap, detektor plastik sintilasi

**DESIGN OF MUON DETECTOR BASED ON
PLASTIC SCINTILLATOR FOR THE COSINE-100
DARK MATTER EXPERIMENT**

By

Hafizh Prihtiadi

NIM : 30214010

Doctoral Program in Physics

Institut Teknologi Bandung

Approved by

Supervisor Team

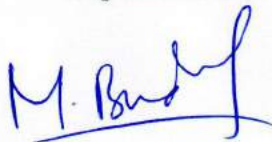
Date: 1 Agustus 2019

Supervisor I



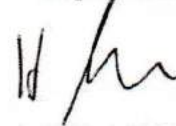
Prof. Dr.-Ing. Mitra Djamal

Supervisor II



Maman Budiman, Ph.D

Supervisor III



Prof. HongJoo Kim, Ph.D

GUIDELINES FOR USE OF THE DISSERTATION

Unpublished Doctoral Dissertation is registered and available in Institut Teknologi Bandung Library. It also opens to the public provided that copyright is on the author by following the rules of Intellectual Property Rights applied in Institut Teknologi Bandung. Literature reference is allowed recorded, but citations or summarizing can only be done with permission from the author and must be accompanied by the scientific habit to mention the source.

Citation of this dissertation can be written in English as follows:

Prihtiadi, H. (2018): Design of muon detector based on plastic scintillator for the cosine-100 dark matter experiment, Doctoral Dissertation, Institut Teknologi Bandung.

and in Indonesian as follows:

Prihtiadi, H., (2018): Desain detektor muon berbasis plastik sintilator untuk eksperimen COSINE-100 materi gelap, Disertasi Program Doktor, Institut Teknologi Bandung.

No part of this publication may be reproduced or distributed in any forms or any by any means or stored in a database of the retrieval system, without the prior written permission of the Director of Graduate Program Institute Teknologi Bandung.

PREFACE

Alhamdulillah, all praises to Allah *Subhanahu Wata'ala* for the strengths, His guidance, and His blessings in completing this dissertation.

A 5-year Doctoral degree is indeed a difficult part of mine, yet is very spectacular due to many extraordinary people surrounding. I would like to dedicate this dissertation to them because of their support, motivation, help, and dua (a prayer of supplication or request).

First, I would like to send my gratitude to my supervisor, Prof. Mitra Djamal, Maman Budiman, Ph.D and Prof. HongJoo Kim, for their kind support, supervision, and guidance during my Doctoral degree. Prof. YeongDuk Kim, Prof. HyunSu Lee, Prof. YongHamb Kim, Prof. MooHyun Lee, Prof. HyangKyu Park, thank you for giving me an opportunity to join a collaboration experiment and to study in astroparticle and nuclear physics field. It was a great experience having meet them. Thank you for helping me with the paper writing, presentations, and some opportunities to attend international conferences. And thank you very much for providing me a great opportunity to have high quality research group at Center for Underground Physics, Institute for Basic Science, Republic of Korea.

Second, I would like to thank COSINE Collaboration for welcome joining in this excellent group. Prof. Reina H Maruyama, Jay, Estella, William, Matt for their experience share in this collaboration.

Third, COSINE student, Pushparaj Adhikari, Govinda Adhikari, and ByungJu park for their kindness.

Fourth, Director of the Doctoral Study Program of Physics, Prof. Suprijadi, Dr. Enjang Mustopa, and Dr. Khairul Basar and Dean of the Graduate Program Prof. Pudji Astuti for the administration procedures during the study.

Fifth, IMNIDA members *Ikatan Muslim Indonesia Daejeon*. May Allah always bless you all.

I would have never been at this stage without strong support dua from the greatest persons in my life. *Ayah dan Ibunda, terima kasih atas doa, motivasi, dan dukungan materiil maupun moril. Keluarga besar di Tulungagung, Bapak Iskandar dan Ibunda yang senantiasa selalu berjuang dan membantu kami dengan segenap upaya dan doa, merawat si Kecil Humaira dengan penuh kasih sayang..*

For my three beloved and beautiful ladies: Herlin, Humaira, and Haura.

Terima kasih tak terkira atas kesabaran, berjuang bersama, doa yang tulus tiap malam dipanjatkan. "Berjuang bersama menempuh S3 adalah bagian dari kisah cinta kita bersama, melalui tiap-tiap langkahnya adalah keharmonisan kisah kita."

I realized that this dissertation is far from perfect, due to the limitation of my ability and knowledge. Therefore, I am looking forward to all of critics and suggestions for the perfection of this dissertation are welcome. I also hope this dissertation can be useful for readers and all parties in adding insight and can be a guide for readers for further research.

Bandung, August 2019

Hafizh Prihtiadi

CONTENTS

| | |
|--|-----|
| ABSTRACT | i |
| <i>ABSTRAK</i> | iii |
| APPROVAL PAGE | v |
| GUIDELINE FOR USE OF DISSERTATION | vi |
| PREFACE | vii |
| CONTENTS | ix |
| LIST OF FIGURES | xi |
| LIST OF TABLES | xv |
| | |
| I Introduction | 1 |
| I.1 Background | 1 |
| I.2 Research of Objectives | 4 |
| I.3 Statement of Problem | 5 |
| I.4 Research Method | 5 |
| I.5 Dissertation Outline | 7 |
| I.6 Contributions | 8 |
| | |
| II Review of Dark Matter | 9 |
| II.1 Evidence of Dark Matter | 9 |
| II.2 Dark Matter Candidates | 11 |
| II.2.1 WIMPs | 12 |
| II.2.2 SUSY Dark Matter | 13 |
| II.2.3 Warm Dark Matter | 14 |
| II.2.4 Axions | 15 |
| II.3 Dark Matter Searches | 16 |
| II.3.1 Collider Production | 16 |
| II.3.2 Indirect Dark Matter Detection | 16 |
| II.3.3 Direct Dark Matter Detection | 17 |
| II.3.3.1 Annual Modulation | 18 |
| II.3.3.2 Status of Dark Matter Experiment | 19 |
| II.4 Background Sources | 21 |
| II.4.1 Cosmic rays and components | 21 |
| II.4.2 Interactions of Muons | 21 |
| II.4.3 Muons in rare event search | 26 |
| | |
| III COSINE-100 Experiment | 27 |
| III.1 Experimental Hall | 27 |
| III.2 The COSINE-100 detector | 28 |
| III.2.1 Liquid Scintillator (LS) detector | 31 |
| III.2.2 Sodium Iodide NaI(Tl) crystal detector | 31 |
| III.2.3 Plastic Scintillator detector | 33 |

| | | |
|---------|---|----|
| III.3 | Data Acquisition System (DAQ) | 33 |
| III.3.1 | Charge-Sensitive M64ADC | 39 |
| III.3.2 | Flash Analog-to-Digital Converter | 40 |
| III.3.3 | High Voltage Supply Mode | 41 |
| III.4 | Slow Monitoring System | 41 |
| III.4.1 | Software architecture | 43 |
| III.4.2 | Alarms | 44 |
| III.4.3 | Data quality monitoring | 45 |
| IV | Muon Analysis of COSINE-100 Experiment | 48 |
| IV.1 | Muons at COSINE-100 | 48 |
| IV.2 | Muon selection procedure | 49 |
| IV.1.1 | Method of μ -threshold determination | 50 |
| IV.1.2 | Time difference cut | 54 |
| IV.3 | Observed muon rate at Y2L | 55 |
| IV.3.1 | Muon in crystal-events | 57 |
| IV.3.2 | DAQ saturation and deadtime | 58 |
| IV.4 | Annual Modulation Analysis of Muon and Temperature | 59 |
| IV.4.1 | Muon Modulation | 59 |
| IV.4.2 | Atmospheric model and effective atmospheric temperature ... | 60 |
| IV.4.3 | Correlation between muon and temperature | 62 |
| V | Conclusions and Future Work | 65 |
| V.1 | Conclusions | 65 |
| V.2 | Future Work for COSINE-200 Experiment | 66 |
| | REFERENCES | 68 |
| | LIST OF PUBLICATIONS | 78 |
| | LIST OF COSINE MEMBER | 80 |
| | APPENDIX | - |

LIST OF FIGURES

| | | |
|------|---|----|
| I.1 | A compilation of WIMP-nucleon spin-independent cross section limits (solid lines) and hints of WIMP signals (closed counters) from current dark matter experiments and projections (dashed) for planned direct detection dark matter experiments. Also shown is an approximate band where neutrino coherent scattering from solar neutrinos, atmospheric neutrinos and diffuse supernova neutrinos will dominate (Billard <i>et al.</i> , 2014) | 2 |
| I.2 | The COSINE-100 detector. The detector comprises a nested arrangement of shielding components, as indicated by different colors. The main purpose of the shield is to provide coverage against external radiation from various background sources. The shielding components include plastic scintillator panels (blue), lead-brick enclosure (grey) and copper box (brown). The eight encapsulated sodium iodide crystal assemblies are located inside the copper box and are immersed in scintillating liquid, as shown in the schematic (right)(Adhikari <i>et al.</i> , 2018) | 6 |
| I.3 | Research diagram of the COSINE-100 experiment | 7 |
| II.1 | SM particles, divided into bosons (red) and fermions. Fermions are further divided into quarks (violet) and leptons (green), with neutrinos. None of these SM particle fulfill the requirements of a dark matter particle, which must therefore be a particle beyond the SM | 11 |
| II.2 | Parameter space of theoretically-motivated dark matter candidates, with particle mass on the x-axis and interaction cross-section on the y-axis. The WIMP (and neutralino) and the axion are preferred candidates, while the neutrino and the WIMPzilla have been excluded. Figure from (Park <i>et al.</i> , 2007) | 13 |
| II.3 | WIMP abundance in the expanding universe. After the WIMP freeze out, dark matter density decreased due to self-annihilation until the universe cooled enough that annihilation was rare. At this point, the WIMP abundance stabilized. The correct density is predicted if the annihilation cross-section is that of weak interaction. Figure from (Paolo <i>et al.</i> , 2005) | 14 |
| II.4 | Table of the Standard Model (left) particles and their hypothetical supersymmetric particle. Figure from (Park <i>et al.</i> , 2007) | 15 |
| II.5 | Expected rate of dark matter interaction during the times of maximum and minimum rate as a function of energy. A low threshold is critical for direct detection experiments because most events are expected in the low energy region. Figure from (Freese, 2013) | 18 |
| II.6 | Annual modulation mechanism for the WIMP flux on Earth. The modulation is a result of changes in the Earth's galactic orbital velocity due to its orbit about the Sun. The SIMP flux maximum is in June, when the Earth's orbital velocity is aligned with the galactic local velocity, and the minimum is in December, when the Earth's solar velocity goes against the | |

| | | |
|--------|---|----|
| | local galactic velocity. The WIMP wind comes from the direction of the constellation Cygnus in the terrestrial frame | 19 |
| III.1 | Yangyang underground laboratory site. The lab is located at the Yangyang pumped storage power plant in the northeast of South Korea | 28 |
| III.2 | The 4π 4-layer shielding enclosure for the COSINE detector. From inside to outward, 8 encapsulated crystal detectors immersed in the 40-cm thick scintillating liquid, a liquid and crystal supporting acrylic box (1 cm thick), 3 cm-thick copper box, 20 cm-thick lead castle, and 37 with 3-cm thick muon panels are shown. Also indicated are the locations of the calibration holes, the size of the PMTs, and labels for sides. The lead shields at the bottom and the front side are omitted for clarity | 29 |
| III.3 | A photo of the COSINE detector room when the front door was opened. Plastic scintillators with black covers and an orange copper box with 5" PMT assemblies on the A-side are shown. A hoist is used to move the 800 kg copper top | 30 |
| III.4 | (a) A prototype liquid scintillator veto detector. (b) Veto efficiencies of internal ^{40}K as function of the thickness between the NaI(Tl) and the LS container for energies between 0-10 keV are presented from simple geometry simulation. Here, square dot not represent result obtained from the prototype detector | 32 |
| III.5 | (a) A acrylic support for the crystals, (b) An array of eight crystal and their position inside the Copper box | 33 |
| III.6 | Assembly procedure of the plastic scintillator panels. (a) The light guide with PMT is attached with BC-600 optical cement. (b) A panel is being wrapped with a TYVEK reflector. (c) A panel is being wrapped with an aluminum foil. (d) Muon panels stacked after being wrapped with a black vinyl sheet | 35 |
| III.7 | Schematic view of a right of left muon panel with assembly parts | 35 |
| III.8 | Experimental setup to test the performance of the muon panels | 35 |
| III.9 | (a) Muon candidate events selected by the trigger counter and modeled by a Landau distribution. (b) Position-dependent charge distributions from three different trigger positions for a 204 cm long muon panel | 36 |
| III.10 | Schematic view of the muon tagging efficiency setup | 37 |
| III.11 | (a) Charge distributions of the two trigger panels in the setup of Fig. III.10. Charge distributions of channel 3 (b) and channel 4 (c) after applying muon selection requirements for channel 1 (>4800) and channel 2 (>5400) | 37 |
| III.12 | The COSINE-100 data flow diagram. A total of 92 channels send signals to two types of digitizers, controlled by a trigger control board. Current DAQ setup consists of total of 32 FADC channels and 60 M64ADC channels. InfluxDB and Grafana are used for storing and visualizing the data (Adhikari <i>et al.</i> , 2018) | 38 |
| III.13 | (a) Series of preamplifiers connected in COSINE-100 station. (b) CAEN high voltage supply module | 42 |

| | |
|--|----|
| III.14(a) Test of temperature sensor thermocouples before installation. (b) Various environmental control system shown in COSINE-100 | 43 |
| III.15 Software architecture of slow monitoring | 44 |
| III.16 Grafana-generated monitoring dashboard. Various monitoring parameters are displayed | 46 |
| III.17 Example plots from the weekly data monitoring. Three plots from M64ADC data are shown here, the LS total charge, the LS charge asymmetry, and the muon rate | 47 |
| IV.1 (a) Schematic of the COSINE-100 shielding structure, (b) Photograph of the installed muon detector captured from the corner between the front and the right side | 48 |
| IV.2 M64 Trigger rates versus time (in h) for the first physics run (~41 days). All of the crystals show stable behavior throughout this running period and the rest of data-taking | 50 |
| IV.3 A scatter-plot of the signal distributions for top- and bottom-side coincident events. The red lines represent the selection criteria for muon candidate events. This method exclusive AND: each signal has to pass its panel threshold independently. An integrated charged is used to define the total charge of side detector | 51 |
| IV.4 In black: all events after coincident with Bottom-side, in blue: events after combined fit exponential and Landau distribution. An exponential function for the remaining background and a Landau distribution for the muons assumed. A peak is about ~26,000 ADC sum is muon peak | 52 |
| IV.5 In black: all events after integrated of 10 PMTs of the top panel. Red is after applying a threshold greater than 14,000 ADC units. Assuming above 14,000 ADC units are muon-like events | 53 |
| IV.6 (a) Time differences (ΔT) between top-side and bottom-side hits for non-muon candidate events and (b) muon candidate events | 54 |
| IV.7 The charge spectrum of muon candidate events in the top-side panels with the charge threshold trigger requirement relaxed. An exponentially decaying background component and Landau-function shaped muon signal component is used to model the data. Here, we consider two Landau functions to take into account events with two hits, visible by the second peak around 44×10^3 ADC counts. The fit results indicate that the normally required threshold for the top-side charge rejects a negligible number of signal muon event (<0.1%) | 55 |
| IV.8 Measurement of the muon flux at the COSINE-100 detector over a two years and 3 months period | 56 |
| IV.9 (a) Mean time distribution of high energy events. Left-blue island represents to alpha events while top-red island classified as muon events, (b) The energy spectrum of crystal 7 at high energy, with muons overlaid in red. Energy is defined as the integrated charge in the waveform | 58 |

| | | |
|-------|--|----|
| IV.10 | Time difference distribution between crystal trigger time and a muon signal from plastic scintillator. The events within 30 ms from a muon hit are removed in crystal event selections | 59 |
| IV.11 | Muon modulation by COSINE-100 data a function of time. The data are shown in monthly bins. Upper plot: cosmic muon modulation observed by COSINE-100 as a function of time. Lower plot: effective temperature, T_{eff} Teff, computed using eq. IV.5 and averaging over the four daily measurements. Monthly binning is used in both panels. The curves show the sinusoidal fit to the data | 60 |
| IV.12 | (a) an average temperature (solid red line), (b) normalized weight $W(X)$ (blue dashed line) as a function of pressure levels computed with pion (π) and kaon (K) contributions | 63 |
| IV.13 | $\Delta I_{\mu}/I_{\mu}^0$ vs $\Delta T_{\text{eff}}/T_{\text{eff}}^0$ for each day in figure for a total of 774 days | 63 |
| IV.12 | Measured values for the effective temperature coefficient, α_T , at varying site depths. The results from this analysis (in blue) as well as those from different experiments are presented. The red line is the value predicted including muon production by pions and kaons. The black line account for one production of pion (π) mechanism only | 64 |

LIST OF TABLES

| | | |
|-------|---|----|
| III.1 | Properties of the Sodium Iodide NaI(Tl) crystal | 32 |
| III.2 | Properties of the EJ-200 Plastic Scintillator | 34 |
| III.3 | Plastic scintillator panels in the muon detector for the COSINE-100 experiment | 36 |
| IV.1 | Solid red color shows integrated charge of side. Solid blue color shows charge distribution of single panel | 51 |
| IV.2 | Charge threshold for each side of muon detector and liquid scintillator . | 53 |
| IV.3 | Input parameters with associated errors for the calculation of the atmospheric effective temperature T_{eff} | 61 |
| IV.4 | Results of the muon and temperature modulation in other experiments.. | 64 |

Chapter I Introduction

In this chapter, we present background, research objectives, statement of the problem, research method, dissertation outline, and contributions of the dissertation.

I.1 Background

There is a huge puzzle about our universe that had led astronomical observations, including the velocities of stars and galaxies and gravitational-lensing measurements. The observations tell us that most of the universe is not made of the ordinary or baryonic matter (Clowe *et al.*, 2004 and Clowe *et al.*, 2006). There is compelling evidence that 96% of the mass and energy in the universe is dark in the sense that although its gravitational influences is readily it does not interact with light and invisible (Persic *et al.*, 1996 and Larson *et al.*, 2011). A variety of observational studies consistently reported that 23% of this dark component is in the form of clusters of dark matter and the rest is homogeneous dark energy. The nature of dark matter and its properties is one of the most important issues in sciences, since it will affect our basic knowledge of the structure and nature of the universe. Perhaps, it provide clues as to what particle physics lies beyond the Standard Model (SM) theory governing the composition and interactions between the most elementary constituents of nature (Bertone *et al.*, 2005 and Bergstrom, 2009). Many theoretical physicists consider that super-symmetric WIMPs (Weakly Interacting Massive Particles) are the most probable particle candidates for dark matter (Lee *et al.*, 1977 and Jungman, 1996). In 1985, Goodman and Witten suggested that very rarely occurring interactions WIMPs in the dark matter halo of our Milky Way Galaxy with nuclei of ordinary matter may be measurable with a very low-background detector in a deep underground environment (Goodman *et al.*, 1985).

This idea motivated a number of active experimental searches for rare events in underground laboratories around the world. With the notable exception of the DAMA/LIBRA experiment no conclusive evidence for a WIMP dark matter signal has been found. If one assumes that the Milky Way's dark matter halo consists of a smooth, non-rotating Maxwell-Boltzmann distribution of WIMPs that is, on average, at rest relative to the galactic center, i.e. the Standard Galactic Halo Model, the experimental results can be translated into cross section limits as a function of WIMP mass. In this context, re-

sults of many recent experiments are shown in Figs. I.1 for the assumption that the WIMP-nucleon interaction is spin-independent. All of the measurements summarized in the figure are upper limits on the cross sections based on null experimental results except for positive signals from the DAMA/NaI and DAMA/LIBRA experiments for which contour indicating allowed cross section vs WIMP mass regions are shown.

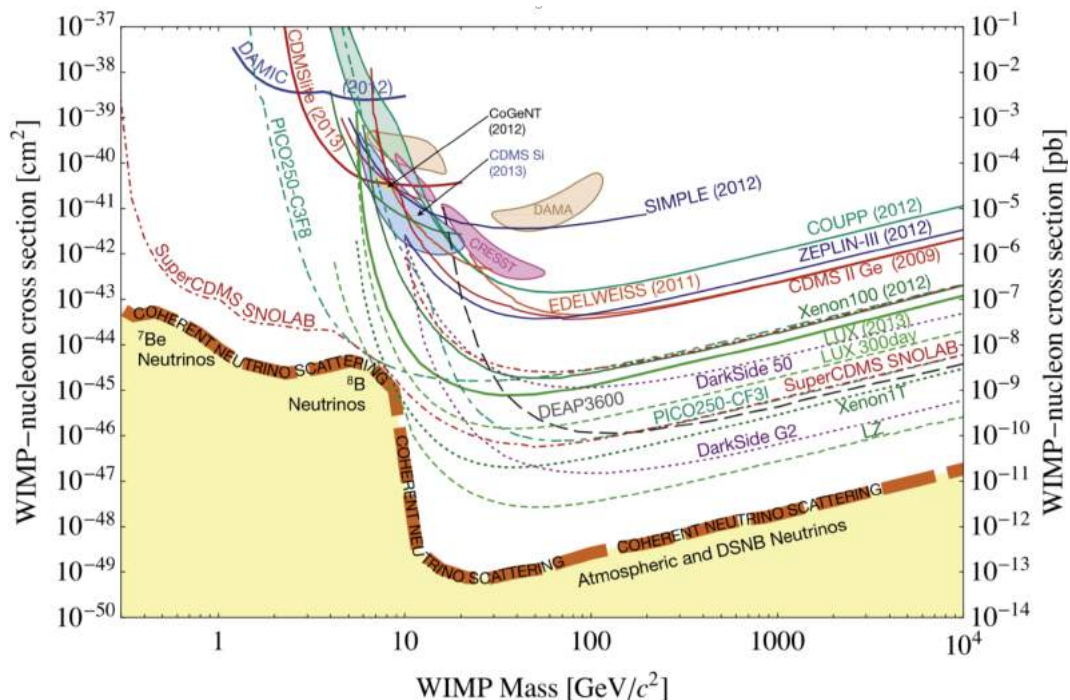


Figure I.1: A compilation of WIMP-nucleon spin-independent cross section limits (solid lines) and hints of WIMP signals (closed counters) from current dark matter experiments and projections (dashed) for planned direct detection dark matter experiments. Also shown is an approximate band where neutrino coherent scattering from solar neutrinos, atmospheric neutrinos and diffuse supernova neutrinos will dominate (Billard *et al.*, 2014)

A series of the DAMA experiment searches for an annual modulation in the nuclear-recoil detection rate in an array of ultra-low background NaI(Tl) crystals caused by the Earth's orbital motion through our Galaxy's dark-matter halo (Savage *et al.*, 2009, Bernabei *et al.*, 2010, and Bernabei *et al.*, 2013). This experiment has been operating for over 15 years and upgraded to Phase-II, has consistently reported a positive signal for an annual modulation signal and has reached 9.3σ . Other experiments, including CoGENT (Aalseth *et al.*, 2011 and Aalseth *et al.*, 2013), CRESST (Angloher *et al.*, 2012 and Angloher *et al.*, 2014), and SuperCDMS (Agnese *et al.*, 2014, Agnese *et al.*, 2014 and

Agnese *et al.*, 2016), have also reported signals that could be interpreted as being possibly due to WIMP interactions. However, these signals have marginal significance at the below of 3 confidence level and some inconsistencies with published null results based on measurements that use similar detectors (Angloher *et al.*, 2014 and Yue *et al.*, 2014). Nevertheless, these marginal signals have motivated the same experimental groups and, in some cases, independent groups to devise experiments to check these signals using similar techniques but with higher sensitivity. In contrast, no independent verification of the DAMA signal in an experiment using the same technique has been done.

The DAMA signal signature has been the subject of a continuing debate that started with the first DAMA result reported 15 years ago. This is primarily because the WIMP nucleon cross section inferred from the DAMA modulation are in conflict with upper limits from other experiments that directly measure the total rate of nuclear recoils, such as LUX (Akerib *et al.*, 2015 and Akerib *et al.*, 2017), XENON100 (Aprile *et al.*, 2012, Aprile *et al.*, 2017, and Aprile *et al.*, 2017), SuperCDMS (Agnese *et al.*, 2014, Agnese *et al.*, 2014, and Agnese *et al.*, 2016). However, there is a room remains for explaining all of these experimental results without conflict in terms of nontrivial systematic differences in detector responses (Plante *et al.*, 2011 and Barker *et al.*, 2012) and uncertainties in the commonly used astronomical model for the WIMP distribution (Mao *et al.*, 2014). An unambiguous verification of the DAMA signal by an independent experiment using similar NaI(Tl) crystals is mandatory.

One reason for the lack of verification of the DAMA result is that a new NaI(Tl) WIMP search would require an independent development of low-background crystals. The crystal-growing company that supplied the DAMA NaI(Tl) crystals no longer produces similar-grade crystals. Several groups including ANAIS (Amare *et al.*, 2014 and Amare *et al.*, 2016), DM-Ice (Cherwinka *et al.*, 2014 and Barbosa *et al.*, 2017), KamLAND-PICO (Fushimi *et al.*, 2016), SABRE (Xu *et al.*, 2015), and KIMS (Kim *et al.*, 2015 and Adhikari *et al.*, 2016), have worked to develop low-background NaI(Tl) crystals suitable for reproducing the DAMA experiment. Among these groups, The COSINE-100 experiment is a collaboration between the Korea Invisible Mass Search (KIMS) (Kim *et al.*, 2015, Adhikari *et al.*, 2016, and Adhikari *et al.*, 2017) and DM-Ice (Cherwinka *et al.*, 2014 and Barbosa *et al.*, 2017) to confirm or refute the annual modulation signal observed by the DAMA/LIBRA experiment. The COSINE-100 experiment was commissioned and has been taking physics

data since September 2016 with a 106kg array of low-background NaI(Tl) crystals in the Yangyang Underground Laboratory (Y2L) in Korea (Adhikari *et al.*, 2018). In experiment to directly detect WIMPs the main problem is, that the rate of WIMPs scattering on nuclei in the detector is expected to be very small with just a few signals per kg and year. Therefore one of the most important issues in the setup and operation of an experiment is the identification, reduction and control of background signals.

The achievable sensitivity of an experiment is limited by background level, muons and muon induced particles. For this reason, it is a particular important to identify muons in the experiment. In underground laboratories the muon flux in experiments is greatly reduced compared to experimental sites on or near the Earth surface. Nevertheless, current low background experiments suffer even from the small muon fluxes in these laboratories of the order of 1 or lower. It is therefore mandatory to understand the muon flux in the experiments and be able to tag muons. This issue is the motivation for this work, which is the part of the COSINE-100 experiment. Design of plastic scintillator-based muon detector for COSINE-100 dark matter searches. An array of muon detector surrounding the dark matter experiment has been designed, installed to COSINE shielding structure and operated during of physics data taking. The results of identifying the muons will give a better understanding of the muon information in experimental site.

I.2 Research Objectives

This work is focused on design, assembly and construction process of muon detector in a particular part of the COSINE-100 detector. Various tests were performed with each muon panel and overall muon detector. Data acquisition system configuration have been tested and pre-running operated before taking physics data. A selection criteria have been developed to tag muons from the signal-events. This selection is used to track and calculate the efficiency of detector, fake-events rate estimation and distribution in signal region. An event selection for crystal study has been developed to tag muons with prompt energy $\geq 4\text{MeV}$. This information is used to model the background understanding of crystal in high energy. Also, low energy effect from first hit muon is studied to prevent crystal-events from the accidental backgrounds induced by muons. An annual muon modulation has been studied with large of statistics as well as calculation of muon flux at experimental site.

I.3 Statement of Problem

COSINE-100 propose to confirm or refute the DAMA annual modulation signature with same target materials in an array of low-background NaI(Tl) crystals. It will directly contribute to the answer of the lack of verification of the DAMA result. COSINE-100 experiment is operated in a recently established experimental area in the Y2L A5 tunnel. With 700m underground level, high energy cosmic-ray muons can reach to the detector. It can unavoidably generate spallation products inside the detector shielding materials. It is also essential to have a better understanding of this source of backgrounds. To have accomplish these events, design and development muon detector and development of muon selection criteria which can identify muon is necessary. The efficiency of panel need to be evaluated from the physics run and both are sufficiently high in order to achieve the detector performance. Based on this issues, the main questions of this study are :

1. How to design, assembly the muon detector and obtain good performance?
2. How to configure the DAQ system which is integrated with crystals and liquid scintillator system ?
3. How to develop muon selection criteria which can account the muons and achieve a good detector efficiency?
4. How to understand the muon impact in low energy and high energy in crystal events? This study is essential to understand the muon events in the crystal detectors which could be contributed from the cosmic-ray muons.
- 5.

I.4 Research Method

The experiment is located at 700m below the surface at Yangyang Underground Laboratory (Y2L). A cut-out view of the COSINE-100 detector is shown in Fig. I.2. It is comprised of an eight crystal array of sodium iodide or NaI(Tl) scintillators (total mass 106 kg) immersed in the center of 2,200 kg of liquid scintillator contained in an acrylic box surrounded by copper and lead shielding. Plastic scintillators surround the entire apparatus and act as muon counters to detect cosmic-ray muons that penetrate the apparatus.

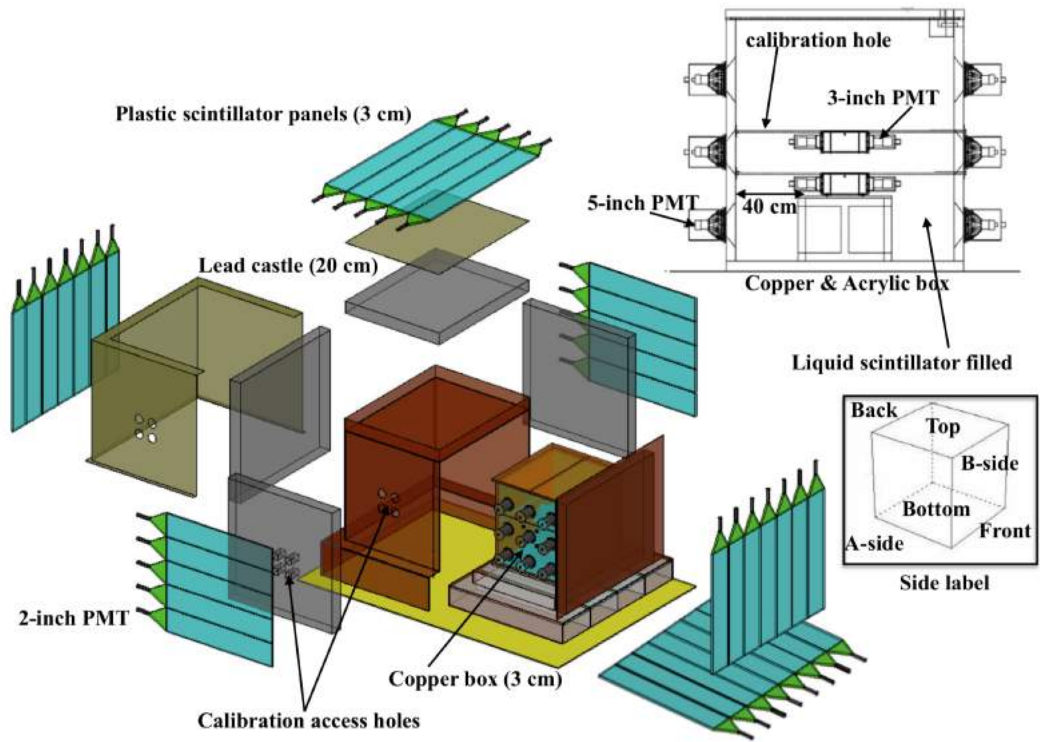


Figure I.2: The COSINE-100 detector. The detector comprises a nested arrangement of shielding components, as indicated by different colors. The main purpose of the shield is to provide coverage against external radiation from various background sources. The shielding components include plastic scintillator panels (blue), lead-brick enclosure (grey) and copper box (brown). The eight encapsulated sodium iodide crystal assemblies are located inside the copper box and are immersed in scintillating liquid, as shown in the schematic (right) ((Adhikari *et al.*, 2018).

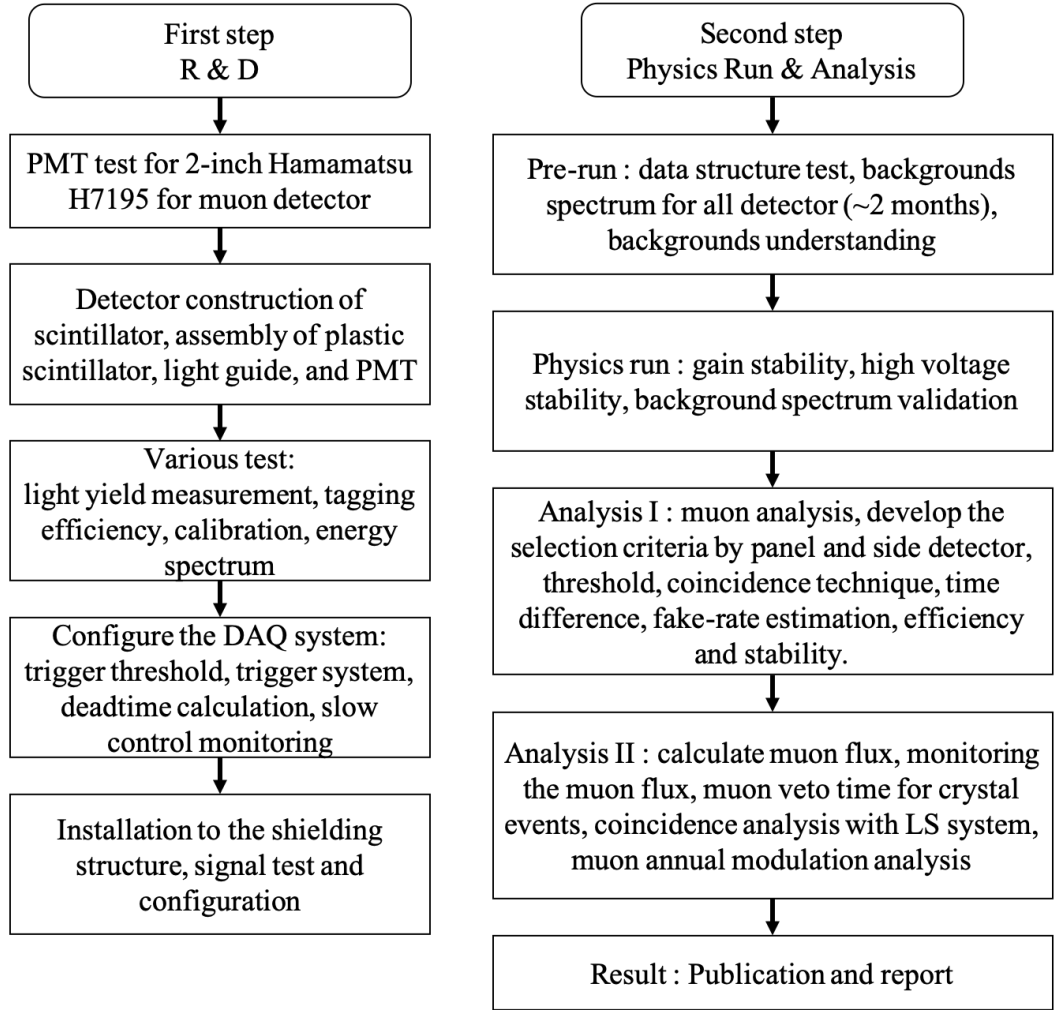


Figure I.3: Research diagram of the dissertation.

This dissertation is focused on assembly and construction of plastic scintillators. Various tests would be performed to understand the light yield, signal characteristics of background and signal, tagging efficiency, calibration, and energy spectrum of each panel. Develop the trigger condition of each panel which is integrated with other detectors. Installation process to the shielding of COSINE-100 experiment and test pre-run before physics data taking. Further, muon detector will take physics data together with crystals and liquid scintillator. From the physics data, we will study and develop the muon selection to obtain the muon signal. The overall works of this dissertation are showed in Fig. I.3.

I.5 Dissertation Outline

This dissertation is systematically organized into several chapters described as follows : Chapter I describes the introduction. It consists of background, research objectives, problem statement, research method, dissertation outline, and contributions. Chapter II discuss the evidences of dark matter particle, dark matter candidates, original background, direct detection method, other group experiments, cosmic-ray muons particle and interactions. Chapter III explains the experimental methods. It consists of preparation, deposition, characterization and analysis steps. Chapter IV presents the results and discussion of the physics run data, which explain the muon efficiency detection, muon flux, and muon modulation. Chapter V contains the conclusions and future work.

I.6 Contributions

In this research activity, the muon detector in the COSINE-100 experiment has been constructed and installed to tag the muon-events in dark matter experiment. Several tests were performed to achieve a good detector performance. Here, muons have been tagged with an event selection technique such as coincidence technique, time-difference cut, efficiency calculation, and fake-event rate estimation. Understanding of low and high energy impact on crystal events have been studied to prevent an accidental background induced by muons and understand the background modelling of crystal signal. Muons has been studied and observed with 2 years of physics data by continuous collecting. The overall of muon efficiency is determined of $99.9 \pm 0.1\%$ and show a muon annual modulation signature. The parts of this study have been reported in several journals and seminars, which are listed in List of Publications.

Chapter II Review of Dark Matter

II.1 Evidence of Dark Matter

The first evidence of dark matter was discovered by Fritz Zwicky in the 1930s from the observation of the velocity of galaxies in the Coma galaxy cluster (Zwicky, 1933). He measured the motions of galaxies within the cluster and estimated the mass of the cluster. He compared it to how much he could actually see by looking at the galaxies. The galaxies were moving too fast within the cluster for the amount of luminous matter. Then, there should have been a 100 times more luminous mass to account for the random speed of the galaxies (Sanders, 2010). The time a galaxy needs to travel through the cluster is much smaller than the age of the universe, it can be assumed that the cluster of galaxies are relatively a bound systems. The cluster is in viral balance and satisfies

$$T = \frac{1}{2}U \tag{II.1}$$

The individual mass, as well as the individual velocity of galaxy members can not be measured directly. It usually assumed that the system is spherically symmetric and in equilibrium, so that the velocity is uniformly distributed over all directions. $\langle v^2 \rangle$ is the mean square velocity of all the galaxies in the cluster. The kinetic energy equals to

$$T = \frac{1}{2}M \times 3\langle v \rangle^2 \tag{II.2}$$

where $\langle v \rangle$ denotes the velocity dispersion, which is assumed to be isotropic (equal in all direction). The potential energy equals to

$$U \sim -G\frac{M^2}{R} \tag{II.3}$$

Putting the equations (II.1), (II.2), and (II.3) together yields for the mass

$$M \sim \frac{3R\langle v \rangle^2}{G} \tag{II.4}$$

Inserting data of the Coma cluster into (II.4) yields $M \sim 10^{15}M_{\odot}$. With $L_{tot} \sim 10^{13}L_{\odot}$ the mass to luminosity ratio can be determined to be

$$\left(\frac{M}{L_{tot}}\right)_{Cluster} \sim 100\frac{M_{\odot}}{L_{\odot}} \quad (\text{II.5})$$

Zwicky observations delivered a first clear impression that there may be more matter in the universe. In 1932 he was one of the first to really grasp the significant presence of dark matter and then called it missing matter (Zwicky, 1933). The luminous matter in clusters is in the form of hot gas in between galaxies. This gas with high temperature ($10^7 - 10^8$ K) is also a hint to the existence of dark matter as the velocity of the gas is higher than the escape velocity deduced from the visually observed matter alone; but the gas is gravitationally bound, pointing to the existence of additional, dark matter, which constitutes at least of 80% of the mass of the galaxy cluster (Freese *et al.*, 2013.).

Today, the identification of dark matter and an elucidation of its properties is one of the most important issues in contemporary science, since it will affect our basic understanding of the structure and, perhaps, provide clues as to what particle physics lies beyond the Standard Model (SM) theory governing the composition of and interactions between the most elementary constituents of nature (Bertone *et al.*, 2005 and Bergstrom, 2009). Particle dark matter is a logical continuation of cosmology, and there are many theories which predict particles which can be suitable for dark matter. In particular, supersymmetric theories would be an interesting extension of the standard model, adding a superpartner to each existing standard model particle with 'mirrored' properties.

Dark matter can be attributed to any substance in the Universe that interacts predominantly via gravity with visible matter as we described in previous section. Dark matter are virtually non-interacting as explained in astrophysical observations like bullet cluster and they are non-baryonic matter as supported by confirmation from Big Bang Nucleosynthesis (BBN) and Cosmic Microwave Background (CMB). Current structure of the universe announce that dark matter is non-relativistic which is named as cold dark matter. Dark Matter do not decayed in the long history of universe so they are very stable. However, dark matter puzzle has led to the proposal of various candidates since dark matter interacts only weakly with ordinary matter, a brief introduction to the prominent candidates will be described.

II.2 Dark Matter Candidates

The Standard Model (SM) of particle physics describes a universe comprised of fermions interacting with each other via fields mediated by bosons. The elementary particles recognized by the SM are shown in Fig. II.1. They are divided first into two categories: fermions, which have a spin of $\frac{1}{2}$ and obey the Pauli exclusion principle, and bosons, which have integer spin and are not restricted by the Pauli exclusion principle.

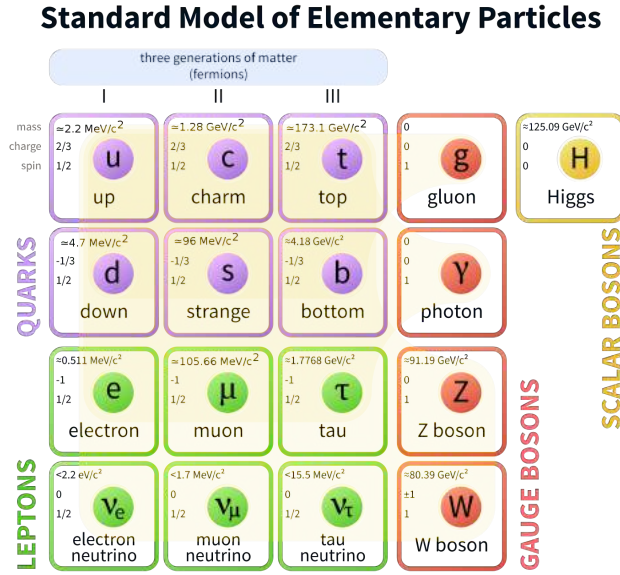


Figure II.1: SM particles, divided into bosons (red) and fermions. Fermions are further divided into quarks (violet) and leptons (green), with neutrinos. None of these SM particles fulfill the requirements of a dark matter particle, which must therefore be a particle beyond the SM. Figure from (Fermilab, 2008).

Fermions are divided into quarks and leptons. Quarks (up, down, charm, strange, bottom, top) are the only particles to interact with all four fundamental forces: electromagnetic, weak, strong, and gravitational. They are never found free, but rather confined in compound systems: baryons comprised of qqq and mesons of $q\bar{q}$. Within the leptons are the three generations of neutrinos (ν_x), which only interact weakly, while the other leptons (e, μ, τ) also interact electromagnetically. All fermions have associated antiparticles of equal mass and opposite charge. The bosons are divided into the gauge bosons (γ, g, Z, W) and the Higgs boson (H). The gauge bosons mediate the fundamental forces, with the photon (γ) mediating the electromagnetic force, gluons (g) mediating the strong force, and the Z and W bosons mediating the weak force.

The hypothesized graviton is believed to mediate the gravitational force. While very successful in describing the physical world, the SM does leave some open questions, and search for physics beyond the SM is a prodigious experimental effort. Notably, there are no SM explanations for gravity (including general relativity), dark matter, dark energy, neutrino masses, or the matter/antimatter asymmetry.

Dark Matter candidates must fulfill certain characteristics that no SM particle can fulfill. They must be massive enough to match observations of gravitational anomalies and structure formation, eliminating photons, gluons, and neutrinos as candidates. They must be electromagnetically neutral otherwise interactions with light would be observed, and these particles would not be dark. This precludes the charged leptons (e , μ , τ), quarks, and (W) bosons from being good candidates. As dark matter cannot be baryonic, compound particles built of quarks are further prohibited. Dark matter particles must be stable, not having decayed since their formation in the early universe, in order to match relic density. This condition eliminates the (Z) and Higgs bosons as candidates. In addition, a good dark matter candidate leaves stellar evolution unchanged, and is compatible with constraints from self-interaction, direct searches, and astrophysics. In addition, possible detection methods are required to experimentally probe the existence of dark matter.

A number of theoretically-motivated dark matter candidates have been proposed, spanning orders of magnitude of mass and interaction phase space, as shown in Fig. II.2.

II.2.1 WIMPs

Weakly Interacting Massive Particles (WIMP) dark matter candidates meet the criteria outlined by Cold Dark Matter (CDM) and return the correct relic density under the assumption that they are weakly interacting. In the early universe ($T > m_{\text{WIMP}}$), WIMP particles and antiparticles were continuously being produced and annihilated until the universe cooled below the temperature of WIMP production, and WIMPs froze out. After freeze out, dark matter numbers decreased because of self-annihilation until the dark matter density became low enough that annihilation was very rare. The dark matter abundance then stabilized, implying that the current density of dark matter is dependent upon the annihilation cross-section, as shown in Figure II.3. If the cross-section is that of the weak interaction ($\sim 10^{-37} \text{ cm}^2$), the correct relic density is predicted. This is known as the WIMP miracle and the remaining

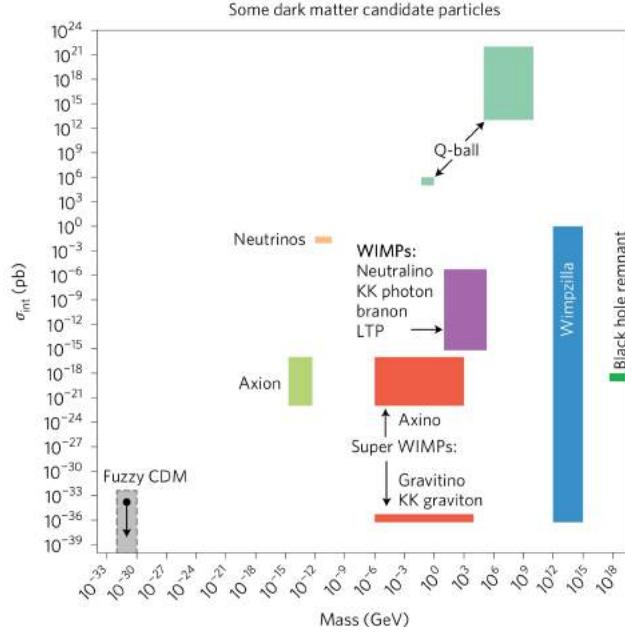


Figure II.2: Parameter space of theoretically-motivated dark matter candidates, with particle mass on the x-axis and interaction cross-section on the y-axis. The WIMP and the axion are preferred candidates, while the neutrino and the WIMPzilla have been excluded. Figure from (Park *et al.*, 2007).

chapters of this work will assume a WIMP dark matter candidate.

II.2.2 SUSY Dark Matter

Supersymmetry (SUSY) proposes a symmetry between fermions and bosons that involves supersymmetric partners for all SM particles, as shown in Figure II.4, one of which may comprise dark matter. Each SUSY particle is heavier than its SM partner and differs in spin by $\frac{1}{2}$. SUSY predicts that in the early universe, supersymmetric partners were in equal abundance to SM particles. By the time the temperature fell below 100GeV, all of the supersymmetric partners except the lightest had decayed, leaving the SM particles. The lightest SUSY particle would be stable due to a postulated new symmetry, R-parity (P_R), that replaces the conservation of baryon (B) and Lepton (L) number and motivates a stable SUSY partner:

$$P_R = (-1)^{2s+3B+L} = (-1)^{2s+3(B-L)} \quad (\text{II.6})$$

Where s is spin. SUSY predicts that all SM particles have $(P_R) = 1$ while SUSY partners have $(P_R) = -1$. The lightest SUSY partner, assuming

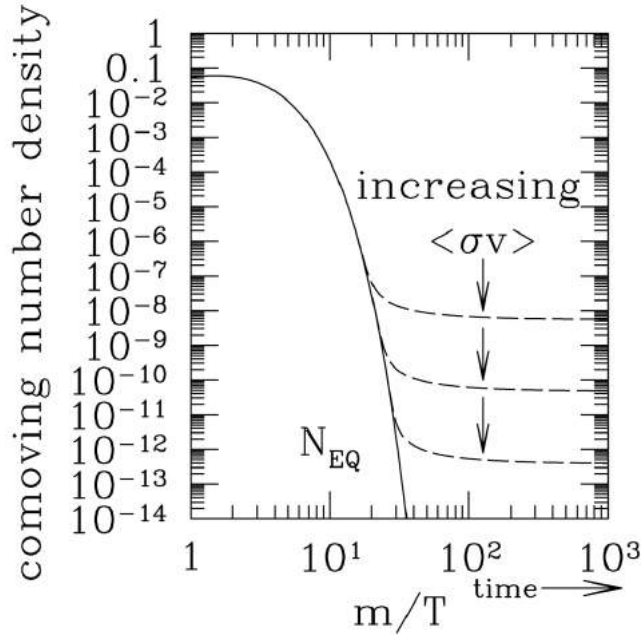


Figure II.3: WIMP abundance in the expanding universe. After the WIMP freeze out, dark matter density decreased due to self-annihilation until the universe cooled enough that annihilation was rare. At this point, the WIMP abundance stabilized. The correct density is predicted if the annihilation cross-section is that of weak interaction. Figure from (Paolo *et al.*, 2005).

R-parity conservation, would have nothing to decay to and would therefore be stable. From this model emerges a WIMP candidate: the Lowest Supersymmetry Particle (LSP). The most popular SUSY WIMP candidate is the neutralino, which is linear combination of neutral supersymmetric particles. The LSP is likely to be the lightest neutralino, a quantum mixture of three SUSY particles with the same quantum numbers: the zino (the Z boson's SUSY partner), the photino (the photon's SUSY partner), and the higgsino (the Higgs' SUSY partner). The neutralino is expected to have a mass of 10-10,000 GeV (Robert *et al.*, 2010).

II.2.3 Warm Dark Matter

Warm Dark Matter (WDM) proposes, as the name implies, an intermediate scenario between Hot Dark Matter (HDM) and Cold Dark Matter (CDM). WDM theorizes that dark matter is comprised of $\sim 2\text{keV}$ particles that were light enough at decoupling to free stream for a non-negligible distance that was much smaller than the causally-connected region. They then became non-relativistic and behaved identically to CDM, matching CDM-consistent observations (de Vega *et al.*, 2013). The success of CDM on a large scale can thus be

| | | | | | | | |
|---------|-----------|------------|----------|-----------------|-------------------|--------------------|------------------|
| u | c | t | γ | \tilde{u} | \tilde{c} | \tilde{t} | $\tilde{\gamma}$ |
| d | s | b | g | \tilde{d} | \tilde{s} | \tilde{b} | \tilde{g} |
| ν_e | ν_μ | ν_τ | Z | $\tilde{\nu}_e$ | $\tilde{\nu}_\mu$ | $\tilde{\nu}_\tau$ | \tilde{Z} |
| e | μ | τ | W | \tilde{e} | $\tilde{\mu}$ | $\tilde{\tau}$ | \tilde{W} |
| | | | H | | | | \tilde{H} |

Figure II.4: Table of the Standard Model (left) particles and their hypothetical supersymmetric particle. Figure from (Park *et al.*, 2007).

integrated into the WDM theory, while inconsistencies on the sub-Mpc scale can be explained by the WDM suppression of structure on this and smaller scales (Matteo Viel *et al.*, 2013). WDM improves dark matter predictions for smaller galaxies, although it requires the inclusion of quantum mechanical effects at small (≤ 100 pc) length scales (de Vega *et al.*, 2013). The most popular WDM candidate is the sterile neutrino, which is a hypothesized right-handed neutrino that only interacts gravitationally (de Vega *et al.*, 2013). WDM searches are underway, notably from X-ray telescope (e.g., Chandra (Watson *et al.*, 2012)) and the XMASS LXe detector (Abe *et al.*, 2014).

II.2.4 Axions

Axion dark matter was first postulated following the unexpected observation that the strong interaction appears to respect Charged-Parity (CP) symmetry, as evidenced by the neutron's lack of electron dipole moment. To resolve this, a quasi-symmetry was proposed that is respected at the classical level but is spontaneously broken by an axion field (Peccei *et al.*, 1977). The axion is predicted to have a mass inversely proportional to the vacuum expectation value that spontaneously breaks CP symmetry. The Axion Dark Matter eXperiment (ADMX) has been searching for axions through the photons that are predicted to arise from axions scattering off of virtual photons in a magnetic field (Asztalos *et al.*, 2001). The frequency of the resulting photons will depend on the axion mass. ADMX looks for these photons using a finely-tuned radio-frequency cavity at low temperature. ADMX ran from 2008-2010 at

Lawrence Livermore National Lab, then moved to the University of Washington. The running temperature was also decreased during this upgrade, from 1.2K to 400mK, with plans to lower down to 100mK to reduce noise (Karl van Bibber *et al.*, 2013). A second detector, ADMX-High Frequency (ADMX-HF) is being built to search in the higher frequency (higher mass) axion signal regime. ADMX-HF, located at Yale University, is smaller than ADMX to probe the higher frequency regime (Karl van Bibber *et al.*, 2013). The axion mass space still has unexplored phase space, but it is severely constrained to within 1-100 μ eV, with significant mass in that region excluded by beam dump experiments, the longevity of red giants, supernova 1987a, and most stringently, ADMX (Bertone *et al.*, 2010).

II.3 Dark Matter Searches

II.3.1 Collider Production

A lepton collider like the Large Hadron Collider should be able to produce WIMPs and detect them as missing energy in an event. In such a search, undetected pair-produced squarks or gluinos will decay down to the neutralino, leading to the missing energy and momentum (Kane *et al.*, 2008).

II.3.2 Indirect Dark Matter Detection

WIMP indirect detection experiments search for an excess of dark matter annihilations products in those areas (solar core, Earth's core, Galactic Center) where dark matter annihilation is most likely to occur. These experiments have observed a number of inconclusive hints but no definitive signals. Positron detectors, which aim to detect dark matter by observing an anomalously high positron-to-electron ratio, have produced the most notable results. An unexplained positron excess above 10GeV is observed by the Alpha Magnetic Spectrometer (AMS (Aguilar *et al.*, 2014)), Payload for Antimatter Matter Exploration and Light-nuclei Astrophysics (PAMELA (Adriani *et al.*, 2009)) and Fermi (Ackermann *et al.*, 2012) space-based detectors. The Advanced Thin Ionization Calorimeter (ATIC) adds to this data with an observed excess of the combined electron and positron flux (Chang *et al.*, 2008). The Wilkinson Microwave Anisotropy Probe and Planck photon detector satellites have observed a haze about the Galactic Center, which may be from radio synchrotron emission from electrons and positrons spiraling in the galactic gravitational field as a result of dark matter annihilation (Bennett *et al.*, 2013, Ade *et al.*, 2012). By contrast, the Very Energetic Radiation Imaging Telescope

Array System (VERITAS (Zitzer, 2013)) and the High Energy Stereoscopic System (HESS (Abramowski *et al.*, 2011)) cosmic ray shower detectors have not seen anything. The IceCube Neutrino Observatory (IceCube) has set the best spin-dependent limits, after observing no excess of neutrinos from the galactic center (Aartsen *et al.*, 2013) or solar core (Aartsen *et al.*, 2013).

II.3.3 Direct Dark Matter Detection

Direct detection experiments aim to observe the recoil of an atomic nucleus from the scattering of an incoming WIMP. The expected WIMP flux is a product of the galaxy being modelled as a disk rotating through a dark halo. This model predicts an effective WIMP wind of ~ 200 km/s and a WIMP flux on Earth, Φ_χ , of :

$$\Phi_\chi \sim 10^5 \frac{100 \text{ GeV}}{M_\chi} \text{cm}^{-2} \text{s}^{-1} \quad (\text{II.7})$$

where M_χ is the WIMP mass (Bertone, 2010). When a WIMP scatters off of a target nucleus of mass M_A , the nucleus recoils with an energy, E_R :

$$E_R = \frac{\mu_{\chi A}^2 v_0^2}{M_A} (1 - \cos \theta), \quad \mu_{\chi A} = \frac{M_\chi M_A}{M_A + M_\chi} \quad (\text{II.8})$$

where $\mu_{\chi A}$ is the reduced mass, v_0 is the WIMP speed, and θ is the scattering angle (Schnee, 2011). As an estimate of the energy scale of interest for detection, the average recoil energy for $v_0 = 220$ km/s and $M_\chi = M_A = 50 \text{ GeV}/c^2$ is 15 keV:

$$\langle E_R \rangle = \frac{\mu_{\chi A}^2 v_0^2}{M_A} = \frac{1}{2} M_\chi v_0^2 = 15 \text{ keV} \quad (\text{II.9})$$

Both the maximum recoil energy and the average recoil energy are at their largest when the target mass is close to the WIMP mass. The recoil energy spectrum is expected to fall exponentially with energy; the number of the events with energy E_R behaves as e^{-E_{thresh}/E_R} , where E_{thresh} is the threshold energy. A low detection threshold is thus critical to detect as many as events as possible, as shown in Figure II.5 The differential rate of interaction (counts/kg/day/keV) in a detector is derived from the number of interactions per nucleon and the number of nuclei in the material:

$$\frac{dR}{dE_r} = \frac{\rho_0}{M_\chi M_A} \int_{v_{min}}^{v_{max}} v f(v) \frac{d\sigma_{\chi A}}{dE_R}(v, E_R) dv, \quad (\text{II.10})$$

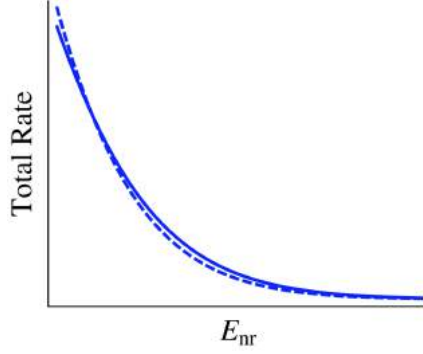


Figure II.5: Expected rate of dark matter interaction during the times of maximum and minimum rate as a function of energy. A low threshold is critical for direct detection experiments because most events are expected in the low energy region. Figure from (Freese, 2013).

where ρ_0 is the local WIMP density, $\sigma_{\chi A}$ is the WIMP-nucleus cross-section, $\frac{d\sigma_{\chi A}}{dE_R}(v, E_R)$ is the differential cross-section, and $f(v)$ is the WIMP velocity distribution. The minimum velocity, v_{min} , is the minimum velocity that can produce a recoil of energy E_r and is thus limited by the detector threshold, and v_{max} is limited by the galactic local escape velocity. Current experiments have already limited the expected WIMP-nucleon interaction rate to ~ 1 events/(kg.day).

II.3.3.1 Annual Modulation

The WIMP flux on Earth is expected to modulate throughout the year due to annual changes in the effective galactic velocity of the Earth. This arises from the combination of the Earth's two orbits: one around the Sun and the other, together with the Sun, around the center of the galaxy. As seen in Figure II.6, the Earth should see a WIMP maximum in June, when its motion around the Sun is in the direction of the galactic rotation velocity (increasing its effective velocity with respect to a galactic halo WIMP). Likewise there should be a WIMP minimum in December when the Earth's velocity is directed against that of the galactic orbit, decreasing its effective velocity. The Earth's velocity in the galactic frame is :

$$v_e(t) = v_{\odot} + v_{\oplus} \cos \gamma \cos \omega(t - t_0) = 232 + 15 \cos\left(2\pi \frac{t - 152.5}{365.25}\right) \quad (\text{II.11})$$

where v_{\odot} is the Sun's velocity with respect to the galactic center; v_{\oplus} is the Earth's velocity around the Sun with an inclination of 60.2° with respect to the galactic plane; $\omega = \frac{2\pi}{1 \text{ yr}}$ is the frequency of the orbit around the Sun, and t_0 is

the time when the Earth’s galactic speed is maximal, in early June (Bernabei *et al.*, 2003). These calculations predict a WIMP signal that modulates with a one year period and has a maximum in early June. In addition, a WIMP signal should be found only in the expected WIMP-induced recoil signal region, should be a single-scatter event, and should modulate with an amplitude $\leq 7\%$.

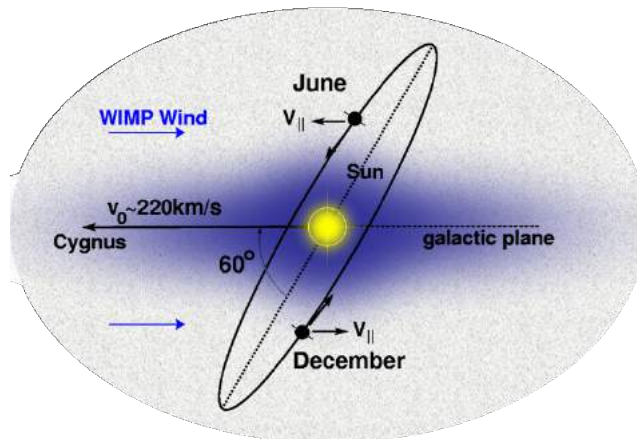


Figure II.6: Annual modulation mechanism for the WIMP flux on Earth. The modulation is a result of changes in the Earth’s galactic orbital velocity due to its orbit about the Sun. The WIMP flux maximum is in June, when the Earth’s orbital velocity is aligned with the galactic local velocity, and the minimum is in December, when the Earth’s solar velocity goes against the local galactic velocity. The WIMP wind comes from the direction of the constellation Cygnus in the terrestrial frame.

II.3.3.2 Status of Dark Matter Experiment

Historically, there have been three dark matter direct detection technique: ionization (using semiconductors and noble liquids/gases), scintillation (using inorganic crystals and noble liquids/gases), and thermal phonons (using cryogenic detectors). Recent experiments have made great strides in background rejection and event identification by integrating multiple readout channels (Freese, 2013).

Thermal phonons: When a nuclear recoils from particle scattering, the temperature of a target material is increased. A detector called the cryogenic detector which is designed and operated to measure phonons (heat) at a very low temperature because of the very small temperature rise in the nuclear recoil process. These detectors are highly sensitive to low energy particles with

very good resolution power for precise measurement of energy. Background level of the cryogenic detector is very low which is advantage for potential background discrimination. Because of the signal for a given event depends on the interaction type, the cryogenic solid state detectors can be instrumented as ionization or a scintillation detector for discrimination of nuclear recoil and electron recoil.

Ionization charge: When a particle interacts in the detector material, electron-hole or electron-ion pairs (ionization) are produced. In order to measure the ionization signal, an electric field has to be applied to collect the charge. There are several experiment running to measure the ionization signal such as DRIFT (Daw *et al.*, 2011) and CoGENT (Aalseth *et al.*, 2011).

Scintillation light” When a WIMP interacts with detector, it will produce the scintillation of light (photon). The scintillation light can be converted to the electron via photoelectric effect and can be measured as electric pulse. Liquid scintillators, noble liquids and highly radio pure scintillating crystals are used as a target material to measure WIMP generated photon. The number of experiments recently reporting very small excesses of signals above the known background is astonishing. For more than 15 years, only the modulation signal claim of the DAMA collaboration, both DAMA/NaI and its successor DAMA/LIBRA (Bernabei *et al.*, 2010), existed in the experimental direct dark matter searches. Other existing experiments conducted significant upgrades in technique and detector mass (CDMS (Agnese *et al.*, 2014), EDELWEISS (Armengaud *et al.*, 2011), CRESST (Angloher *et al.*, 2012), and were complemented by new experiments with solid state (CoGENT) and increasingly liquid noble gas detectors (XENON10, XENON100, also with its upgrade to 1Ton, LUX, WARP, and several more). The increasing sensitivity created the situation that more than one experiment found a small number of signals, which could not be explained by the known background sources. However, since the signals are sparse and just at the edge of the experiments sensitivity, and also most of the detectors have not been taking data for several annual cycles, none of the new results can be considered as clear and concise evidence for dark matter detection.

II.4 Background Sources

Dark matter experiments require low backgrounds to detect such a rare signal, so shielding from the environment, the detector, and even the target is an important experimental factor. Placing experiments deep underground shields

them from cosmic ray backgrounds, and additional shielding is used for local environmental backgrounds. As most backgrounds will produce electron recoils rather than nuclear recoils, discrimination between nuclear recoils and electron recoils can reject almost the entire background. To achieve this sensitivity, the background suppressions are a must in rare event searches, especially muons from cosmic-ray shower. A short overview of the origin, main components and spectra of cosmic rays and their flux in underground experiments is given here for the aspects needed to understand the importance of a muon veto in underground and low background experiments such as COSINE, as muons are the main cosmic ray component influencing such experiments.

II.4.1 Cosmic rays and components

Cosmic rays are particles coming from space into the atmosphere of the Earth, discovered by Viktor Hess in 1912 (Hess, 1913). Their study is interesting not only by itself but has also triggered many important developments in physics. Cosmic rays originate mainly in our galaxy; however, the origin of the particles with the highest energies (above 10^{20} eV) is still unclear. Charged primary cosmic rays (i.e. the ones coming directly from the original sources) consist of 86% protons, 11% α -particles, 1% heavier nuclei and 2% electrons. The small amounts of positrons and antiprotons observed are believed to originate from interactions of the primary particles with the interstellar gas. The chemical composition of the cosmic rays is also modified by interactions: most of it is comparable to the distribution of elements in the solar system; however; Li, Be, B as well as Sc, Ti, V, Mn, which are quite rare in the solar system as they are easily destroyed during stellar nucleosynthesis, are significantly more abundant in the cosmic rays since they are produced by spallation of the abundant C, O and Fe, Ni nuclei (Nakamura *et al.*, 2010).

Charged cosmic rays interact in the atmosphere producing especially pions and kaons. Pions can be either charged (π^+ , π^-) or neutral (π^0). Both pions and kaons are extremely short lived, and were they to not interact on their descent through the atmosphere to produce extensive air showers. Charged pions with energies below about 100 GeV mainly decay in flight, resulting in muons with branching ratios are :

$$\begin{aligned}
 \pi^\pm &\rightarrow \mu^\pm + \nu_\mu(\bar{\nu}_\mu) (\sim 100\%) \\
 \pi^0 &\rightarrow 2\gamma (\sim 98.8\%) \\
 K^\pm &\rightarrow \mu^\pm + \nu_\mu(\bar{\nu}_\mu) (\sim 63.5\%)
 \end{aligned}
 \tag{II.12}$$

where γ here refers to a photon, rather than the spectral index as it has been used before. Muon decay is a prominent source of neutrino. At low energies (or after a very long amount of time), muons will decay as

$$\mu^\pm \rightarrow e^\pm + \nu_e(\bar{\nu}_e) + \bar{\nu}_e(\nu_e) \quad (\text{II.13})$$

Higher energy pions often undergo nuclear interaction instead of decaying, therefore the energy spectrum of the daughter muons is steeper by $1/E$ than that of the pions or the primary protons. As charmed particles decay rather than interact because of their short lifetimes, the spectrum of these prompt muons is not steepened by $\frac{1}{E}$ but has the same exponent as the primary spectrum, therefore at very high energies prompt muons will dominate the muon flux although their parents initially are produced in much smaller quantities. Prompt muons are distributed isotropically (Geisser, 1990).

Due to their relatively long lifetime 2.2×10^{-6} s and small cross section high energy muons are the most penetrating component of cosmic rays. For example, a 3GeV muon has decay length of 20 km and can pass the entire atmosphere without decay or interaction. Higher energetic muons can even propagate through large amounts of rock. This is the reason why Dark Matter searches and other low background experiments have to be carried out at as large depths underground as possible. On the surface, muons are distributed isotropically in azimuthal angle, while their zenith angle distribution varies with $\frac{1}{\cos\theta}$ due to the large thickness of atmosphere they have to cross. The differential muon energy spectrum on Earth at energies above 10 GeV, at which muon decay and energy loss may be neglected, can be approximately by (Geisser, 1990) :

$$\frac{dN_\mu}{dE_\mu} \approx \frac{0.14E_\mu^{-2.7}}{cm^2s sr GeV} \left\{ \frac{1}{1 + \frac{1.1E_\mu \cos \theta}{115 GeV}} + \frac{0.54}{1 + \frac{1.1E_\mu \cos \theta}{850 GeV}} \right\} \quad (\text{II.14})$$

The first term inside the brackets represents the muons originating from pion decay, the second the ones from kaon decay. At angle θ larger than 60° the curvature of the Earth has to be taken into account. The zenith angle θ on the surface of the Earth is connected to the zenith angle θ at the top of the atmosphere by the relation $\sin \theta = \sin \theta \frac{R_E + H_{int}}{R_E}$ with $R_E = 6.600$ km being the Earth radius = 18.6 km the mean interaction height for primary particles in the atmosphere (Horn, 2007 and Rhode, 1993). Underground the muon distribution reflects the topography of the rock overburden. Therefore,

to study the muon background in an underground experiment the mountain profile has to be known as precisely as possible.

II.4.2 Interactions of Muons

Muons can interact with matter either continuously by ionization of the surrounding material or discretely by the radiative processes bremsstrahlung, pair production and nuclear interaction. In bremsstrahlung and pair production electrons, positrons and gammas are produced, which in turn can undergo bremsstrahlung and pair production, leading to the development of electromagnetic showers. In a similar way, hadronic showers can be induced by the nuclear interaction of muons. In hadronic showers also neutrons are produced which are the most dangerous background in Dark Matter search experiments, therefore it is important to know the numbers of neutrons as precise as possible.

II.4.2.1 Ionization

The energy loss of muons by ionization is given by the Bethe-Bloch formula (Bethe, 1930 and Nakamura *et al.*, 2010) :

$$-\frac{dE}{dx} = 4\pi N_A r_e^2 m_e c^2 z^2 \frac{Z}{A} \frac{1}{\beta^2} \left[\frac{1}{2} \ln \frac{2m_e c^2 \beta^2 \gamma^2 T_{max}}{I^2} - \beta^2 - \frac{\delta(\beta\gamma)}{2} \right] \quad (\text{II.15})$$

with N_A Avogadro's number, $r_e = \frac{e^2}{4\pi\epsilon_0 m_e c^2}$ the classical electron radius, m_e the mass of electron, z_e the charge of the incoming particle (in this case the muon), Z the atomic number and A the atomic mass of the absorber, T_{max} the maximum kinetic energy which a free electron can obtain in a single collision, I the mean excitation energy, $\beta = \frac{v}{c}$ and $\gamma = \frac{1}{\sqrt{1-\beta^2}}$ the usual kinematic variables and $\delta(\beta\gamma)$ the density effect correction. T_{max} is given by

$$T_{max} = \frac{2m_e c^2 \beta^2 \gamma^2}{1 + 2\gamma m_e / m_\mu + (m_e / m_\mu)^2} \quad (\text{II.16})$$

with m_μ the mass of the muon. The determination of I is difficult; values are recommended by the International Commission on Radiation Units and Measurement (ICRU). The density effect correction is usually calculated by Sternheimer's parametrization (Sternheimer *et al.*, 1971). The ionization energy loss is approximately $2\text{MeV}/(\text{g}\cdot\text{cm}^2)$.

II.4.2.2 Bremsstrahlung

In bremsstrahlung, a photon is emitted by the interaction of the muon with matter. The cross section has originally been calculated by Bethe and Heitler (Bethe *et al.*, 1934). In GEANT4 an improved version by Kelner, Kokoulin and Petrukhin is used (Kelner *et al.*, 1995) :

$$\begin{aligned} \frac{d\sigma(E, \epsilon, Z, A)}{d\epsilon} &= \frac{16}{3} \alpha N_A \left(\frac{m_e}{m_\mu} r_e \right)^2 \frac{1}{\epsilon A} Z(Z\Phi_n + \Phi_e) (1 - v + \frac{3}{4}v^2) \\ &= 0 \text{ if } \epsilon \geq \epsilon_{max} = E - m_\mu \end{aligned} \quad (\text{II.17})$$

with α the fine structure constant, N_A Avogadro's number, m_e and m_μ the mass of the electron and muon, respectively, r_e the classical electron radius, E the initial total energy of the muon, $\epsilon = E - E'$ the energy of the emitted photon, Z the atomic number and A the atomic mass of the absorber and $v = \epsilon/E$ the relative energy transfer of the muon. Φ_n and Φ_e are the contributions of the nucleus and of the electron, respectively.

II.4.2.3 Pair Production

In pair production, an electron-positron pair is generated by the muon. The differential cross section is given

$$\begin{aligned} \sigma(Z, A, E, \epsilon) &= \frac{4}{3\pi} \frac{Z(Z + \zeta)}{A} N_A (\alpha r_0)^2 \frac{1 - v}{\epsilon} \int_0^{\rho_{max}} G(Z, E, v, \rho) d\rho \\ &\text{with} \\ G(Z, E, v, \rho) &= \Phi_e + \left(\frac{m_e}{m_\mu} \right)^2 \Phi_\mu \end{aligned} \quad (\text{II.18})$$

ζ is the inelastic atomic form factor contribution from pair production on atomic electrons. Z the atomic number and A the atomic mass of the material, N_A Avogadro's number, α the fine structure constant, ϵ the total energy of the produced pair corresponding to the energy loss of the muon $E - E'$, $v = \epsilon/E$ the fractional energy loss. Φ_e and Φ_μ are complicated QED functions and also take atomic and nuclear cross sections into account; formulas are given in (Lohmann *et al.*, 1985).

II.4.2.4 Nuclear Interaction

Muon nuclear interaction is especially important at high muon energies ($E \geq 10\text{GeV}$), high energy transfers ($\nu/E \geq 10^{-2}$) and for light target materials.

The contributions of this process to the total energy loss increases almost linearly with energy, reaching about 10% for TeV muon energies. The cross section and energy loss is dominated by the low Q^2 region ($Q^2 \ll 1\text{GeV}^2$). The electromagnetic interaction of the muon with the nucleus is mediated by a virtual photon. In this sense the muon nuclear interaction is comparable to the photonuclear interaction.

It can be described by the Borog and Petrushkin formula for the cross section (Borog *et al.*, 1975), which is based on Hand's formalism for inelastic muon scattering (Hand *et al.*, 1963), a vector dominance model with parameters estimated from experimental data for the inelastic form factor and theoretically parameterized nuclear shadowing effect (Brodsky *et al.*, 1972). If the same photonuclear cross section is used it agrees to better than 10% with the formula given by Bezrukov and Bugaev. For $E \geq 10\text{GeV}$ it can be written as

$$\begin{aligned}\sigma(E, \nu) &= \Psi(\nu)\Phi(E, v) \\ \Psi(\nu) &= \frac{\alpha}{\pi} \frac{A_{eff} N_A}{A} \sigma_\gamma N(\nu) \frac{1}{\nu} \\ \Phi(E, v) &= v - 1 + \left[1 - v + \frac{v^2}{2} \left(1 + \frac{2m_\mu^2}{\Lambda} \right) \right] \ln \frac{\frac{E^2(1-v)}{m_\mu} \left(1 + \frac{m_\mu^2 v^2}{\Lambda^2(1-v)} \right)}{1 + \frac{Ev}{\Lambda} \left(1 + \frac{\Lambda}{2M} + \frac{Ev}{\Lambda} \right)}\end{aligned}\tag{II.19}$$

with α the fine structure constant, N_A Avogadro's number, A the atomic mass of the material, ν the energy lost by the muon, $v = \nu/E$, m_μ the muon and M the nucleon mass. Λ is a vector dominance model parameter estimated to be $\Lambda^2 = 0.4\text{GeV}^2$. The effect of nuclear shadowing is included in A_{eff} , which is parameterized as

$$A_{eff} = 0.22A + 0.78A^{0.89}\tag{II.20}$$

A possible dependence on ν and E is currently neglected in this formalism. For the photonuclear cross section $\sigma_\gamma N$ the parameterization of Caldwell of experimental data of real photoproduction is chosen:

$$\sigma_{\gamma N} = (49.2 + 11.1 \ln K + 151.8K^{-1/2}).10^{-30} \text{ cm}^2, K \text{ in GeV}\tag{II.21}$$

which should be valid at least up to 100 TeV.

II.4.3 Muons in rare event search

On their way through atmosphere and rock muons lose about $2\text{MeV}/(\text{g}\cdot\text{cm}^2)$ by ionization; at higher energies the energy loss rate $\frac{dE}{dx}$ increases slowly with muon energy E_μ and can be approximated to better than 5% for $E_\mu \geq 10\text{GeV}$ by (Gaisser, 1990).

$$-\frac{dE}{dx} \approx \left(1.9 + 0.08 \ln \frac{E_\mu}{\text{GeV}} \right) \left[\frac{\text{MeV}}{\text{g}/\text{cm}^2} \right] \quad (\text{II.22})$$

At even higher energies also the other energy loss processes bremsstrahlung, pair production and inelastic scattering on nuclei become important; their energy loss rate is proportional to the muon energy. Therefore, the average muon energy loss can be written as

$$-\frac{dE(E_\mu)}{dx} = a(E_\mu) + b(E_\mu)E_\mu \quad (\text{II.23})$$

with $a(E_\mu)$ the ionization energy loss and $b(E_\mu) = b_{\text{brems}}(E_\mu) + b_{\text{pair}}(E_\mu) + b_{\text{inelastic}}(E_\mu)$ the sum of the radioactive contributions. Neglecting fluctuations the relation between the initial and final energies of a muon passing a distance x is given by

$$x = \int_E^{E_0} \frac{dE_\mu}{\langle dE(E_\mu)/dx \rangle} \quad (\text{II.24})$$

If a and b are energy-independent, this can be expressed as

$$E = (E_0 + \epsilon)e^{-bx} - \epsilon \quad (\text{II.25})$$

where $\epsilon = a/b$ is the critical energy above which the radiative energy losses become more important than the ones due to ionization.

Chapter III COSINE-100 Experiment

In this chapter, all the elements of the experimental requirements, experiment site, set-up including shielding structure, crystal detectors, veto systems, photomultipliers, electronics and data acquisitions, slow control monitoring will be described. This the 1st generation of the experiment with 106 kg NaI(Tl) crystal has been operating and collecting of the physics data, called COSINE-100.

III.1 Experimental Hall

The COSINE experiment is located in a recently established experimental area in the Y2L A5 tunnel. The Y2L facility is situated next to the underground generators of the Yangyang pumped-storage hydroelectric power plant under Mount Jumbong, 200 km east of Seoul in Korea (38° 01' 09.1" N, 128° 29' 58.6" E). The laboratory consists of experimental areas located in the A5 and A6 tunnels and are accessible by car via a 2km horizontal access tunnel shown in Fig III.1. The experimental area has an overburden of a 1800 meter-water equivalent depth. The cosmic-ray flux in A6 is measured to be $2.7 \times 10^{-7} \text{ cm}^{-2} \text{ s}^{-1}$ (Zhu *et al.*, 2013). Automatically regulated electrical power, conditioned by uninterruptible supplies, is provided to experimental area, with voltages that are continuously monitored. Additionally, a humidity control system, radon reduction system, and gas supply facility are provided.

The COSINE-100 detector room is 44 m² wide and is an access-controlled clean air environment. The room is designed to be self-contained and properly sealed to minimize contact with outside air containing high humidity and large amount of Radon and other background. The air in the room is continuously circulated and filtered through a high-efficiency particulate arrestance mechanism with the maximum number of dust particle larger than 0.5 μm is kept below 1500 per cubic foot. The physical condition of room is monitored with several temperature and air control system, and other measurement equipment. The main design requirement for the room is to provide a temperature stability of $\pm 1.0 \text{ }^\circ\text{C}$ throughout the year, a humidity control at $\pm 3.0 \%$, and Radon level below 40 Bq/m³. The room is also equipped with a backup cooling system, a Radon-free air supply, and an access buffer booth. The room is only accessed through the buffer in the events of a calibration campaign or a regular maintenance.



Figure III.1: Yangyang underground laboratory site. The lab is located at the Yangyang pumped storage power plant in the northeast of South Korea.

III.2 The COSINE-100 detector

The COSINE shielding structure inherited many features from KIMS [40,41]. The detector is contained in a 4-layer box-shaped shields shown in Fig III.2 that provide a 4π containment to reduce external and internal backgrounds from cosmic-rays and cosmogenic radioisotopes. From the center outward, the four shielding layers are scintillating liquid, copper, lead, and plastic scintillator panels. The liquid scintillator and plastic scintillators work as both passive and active shields against the external radiation and muons, respectively, while the two other layers provide passive background reduction. The eight NaI(Tl) crystal assemblies and their support table are immersed in the scintillating liquid. The shield is supported by a steel skeleton that surrounds a 300 cm (L) \times 220 cm (W) \times 270 cm (H) volume. The front side of the shield can slide open at a speed of 40 cm per minute through a linear rail. Details of the each components including physical conditions, R&D results and initial performances will be described in below subsections.

A layer of lead bricks has been installed with enclosing the copper box. Gamma rays from the external sources are attenuated by a 20 cm-thick lead

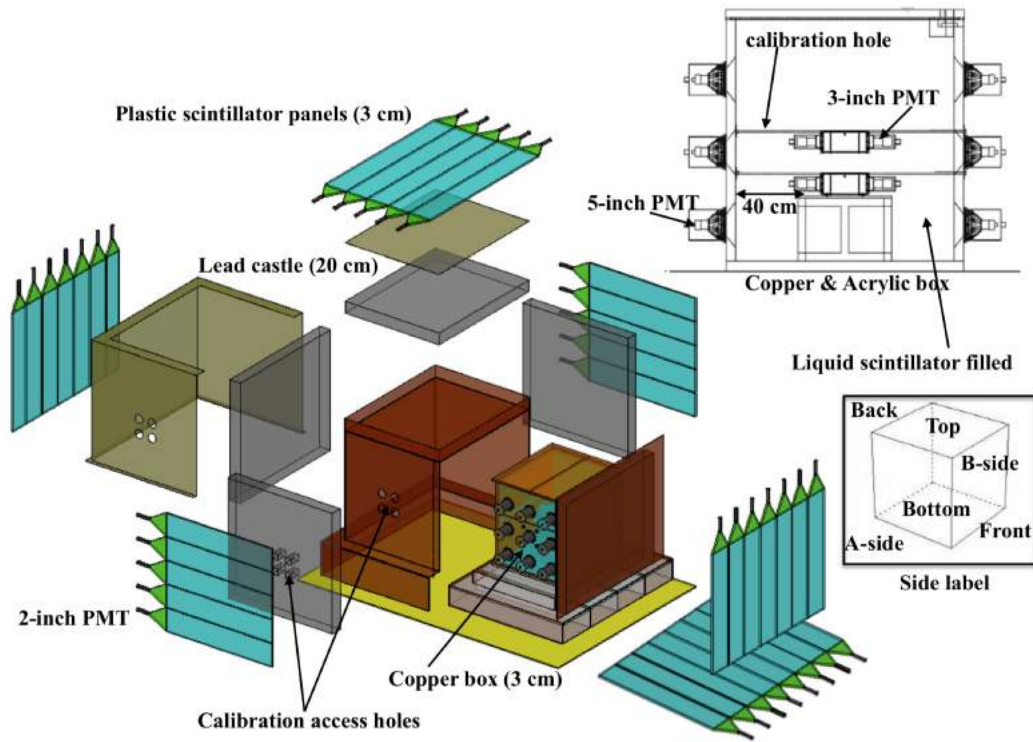


Figure III.2: The 4π 4-layer shielding enclosure for the COSINE detector. From inside to outward, 8 encapsulated crystal detectors immersed in the 40-cm thick scintillating liquid, a liquid and crystal supporting acrylic box (1 cm thick), 3 cm-thick copper box, 20 cm-thick lead castle, and 37 with 3-cm thick muon panels are shown. Also indicated are the locations of the calibration holes, the size of the PMTs, and labels for sides. The lead shields at the bottom and the front side are omitted for clarity.

wall that surrounds the copper box as shown in Fig. III.3. The inner half of this shield is made with low-contamination ancient lead that has measured U and Th concentrations of 6.9 and 3.8 ppt, respectively. The ^{210}Pb content was measured to be 30 ± 1 Bq/kg at y2L using alpha counting of ^{210}Po decay while the supplier's specification shows 59 ± 6 Bq/kg using ^{210}Bi beta counting. The outer half of the shield is made from normal lead supplied by a domestic dealer with 99.99% purity. The lead is in the form of $20\text{ cm} \times 10\text{ cm} \times 5\text{ cm}$ rectangular bricks and are stacked in such a way that there is no open channel between the outer and inner layer. Four calibration window of dimension $20\text{ cm} \times 20\text{ cm}$ each are designed in such a way that lead bricks can remove and install the source and sealed again for data taking.



Figure III.3: A photo of the COSINE detector room when the front door was opened. Plastic scintillators with black covers and an orange copper box with 5" PMT assemblies on the A-side are shown. A hoist is used to move the 800 kg copper top.

The lead bricks were wiped with 100% isopropyl alcohol thoroughly prior to installation. The total weight of the lead is 56 tons. The copper box serves as a shield for γ -rays as well as a support for the liquid scintillator. ICP-MS measurements of the copper were 27 and 51 ppt of ^{238}U and ^{232}Th , respectively. The outer dimensions of the box are $152\text{ cm (L)} \times 142\text{ cm (W)} \times 142\text{ cm (H)}$. The wall thickness is 3 cm and the total mass is 6.4 tons. It is made of oxygen-free copper (OFC). A 1 cm-thick acrylic container for the liquid scintillator is nested inside of the copper box.

III.2.1 Liquid Scintillator (LS) Detector

A variety of backgrounds produced by radiogenic particles from components in and near the NaI(Tl) crystals, including the crystal PMT-originating and the NaI(Tl) internal backgrounds, are efficiently rejected by an anticoincidence requirement with PMT signals from the liquid scintillator (LS) and neighboring crystal signals. This innermost active and passive shielding is provided by 2,200 L of Linear Alkyl-Benzene (LAB)-based LS contained in the acrylic box. The inner walls of the acrylic container and the outer surfaces of the crystal assemblies are wrapped with specular reflective films to increase the LS light collection efficiency. The LS-produced photons are detected by eighteen 5-inch Hamamatsu PMTs (R877) that are attached to the two sides of the box. The minimum distance between the crystal PMTs and the copper box inner wall is approximately 40cm.

The LAB-based liquid scintillator has a LAB base with 3g/l PPO and 30 mg/l bis-MSB as flour and wavelength shifter (Park *et al.*, 2013). We used LAB from a domestic company, neutrino grade PPO, and scintillation grade bis-MSB. The LS production is performed in a ground laboratory in Chonnam University, 350 from Y2L. After production, the LS was moved to the A5 tunnel for filling process into the acrylic container of the COSINE shield. We filled the total 2,200l LAB-based LS corresponding up to 9 cm below the top of the copper box. This 9 cm marginal space is a safety precaution in the event of any sudden temperature increase that might cause an expansion of the LS volume.

The detector tags 48% of the internal ^{40}K background in the 0-10 keV energy region. We also measure the tagging efficiency for events at 6-20 keV to be $26.5 \pm 1.7\%$ of the total events, which corresponds to 0.76 ± 0.04 events/keV/kg/day. According to a simulation, about 60% of the background events from U, Th, and K radioisotopes in photomultiplier tubes are tagged at energies of 0-10 keV. Full shielding with a 40 cm thick liquid scintillator can increase the tagging efficiency for both the internal ^{40}K and the external background to about 80% Fig. III.4.

III.2.2 Sodium Iodide NaI(Tl) crystal detector

NaI(Tl) has high scintillation efficiency so it is widely used as a scintillation detector. Because of its hygroscopic nature they are easily damaged when exposed to moisture at normal humidity levels. Hydration appears as yellow or green spots on the surface, which absorbs blue scintillation light from the crys-

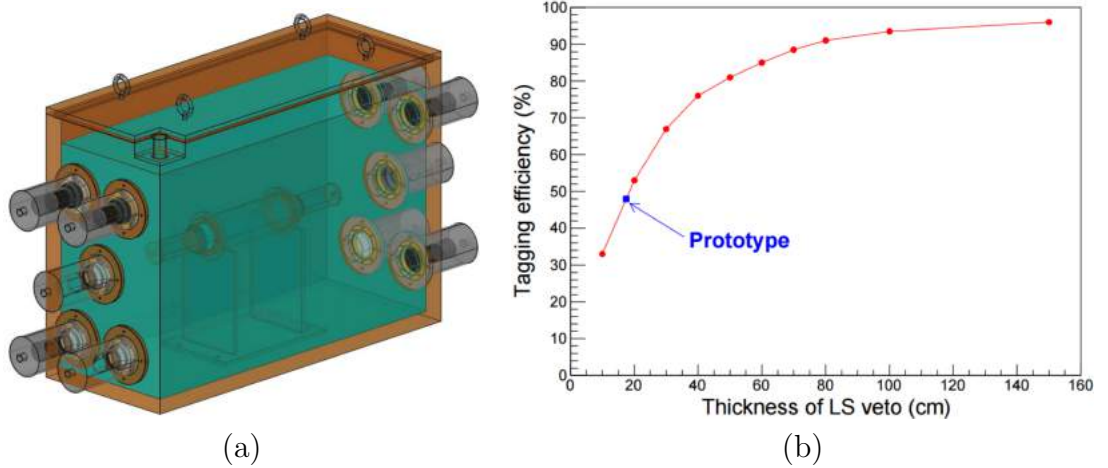


Figure III.4: (a) A prototype liquid scintillator veto detector. (b) Veto efficiencies of internal ^{40}K as a function of the thickness between the NaI(Tl) crystal and the LS container for energies between 0-10 keV are presented from simple geometry simulation. Here square dot not represent result obtained from the prototype detector.

tal and as a result degradation of the light output and resolution of the crystal. Therefore NaI(Tl) crystals need very attentive treatment and handling. The primary decay constant of the NaI(Tl) crystal is 250 ns at room temperature. General properties of the NaI(Tl) crystal are described in Table III.1.

Table III.1: Properties of the Sodium Iodide NaI(Tl) crystal

| | |
|----------------------------|------------------------|
| Density | 3.67 g/cm ³ |
| Wavelength of emission max | 415 nm |
| Primary decay time | 250 ns |
| Light yield | 40 photons/keV |
| Hygroscopic | yes |

We have developed the ultra-low background NaI(Tl) crystals in cooperation with the Alpha Spectra Inc. (AS). Eight NaI(Tl) crystals were produced (labeled Crystal-1 to Crystal-8), or C1-C8) at a sequence of steps in which the initial powder purification was carried out following different procedures before the crystal was grown by the Company. The final crystals are cylindrically shaped and are hermetically encased in an Oxygen-Free Copper (OFC) tube with Quartz end windows. After the performance of various surface treatment procedures, the crystals were wrapped in a Teflon reflector and inserted into the OFC cylinder and encapsulated, all in a Radoo-free nitrogen gas environment. A 12.7 mm-thick quartz window is coupled to each end of the cylinder with an optical interface (7 mm optical pad) between the crystal

and the quartz windows. These are, in turn, light-couple to 3" Hamamatsu R12669SEL (selected for high quantum efficiency) PMTs via a small amount of optical grease.

The crystals were installed inside the copper box in a two-story acrylic support. An acrylic table having eight bow-shaped structure (Fig. III.5) to fix eight crystals has been install inside the copper box, at the center of the copper box floor. Fig III.5, (b), shows the array of eight crystal and their position. Overall, these crystals show high light output and tiny ^{238}U and ^{232}Th contaminations. Also, the powder grade is closely correlated with the contamination level of the grown crystals, as can be seen the level of ^{40}K depending on the powder batch. Within a specific batch of powders, radioactivities are consistently reproduced. However, the level of alpha particles due to ^{210}Po is higher than that achieved by DAMA. Its origin is not fully understood at the moment. Chain equilibrium is assumed for the interpretation of ^{238}U and ^{232}Th related radioactivity measurements, with the exception of ^{210}Pb .

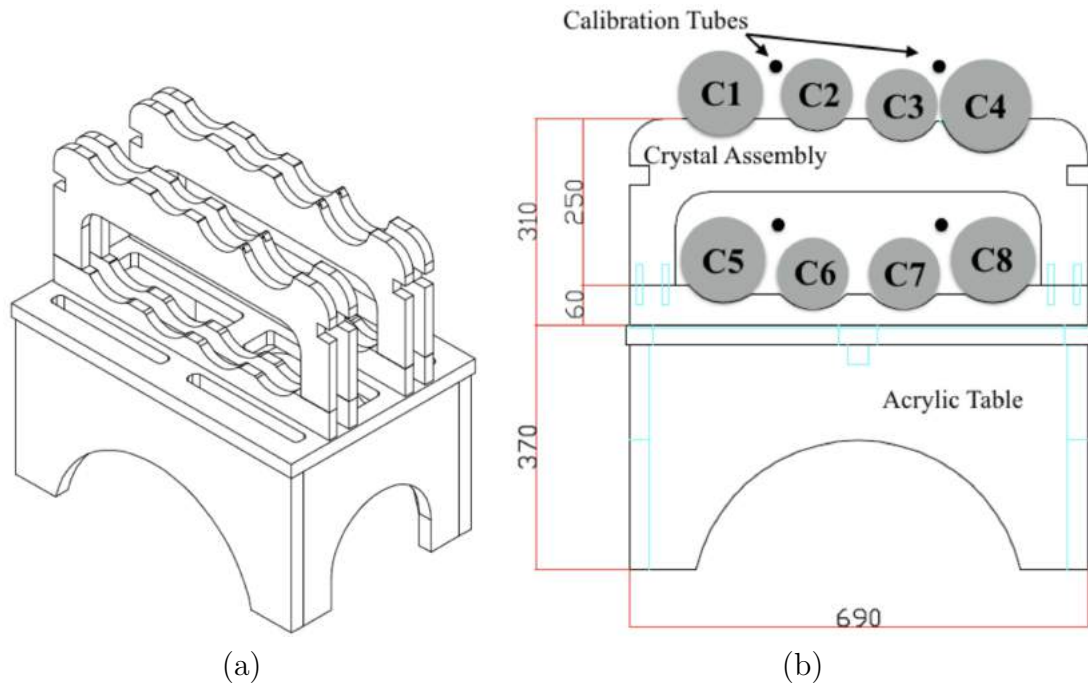


Figure III.5: (a) A acrylic support for the crystals, (b) An array of eight crystal and their position inside the Copper box.

III.2.3 Plastic Scintillator Detector

The outer detector shielding is consist of 42 PMTs of 2-inch PMT from Hamamatsu Photonics and 37 plastic scintillator with 3-cm thickness of type EJ-200

having maximum light output at wavelength 425 nm¹. General properties of the EJ-200 are described in Table III.2. Twenty seven of the panels are 40 cm wide, ten are 33 cm wide in order to fit into the shielding structure. The array forms a near cubic structure with sides labeled as top, bottom, front, back, left, and right. The top-side panels are 282 cm long and are read out by a photomultiplier tube (PMT) at both ends. The panels on the other side are approximately 200 cm long and their signals are read out by one PMT.

Table III.2: Properties of the EJ-200 Plastic Scintillator

| | |
|--------------------------------|---------------------------|
| Light Output | 64 % Anthracene |
| Scintillation Efficiency | 10,000 photons/1MeV e^- |
| Wavelength of Maximum Emission | 425 nm |
| Light Attenuation Length | 380 cm |
| Decay Time | 2.1 ns |
| Polymer Base | Polyvinyltoluene |

Table III.3 lists dimensions of the muon panels for the six sides. Each panel is polished and coupled to an acrylic light guide using BC-600 optical cement from Saint-Gobain². Two-inch H7195 PMTs from Hamamatsu Photonics³ are mounted with the optical cement at the end of the light guides. The optical coupling was visually inspected, as shown in Fig. III.6 (a). To increase the light collection, a Vikuiti reflector film is attached with the optical grease at one end of the scintillator for the 200 cm-long panels. The muon panels are wrapped with a TYVEK reflector to collect light efficiently, as shown in Fig. III.6 (b). Then, the panel is covered with a 50- μ m-thick aluminum foil [Fig. III.6 (c)] and a black vinyl sheet [Fig. III.6 (d)] to prevent external light from leaking inside and physical damage. A schematic of the muon panel used for the left or right side is shown in Fig. III.7.

Various tests were performed with the muon panels in a ground laboratory where the cosmic ray muon flux is reasonably high. A small trigger counter made of the same plastic scintillator was placed above the muon detector panel as shown in Fig. III.8. Coincident signals from the muon panel and the trigger counter are used to select muon candidates. With a sufficiently high energy threshold for the signals in the trigger counter, muon candidate events in the panel can be selected as shown in Fig. III.9 (a). The muon candidate signals in the panels are well modeled by a Landau distribution.

¹<http://www.eljentechnology.com>

²<http://www.crystal.saint-gobain.com>

³<http://www.hamamatsu.com>

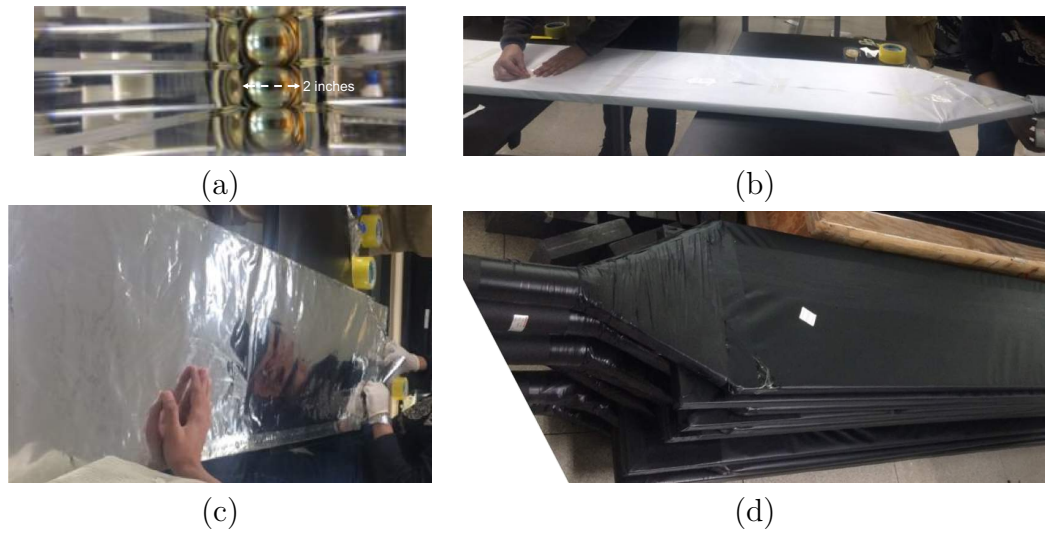


Figure III.6: Assembly procedure of the plastic scintillator panels. (a) The light guide with PMT is attached with BC-600 optical cement. (b) A panel is being wrapped with a TYVEK reflector. (c) A panel is being wrapped with an aluminum foil. (d) Muon panels stacked after being wrapped with a black vinyl sheet.

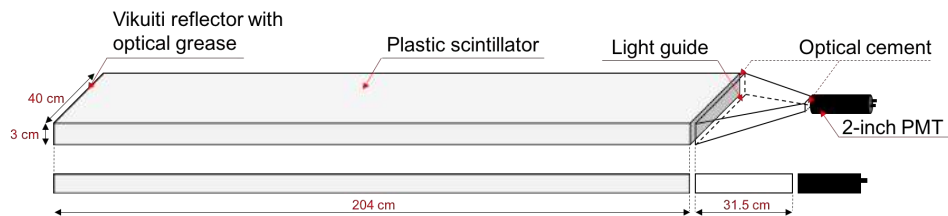


Figure III.7: Schematic view of a right or left muon panel with assembly parts.

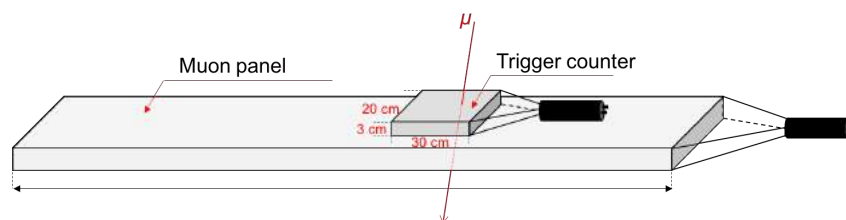


Figure III.8: Experimental setup to test the performance of the muon panels.

Table III.3: Plastic scintillator panels in the muon detector for the COSINE-100 experiment.

| Position | Length (cm) | Width (cm) | Thickness (cm) | Panels | PMTs |
|----------|-------------|------------|----------------|--------|------|
| Top | 282 | 40 | 3 | 5 | 2 |
| Front | 205 | 40 | 3 | 5 | 1 |
| | 207 | 33 | 3 | 2 | 1 |
| Back | 202 | 40 | 3 | 5 | 1 |
| | 202 | 33 | 3 | 2 | 1 |
| Right | 204 | 40 | 3 | 5 | 1 |
| Left | 204 | 40 | 3 | 5 | 1 |
| Bottom | 207 | 33 | 3 | 6 | 1 |
| | 205 | 40 | 3 | 2 | 1 |

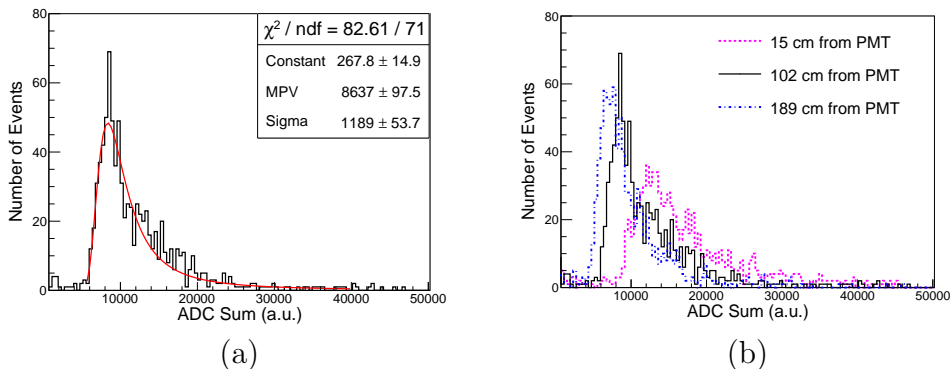


Figure III.9: (a) Muon candidate events selected by the trigger counter and modeled by a Landau distribution. (b) Position-dependent charge distributions from three different trigger positions for a 204 cm long muon panel.

The most probable value (MPV) of a Landau function fit to the distribution is used to estimate the relative light collection efficiency of each panel from muons and found to be approximately 250 photoelectrons with 20% panel to panel deviations. To study the position dependence of the light collection, the trigger counter was placed in three different positions: 15 cm (the closest), 102 cm (center), and 189 cm (the farthest) from the PMT. As shown in Fig. III.9 (b), the light collection strongly depends on the distance between the muon hit and the PMT; the maximum difference in the light collection was 45%. Nonetheless, muon candidate events far from the PMT were well separated from background events. The muon selection threshold for each panel is determined from the data accumulated at the lowest light yield location.

To estimate the muon detection efficiency as well as measure the muon flux, four panels were stacked as shown in Fig. III.10. A trigger for muon candidate events requires coincident signal in top (channel 1)–bottom (channel 2)

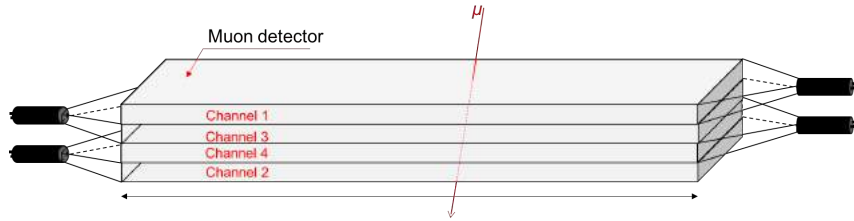


Figure III.10: Schematic view of the muon tagging efficiency setup.

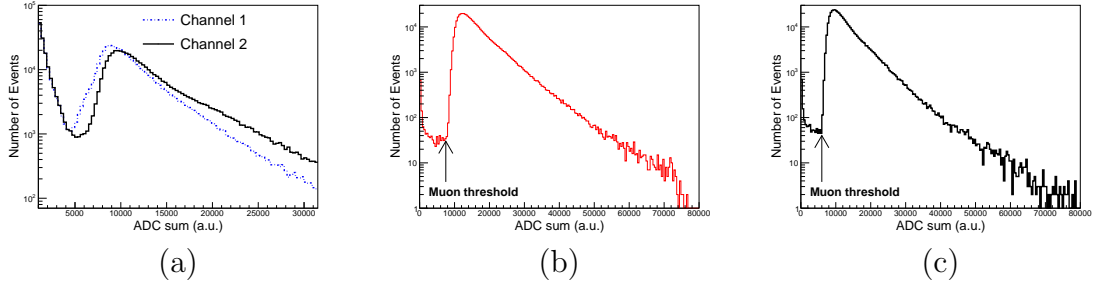


Figure III.11: (a) Charge distributions of the two trigger panels in the setup of Fig. III.10. Charge distributions of channel 3 (b) and channel 4 (c) after applying muon selection requirements for channel 1 (>4800) and channel 2 (>5400).

pair. When the trigger condition is satisfied, data are recorded from all four channels. If muons are passing through the top–bottom pair, these muons should also pass the middle two panels. An offline selection signal threshold for muon candidates is applied for the top and bottom panels to remove the environmental γ - or β -induced backgrounds as shown in Fig. III.11 (a). The charge distributions of the middle two panels after the offline selection cuts to the top and bottom panels are shown in Figs. III.11 (b) and III.11 (c). A total of 425,824 events are selected as muon candidates from the top–bottom pairs. From this result, muon detection efficiency for the muon panels is measured approximately to be 99.6%; the 0.4% loss could include a systematic uncertainty due to minor misalignments of the panels. Muon candidate events selected by coincident signals from the two middle panels are used to estimate the muon flux at the ground laboratory, which is 136 ± 7 muons/m²/s.

III.3 Data Acquisition System (DAQ)

The COSINE-100 data acquisition system incorporate with 8 Flash Analog-to-Digital Converter (FADC) modules, 2 charge-sensitive flash-analog-to-digital converter (M64ADC) modules, 1 Trigger and Clock Board (TCB), 4 pre-amplifiers, a High Voltage (HV) supply system, and Linux machines. Liquid

scintillator signals are connected to M64ADC modules amplifying by a factor of 30, while the plastic scintillator signals are directly connected to M64ADCs without any amplification. Eight crystals have 16 PMTs, two readouts each, a high-gain signal from the anode and a low-gain signal from the 5th stage dynode, collected by FADC modules.

The anode signal is amplified by a factor of 30 and the dynode signal is amplified by a factor of 100. The DAQ system consists of total 92 signal channels accounting two readouts per PMT from the crystals, 42 channels from the plastic scintillator veto, and 18 readouts from the liquid scintillator veto system to record the signals from each detector components. The global trigger decisions are made by the TCB, which also synchronized the times of all modules, the raw data is stored at DAQ computer in ROOT format. Fig. III.12 summarizes the overall data flow of the COSINE-100 experiment.

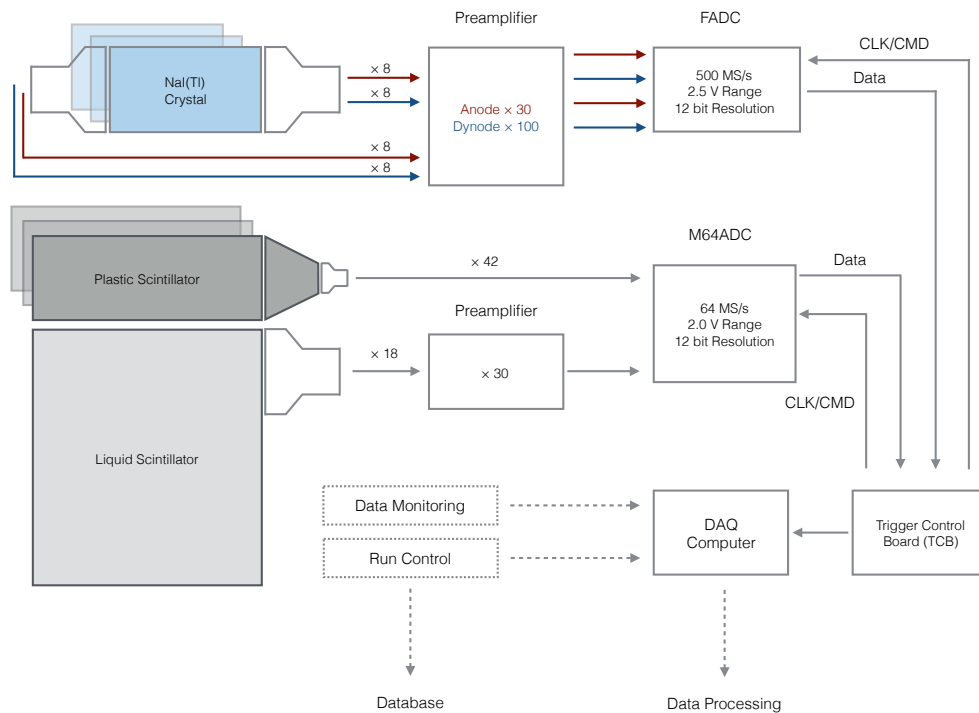


Figure III.12: The COSINE-100 data flow diagram. A total of 92 channels send signals to two types of digitizers, controlled by a trigger control board. Current DAQ setup consists of total of 32 FADC channels and 60 M64ADC channels. InfluxDB and Grafana are used for storing and visualizing the data (Adhikari *et al.*, 2018).

III.3.1 Charge-Sensitive M64ADC

Two charge-sensitive M64ADC modules with a 64 MS/s sampling rate are used to collect data from the active LS veto and the plastic scintillator muon veto. Each M64ADC module has 32 channels and $2 V_{pp}$ of input dynamic range with 12-bit resolution for each channel. 18 PMTs from the LS and 42 from the PS, a total of 60 PMTs, are connected to the modules with BNC-type input connectors. Signals from LS veto detector are amplified by a factor of 30 for higher gain and lower trigger threshold, where signals from plastic scintillator muon panels are not amplified and directly connected to M64ADCs. The local trigger report from the ADC modules passed to TCB for a global trigger decision, and the final data is transferred by USB3 to the DAQ computer.

The charge-sensitive M64ADCs return the integrated charge by integrating the input signal according to a preset Field Programmable Gate Arrays (FPGA) setting without saving raw waveform of the data. In an every 16 ns the analogue signal input to the M64ADC is digitized and when the FPGA receives a trigger it adds the digitized signal within the following 192 ns, returning a charge sum in ADC counts. In order to capture the whole signal, an internal trigger crossing defines the window start with the integration width of 192 ns for all the M64ADC modules which is longer than the decay time of the plastic scintillator (~ 12 ns) and the LAB-based organic scintillator (~ 4 ns for fast component and ~ 18 ns for slow component).

Integrated charge trigger threshold has been set to 4,000 ADC counts (equivalent to approximately 125 pC) to select muon events by removing γ background events coming from outside the panels, whereas the integrated charge of most of muon-like events is larger than 12,000 ADC counts (15,000 ADC counts for the top panels) (Prihtiadi *et al.*, 2018). In the top panels two PMTs attached instead of one, either one of two PMTs need to have the integrated charge more than 4,000 ADC counts to be triggered. If a muon passes through the detector, it will deposit energy in at least two different muon detector panels, and the LS Veto as well depending on the muon path. If a muon stops inside the LS, it will deposit energy in a single muon detector panel and the LS veto. Therefore, we require coincidence of at least two PMTs (which cannot be from the same top muon panel) to tag both cases: at least two muon detector PMTs or at least one muon detector PMT and one LS veto PMT each. When the integrated charge of a single channel is larger than the preset threshold, a coincidence window with a 400 ns width is opened. If any other channel triggers within the coincidence window, the M64ADCs sends a

trigger signal to the TCB. When the TCB sends a signal to the FADCs and M64ADCs to save an event, the M64ADCs open a $4 \mu\text{s}$ gate window, with the end of the TCB time in the middle of the window. Within the gate window the M64ADC searches and saves the maximum integrated charge values and their corresponding times for all channels.

III.3.2 Flash Analog-to-Digital Converter

To digitize analogue signals of NaI(Tl) crystal events eight 500MS/s FADC modules are used. Each FADC has 4 channels with SMA type input connectors, each channel having a dynamic range of 2.5 V and a 12-bit resolution. Different algorithms are installed in a FPGA within the FADC to determine self and local trigger for each module. As discussed in previous sections, COSINE-100 has one 3-inch PMT at each end of individual crystals and each PMT has two output channels, namely an anode channel for low energy with high gain and a dynode channel for high energy with low gain. The anode signal is sensitive to the level of single-photoelectron and is used for the dark matter search analysis.

For the understanding of alpha background and other high energy gamma/beta events analysis, dynode recorded signal from the 5th dynode of the PMT were used. PMT base structure was modified to extract both anode and the 5th dynode signals and connected to separate FADC channels. The signal from anode is amplified by 30 to increase gain and achieving a linear response for energies up to 100keV using a preamplifier but the signal from 5th dynode is relatively small so a factor of 100 preamplifier is used in dynode readout to achieve linear energy response up to 3 MeV.

If there is a coincidence of high-gain anode signal larger than the preset threshold (6mV, equivalent of 10 ADC counts or 0.2 photoelectron) within a time window of 200 ns between the two PMTs in crystal, then only waveforms from each of the two PMTs are recorded. The FADC module generates a trigger output signal if and only if both PMTs are triggered within the time window, as determined by the anode signal. The dynode signals are recorded when a global trigger is issued by the TCB, only when anode channels pass a 10 ADC counts trigger threshold, so they record a data as a passive trigger. If any one of the eight crystals matches the coincidence condition, then a trigger signal is transferred to the TCB and the FADCs save the waveforms of all the channels. The recorded waveform is $8 \mu\text{s}$ long, starting approximately $2.4 \mu\text{s}$ before the trigger occurs. The pre-trigger information is stored in DRAM on

the FADC board, which can store a waveform with up to 64 μs length. For FADCs, if each anode channel of PMT does not have any trigger generated and have only baselines, the contents of waveforms for the both anode and dynode channels are suppressed to zero. This zero suppression algorithm is critical to reduce the data size, as when DAQ is triggered only one or two crystals have signals and all other channels are recording baseline data. With the zero suppression, the data size can be reduced by $\sim 80\%$.

The signal region before the trigger occur, in our case starting to 2 μs is called pedestal, and which is useful for the calibration of baseline, estimation of dark count rate and also for the event reconstruction, this will be explained in chapter 4.

III.3.3 High Voltage Supply Mode

CAEN high voltage supply modules are used to supply high voltage to PMTs. 8 CAEN A1535N HV supplies with two 24-channel and six 12-channel modules, which are all installed at a CAEN VME4527 VME crate were used. All modules can supply voltages up to 3.5 kV with negative polarity, sufficient for all the PMTs used in the COSINE-100 detectors as the highest magnitude of the voltage applied does not exceed 2500 V after the PMT gain correction. High voltage scan was performed for all the channels prior to the physics run, followed by gain matching and light yield measurement. All the HV modules' SHV connector points are wrapped with bare ground cables to reduce noise, just like the pre-amplifier. A photo of High Voltage Supply Module is shown in Fig. III.13.

III.4 Slow Monitoring System

For stable data-taking and systematic analyses of seasonal variations. It is important to monitor continuously environmental parameters such as detector temperatures, high voltage variations, humidities, etc. We have developed slow monitoring system for specific monitoring purposes but all the monitors are controlled by a common database server and visualization program.

Temperature: To monitor temperatures at various positions, we used an 8-channel thermocouple data logger, TC-08, from Pico Technology. Eight K-type thermocouples are connected to the data logger. Three sensors are installed inside the Copper chamber and are placed in contact with the liquid scintillator. The room and outside-tunnel temperatures are also measured continuously. Test of thermocouples before the installation is shown in Fig. III.14.

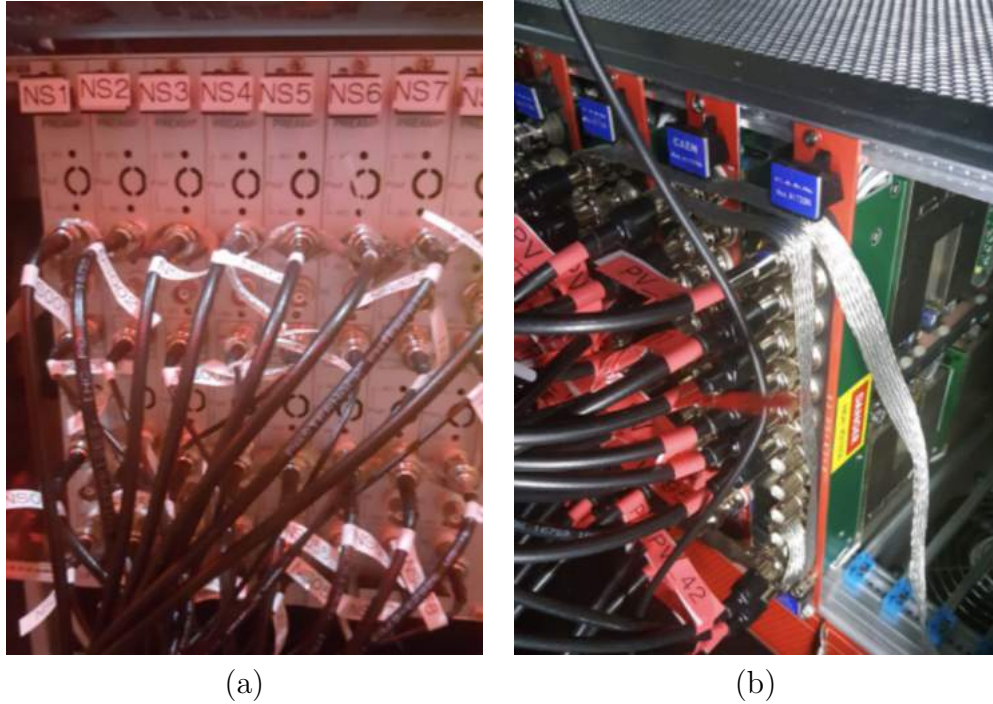


Figure III.13: (a) Series of preamplifiers connected in COSINE-100 station. (b) CAEN high voltage supply module.

High voltage equipments: The CAEN HV crate is monitorized with a wrapper provided by the Company. All of the supplied HV, currents, and status are monitored every minute.

Relative Humidity: Three MM2001 analog sensors, manufactured by Maxdetect are used to measure the relative humidity. The humidity sensors are connected to the slow monitoring server via a Labjack U3 DAQ module and also use a U3 DAQ module to monitor the applied low voltage for the preamplifiers. Three Labjack analog inputs for the amplifiers and three analog inputs for the humidity sensors are assigned.

Oxygen level: Oxygen level of the detector room is monitored with a Lutron O2H-9903SD device that contains an RS-232 port for serial communication. For safety purposes, oxygen level data are displayed in the front of detector room.

Air conditioning: Korea Air Conditioning Technology provides a communication protocol based on RS-485 and Modbus to monitor the status of the air conditioner. We convert the RS-485 signal to USB for continuous monitoring. The air conditioner data include the status of the equipment, the temperature and humidity, and various alarms.

Electricity: The monitoring equipment is protected by a 80 KVA on-



Figure III.14: (a) Test of temperature sensor thermocouples before installation. (b) Various environmental control system shown in COSINE-100.

line UPS. The UPS, manufactured by Ewha Electronics, has a network-based monitoring module that provides various protocols. Slow monitoring system checks its status in every 5 seconds via a Simple Network Management Protocol (SNMP) that monitors input and output voltages as well as various event logs.

Radon Detection: One RAD7 from Durrige Company is installed for regular monitoring of the Radon level in the detector room. The Radon level is measured every 30 min, and the data are sent to the slow monitoring server.

III.4.1 Software architecture

Monitoring system consists of simple programs and these monitoring programs communicate each other using standardized protocols and data format in order not to depend on a particular platform or database. The monitoring system is based on publish-subscribe messaging. A publisher program collects metrics from sensors and then publish the metrics to one or more subscribers. A subscriber program stores or analyze collected messages. The monitoring messages are published and subscribed via AMQP or MQTT protocol. These protocols can send not only a message body but also a routing key or topic. We use the key to distinguish monitoring programs. The monitoring message data format is JSON. We follow InfluxDB data structure.

The message contains measurement name, tags, fields. Measurement name is a string data like an "air-conditioner". Tags and fields are a list of key-values. Tags is not always required however it is necessary to distinguish sensor locations, computers. Fields are metric names and values of a sensor. E.g. temperature, humidity, memory usage, etc. We use RabbitMQ as a message

broker. Every monitoring programs are connected to message broker. Each region in underground laboratory has a RabbitMQ server that is responsible for the area. These underground RabbitMQ servers send their messages to another RabbitMQ server in ground using a federation plugin. The federation is a loosely coupled method but it is more robust for unstable network connection than a clustering. And we have several experimental groups in a same region, each of which requires an independent message broker for security. So we use the virtual hosting of RabbitMQ to provide the broker for each experiment group. Metrics data are stored into two InfluxDB servers. One is local database server, the other one is located in AWS Seoul region. Because the duplicated database is located outside the lab, researcher can monitor the lab even if we lose connection to the lab completely. And the server in AWS provides a visualization service using Grafana.

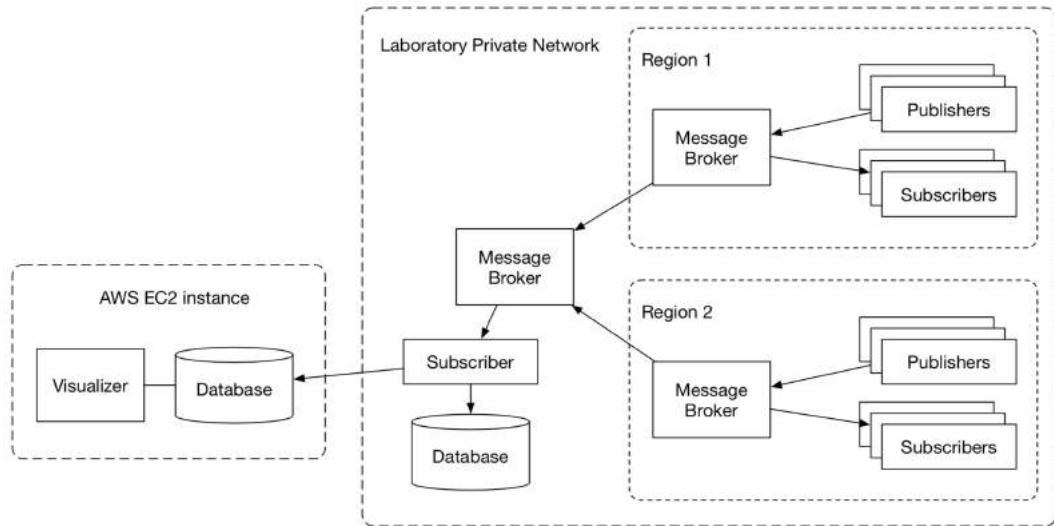


Figure III.15: Software architecture of slow monitoring.

III.4.2 Alarms

An alarm server requests or responses messages via HTTP. The server program isolates from the monitoring system so that it can operate even if the monitoring system fails. We have chosen HTTP based API to take advantage of its ecosystem. The alarm servers store received messages and analyze emergency status. These informations are shared by database server. Alarm alert programs watch changes of status informations. The programs send email or SMS to people or control sirens and lamps in underground laboratory. The system

can be separated external and internal alarm system. External alarm system means email, SMS, messengers for people outside the underground. Internal alarm system are lamps, sirens in the underground.

III.4.3 Data Quality Monitoring

The COSINE-100 experiment has established an online data monitoring system with a dedicated web server to monitor the data quality. The raw data are converted to a ROOT format and saved in the DAQ computer every 2 hours and the data is processed to extract monitoring variables. The monitoring system displays 26 variables for FADC (1 for total trigger rate, 8 for crystal's data analysis variables, and 17 for PMTs variables) and 6 for M64ADC (1 for total trigger rate, 2 for plastic scintillator PMTs, and 3 for liquid scintillator PMTs). All the variable plots are overlaid with reference plots, with known good data quality, to highlight possible deviation of the monitoring variables. The reference plot is frequently updated to account for time variation of the variables. Fig. III.16 shows example plots of one of the monitoring variables, low energy spectrum with basic noise event removal, details of noise removal will be explained in Chapter 3. Blue line indicates the data from the 2-hour-long subrun file where red lines represents the reference plots from a "good" subrun data. Any deviation from the reference plot will be examined afterwards.

In order to monitor longer term data accumulation, total of 7 weekly monitoring plots are also generated automatically: Live-time, crystal's trigger rate, M64ADC trigger rate, LS total charge, LS charge asymmetry, and muon event rate. These plots help to identify any long term trends in data, such as gradual and slow increase in event rate is shown in Fig. III.17.

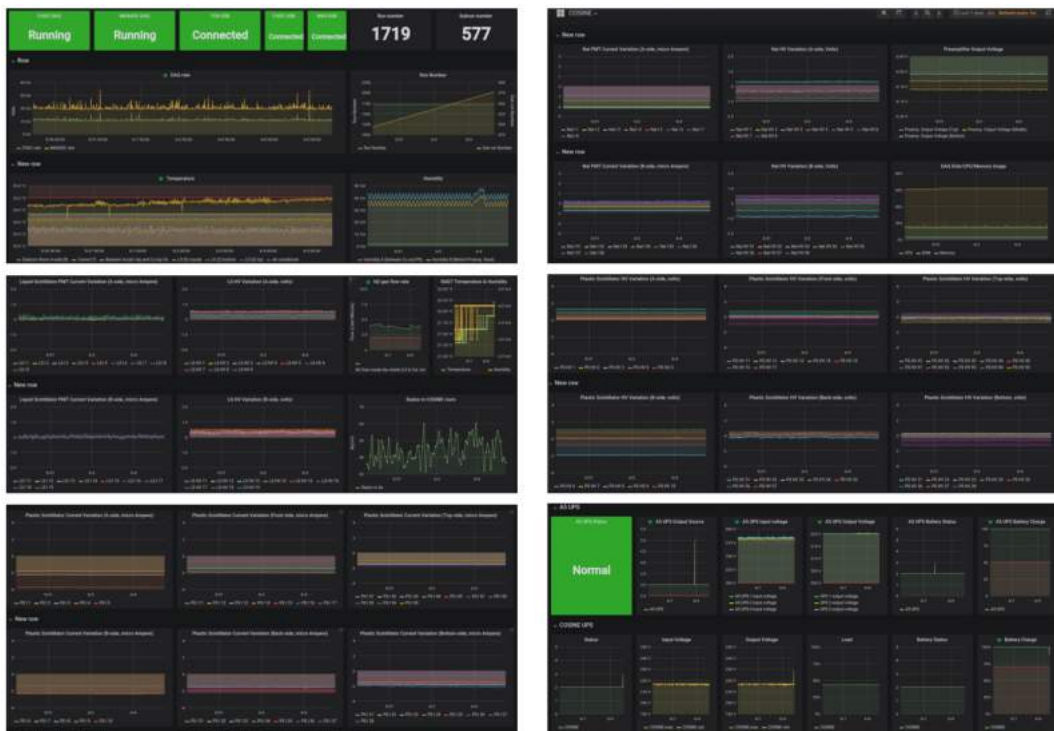


Figure III.16: Grafana-generated monitoring dashboard. Various monitoring parameters are displayed.

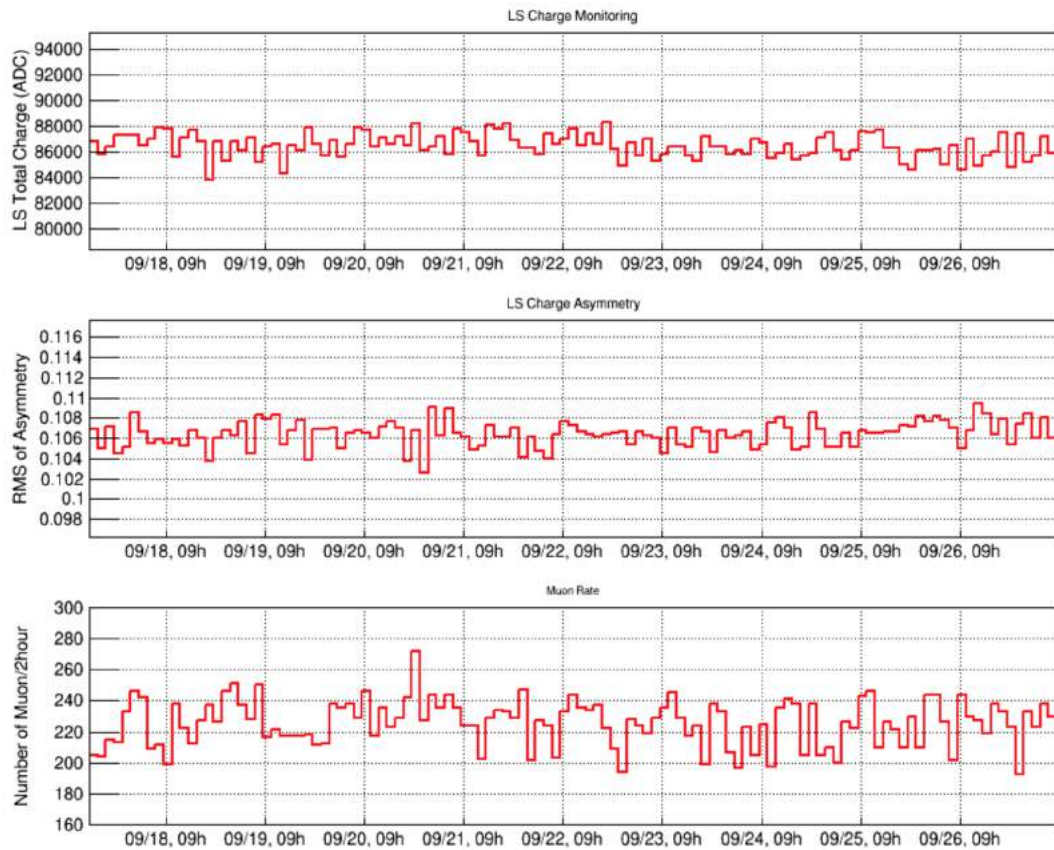


Figure III.17: Example plots from the weekly data monitoring. Three plots from M64ADC data are shown here, the LS total charge, the LS charge asymmetry, and the muon rate.

Chapter IV Muon Analysis of COSINE-100 Experiment

In this chapter, the first analysis of data taken with the COSINE muon detector will be presented. The analysis way is accomplished with analysis framework ROOT. CERN developed the framework for data processing, nowadays many experiments in particle physics field and most current experimental plots and results in those subfields are obtained using ROOT. The DAQ collects the data and saves in root format, although an offline analysis is still required in order to understand a physics analysis result. The data, which are analyzed here, were taken during the period from 23rd of September 2016 to 31th of December 2018.

IV.1 Muons at COSINE-100

After the ground laboratory measurement, the muon panels were subsequently installed in the COSINE-100 room at Y2L as an active muon shield. The entire array of 37 panels surrounds the detector with a full 4π solid angle coverage. The general layout of the COSINE-100 muon detector and a photograph of the installed detector are shown in Fig. IV.1.

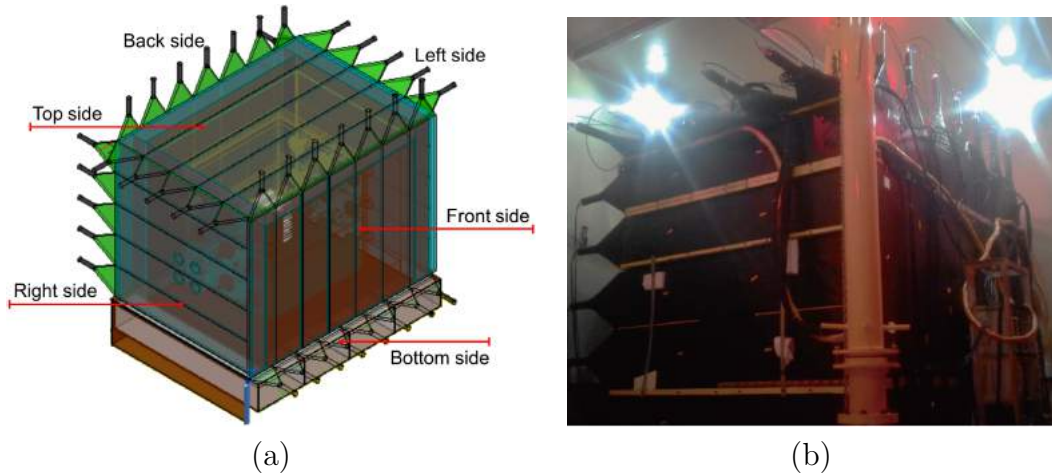


Figure IV.1: (a) Schematic of the COSINE-100 shielding structure, (b) Photograph of the installed muon detector captured from the corner between the front and the right side.

Muon fluxes in underground laboratories show significantly reduced rates (Hime *et al.*, 2006). Because the surviving muons at deep underground places still have high energies, most of the muons penetrate through all of the detector materials while leaving relatively large energy depositions. Energetic muons

should deposit energies that are greater than the minimum ionization energy, which is approximately 6 MeV for a 3-cm-thick plastic scintillator (Nakamura *et al.*, 2010) and is much larger than the typical γ or β -energies produced by environmental background components. In addition, because the muon detector provides 4π coverage of the COSINE-100 detector, muon signals can be observed in at least two sides of the detector. Therefore, muon candidate events can be selected according to their energy deposits and coincidence requirements.

A total of 42 PMT signals are digitized by charge-sensitive 62.5 Megasamples per second (MS/s) ADCs from Notice Korea that are called SADC¹. One SADC module contains 32 channels with field-programmable gate arrays for signal processing and trigger generation. The dynamic range is 2 V with 12-bit resolution and two modules are dedicated for muon detection. The SADC continuously calculates the integrated charges using a 192 ns integration time window with 16 ns time bin. The trigger thresholds are set to be approximately one-third of the typical muon selection threshold. At least two PMTs from independent panels should exceed the trigger threshold at 4000 ADC within a 400 ns coincident time window. If this trigger condition is satisfied, each SADC channel records the maximum value of the 192 ns integrated charges and its time position within a 4 μ s search window (a range of approximately -2 to 2 μ s from the trigger position). Information for the six sides is calculated by combining the information of the panels constituting each side. The charges of all panels from one side are added for a given side, but the timing is selected from the one which has the maximum charge.

The first monitoring parameter naturally is the event rate. Fig. IV.2 is shown for M64 trigger rate for ~ 41 days accumulated data since September 2016. It shows the trigger rate is about 30Hz. There is a very sharp event rate in some moments due to high energy muons that give a phosphorescence events in crystal. The highest energy muon events induce long-lived phosphorescence in crystal events and produces a thousand events in low energy crystals.

IV.2 Muon Selection Procedure

The goal is to develop a procedure that will identify muons which passed all of detector components in COSINE-100. The deposit of muons can be selected by applying a selection criteria to obtain the muon-like events. The ADC sum refers to energy equivalent of events that digitized from DAQ. Above of

¹<http://www.noticekorea.com>

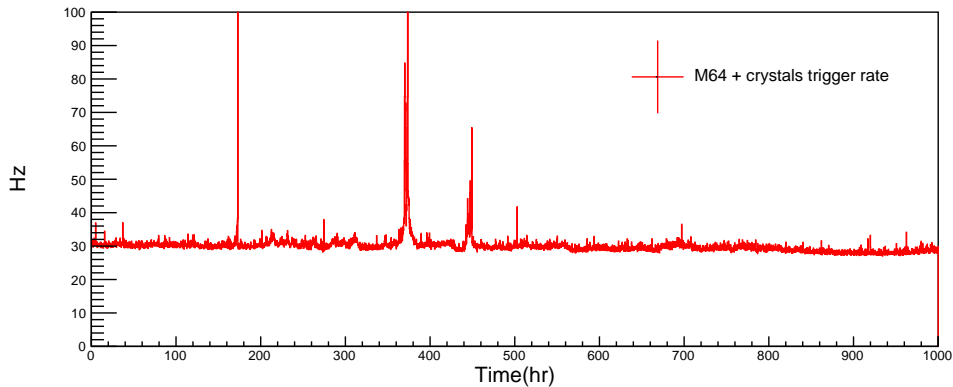


Figure IV.2: M64 Trigger rates versus time (in h) for the first physics run (~ 41 days). All of the crystals show stable behaviour throughout this running period and the rest of data-taking.

a certain value is used for considering as muon-like events. The DAQ has set a trigger condition for muon detector and liquid scintillator to record events which has ADC sum larger than 4,000 ADC. This condition is significantly reduced and suppressed the dominant background of γ -like events. It is also has advantage in reducing the data capacity of raw-data. Therefore, this method is strongly dependent on the fit onset, which is critical for the fit to coverage and to especially obtain the acceptable of muon. For these reasons, an improved method to extract the threshold information for muon identification was developed. Here is only the highest sum signals, i.e. $\text{sum} \geq 4,000$ ADC counts were selected.

IV.2.1 Methods of μ -threshold determination

We used a technique that commonly used in nuclear and particle physics which called coincidence method. This basic technique will search if the two signals are, in fact, "coincident", then this is counted as single events from the same particle. A coincidence analysis is pervasive technique and to use for estimating the closest events between at least two panels in coincidence window. This method can determine the region for perspective part of spectrum, which is either region for low energy background or high energy of muons as shown

In Fig. IV.3, a 2D plot is shown, with the signal in the top-side on the y-axis and the signal in the bottom-side on the x-axis. One can clearly see signals in both layers, and two groups of signals along the axes, meaning almost no signal in one of the layers. In between, there is a gap. This gap can be used to cut on "real" coincidences. An easy cut would be to ask form a sum

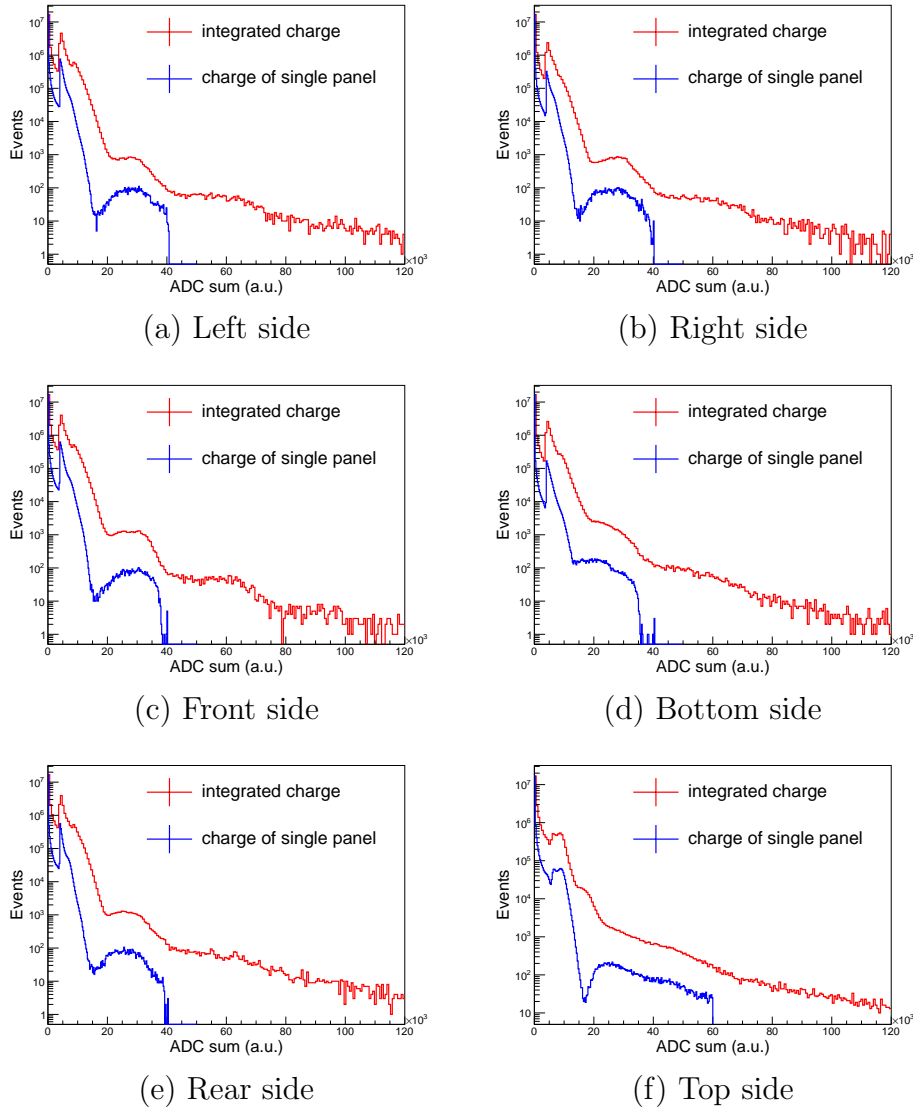


Table IV.1: Solid red color shows integrated charge of side. Solid blue color shows charge distribution of single panel

of top and bottom higher than a threshold. The threshold must be selected in a way that rejects as much as noise as possible. A threshold cut of each side is needed, which would cause a horizontal and a vertical lines. This can remove low energy background and it will remain muon-like events in high energy region. By applying these requirements, most of non-muon events or backgrounds are rejected. The threshold is set to each side, with coincidence between an integrated sum of each side.

In Fig. IV.4, the total charge of the top side (i.e. the projection to the y-axis of Fig. IV.3) is shown. Without applying a cut, one gets a huge amount of low light events. This may be electrons or γ 's coming from the surrounding rock.

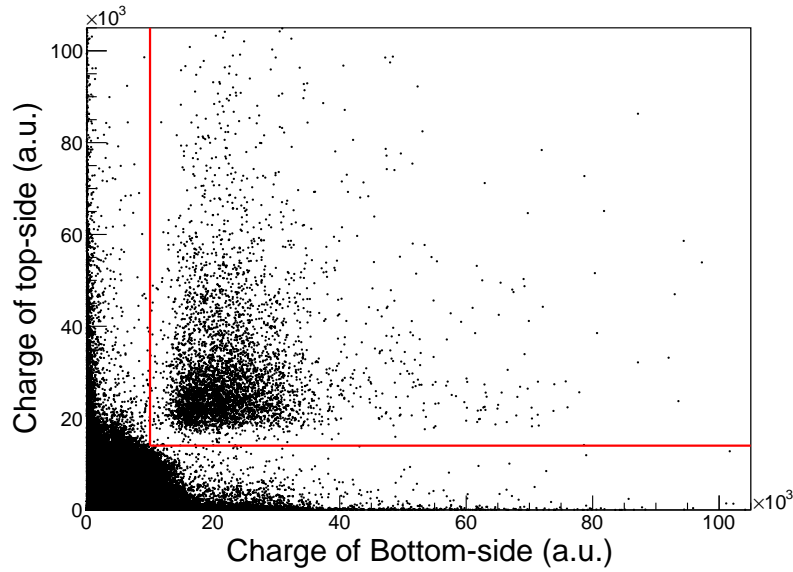


Figure IV.3: A scatter-plot of the signal distributions for top- and bottom-side coincident events. The red lines represent the selection criteria for muon candidate events. This method exclusive AND: each signal has to pass its panel threshold independently. An integrated charged is used to define the total charge of side detector.

If one applies the product cut, the muon peak survives the cut almost without a change. This cut can now be applied to select muons which are traversing plastic veto and Cherenkov veto while histogramming the multiplicity of the Cherenkov PMTs.

The maximum of the Landau distribution defines the most probable value (mpv), where the maximum of the muon distribution is expected. Therefore more muon safe threshold is defined here in view of the focus on muon identification. Selecting the muon-like events, a Landau distribution can be used for determining an approximate minimum between the low energy slope and the muon peak energy. Therefore, applying cut threshold is slightly chosen the muon candidate events at drop or baseline corrections at least 14,000 in ADC units. The summary of charge threshold of each panel is shown in Table IV.2. Fig IV.5 is shows the integrated charged of top-side detector after digitized from DAQ. Also, an integrated time is the time information when a PMT has fired at the highest charge information.

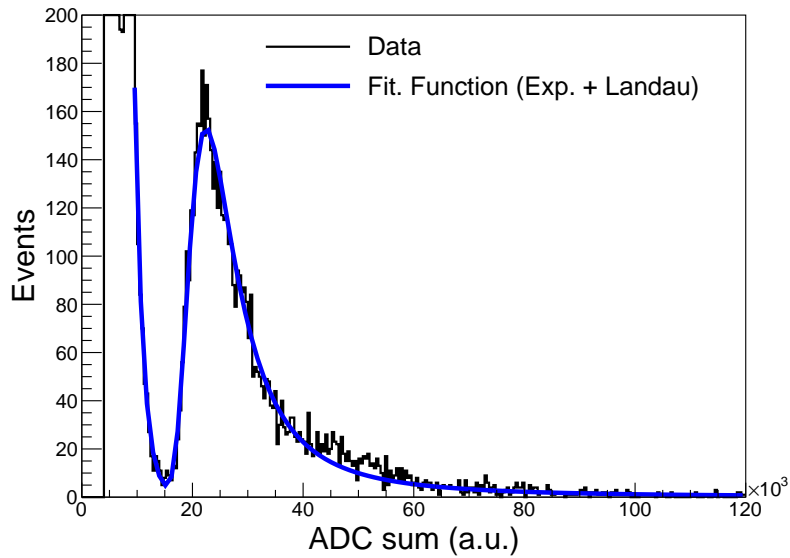


Figure IV.4: In black: all events after coincident with bottom-side, in blue: events after combined fit exponential and Landau distribution. An exponential function for the remaining background and a Landau distribution for the muons assumed. A peak at about $\sim 26,000$ ADC sum is muon peak.

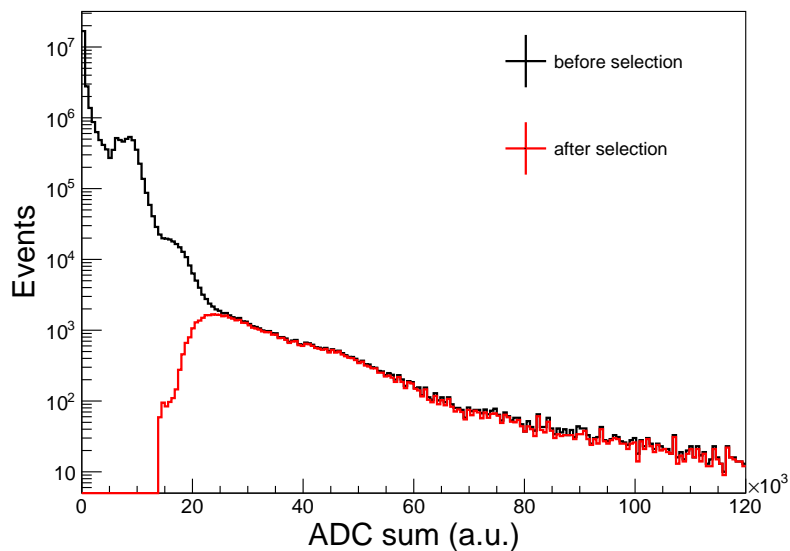


Figure IV.5: In black: all events after integrated of 10 PMTs of top panel. Red is after applying a threshold greater than 14,000 ADC units. Assuming above 14,000 ADC units are muon-like events.

Table IV.2: Charge threshold for each side of muon detector and Liquid Scintillator

| Side Detector | Threshold Value (in ADC units) |
|---------------|--------------------------------|
| Left Side | 12,600 |
| Right Side | 12,000 |
| Front Side | 10,000 |
| Bottom Side | 10,000 |
| Rear Side | 12,000 |
| Top Side | 14,000 |
| LS Veto | 431,400 (3MeV) |

IV.2.2 Time Different Cut

As an example, a scatter plot from the top and bottom sides is shown in Fig. IV.3. The time differences (ΔT) between the bottom-side and top-side signals are shown in Fig. IV.6 (b), where muon candidate events exhibit a clear coincidence, while the γ/β background events have a random distribution as shown in Fig. IV.6 (a). On the basis of the time correlation observed for the muon candidate events, an additional selection criterion of ΔT is applied containing a 5σ range of signal events, in this example -100 ns ΔT 115 ns as shown in Fig. IV.6 (b).

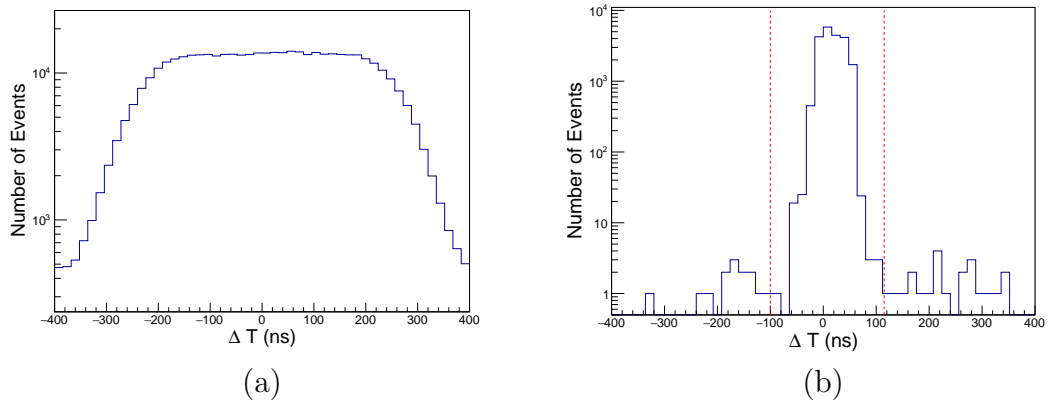


Figure IV.6: (a) Time differences (ΔT) between top-side and bottom-side hits for non-muon candidate events and (b) muon candidate events.

Using the ΔT distribution of the signal events, the background contamination in the signal region can be estimated. The number of events outside the signal region (-200 ns $< \Delta T < -100$ ns or 115 ns $< \Delta T < 215$ ns) is counted in Fig. IV.6 (b). Considering the background distribution in Fig. IV.6 (a), the background contamination in the signal region is calculated to be 0.2%.

The muon coincident signal is shown in Fig. IV.6, a Δt distribution of

coincidence events of Top and Bottom side. In contrast, muon-like events show a much more confined in distribution of time-differences within the gap of signal is 16ns time resolution in M64ADC DAQ. The signal distribution is well performed by Gaussian fitting and selecting signal region by statistical significance of 5σ . Here, we defined to signal region in range of -60ns up to 80ns region for muon-like events. Due to the different length signal cable, we applied the global timing cut in our selection criteria in range -115ns up to 115ns. In this distribution, an accidental background coincidence are occurred in low energy region. It also possible, the signal region has accidental background that contributed in muon-like events. We called fake-event which is random coincidence in signal region. We counted the total random-events in outside of signal region and estimating the events/per-binsize in the signal region. On average, the fake-event is found to be 0.1% and can be neglected.

The muon selection criteria discussed above were applied to determine the charge distribution of the top-side panels. Here, the muon selection threshold for the top side is ignored to reveal the background shape as shown in Fig. IV.7. Muon candidate events are fitted with the expected signal shape, Landau distributions, together with an exponential background component. Because the muons induce spallation that makes multiple hits on the top-side, two Landau distributions are considered for signal modeling. From this fit, the background contribution in the signal region can be estimated as approximately 0.1%, which is consistent with the background contamination rate estimated with the ΔT distribution. Furthermore, the muon selection efficiency was estimated to be 99.9 ± 0.1 % when the charge threshold cuts mentioned previously are applied. A similar muon selection technique is applied for all pairs of different sides to tag muon candidate events.

IV.3 Observed Muon Rate at Y2L

The muon flux at the COSINE-100 experimental site is determined from all of two-side hit events including signals in the top-side panel array. A muon event with hits in more than two sides are also counted as a single muon event. To normalize the muon rate, the effective area of the top-side is calculated as $A_d = 5.48 \pm 0.16$ m², where the uncertainty reflects the area of the top-side panels that extend beyond the sides of the array and its muon tagging is not fully active. This uncertainty is expected to be reduced with simulation-based studies.

A total number of 144,325 muon candidate events (N_μ) were observed dur-

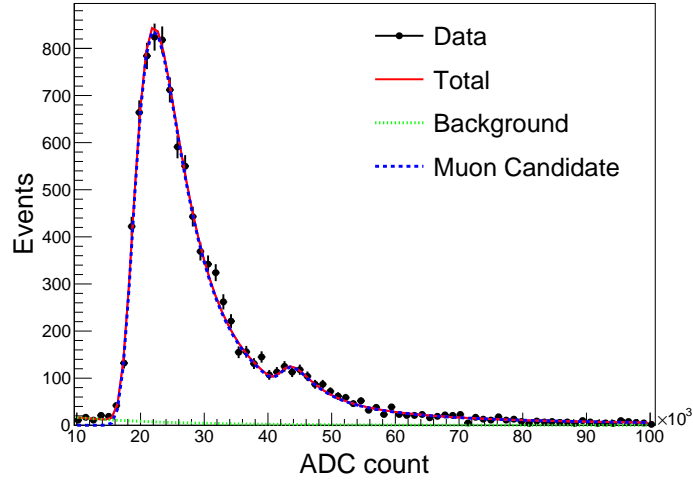


Figure IV.7: The charge spectrum of muon candidate events in the top-side panels with the charge threshold trigger requirement relaxed. An exponentially decaying background component and Landau-function shaped muon signal component is used to model the data. Here we consider two Landau functions to take into account events with two hits, visible by the second peak around 44×10^3 ADC counts. The fit results indicate that the normally required threshold for the top-side charge rejects a negligible number of signal muon events ($<0.1\%$).

ing a period of approximately three months. Because the non-muon contribution is negligible, the muon flux Φ_μ can be calculated as follows:

$$\Phi_\mu = \frac{N_\mu}{t_d \cdot A_d \cdot \epsilon_\mu}, \quad (\text{IV.1})$$

where ϵ_μ is the muon selection efficiency, and t_d is the total data acquisition time. This returns a measured muon flux at the COSINE-100 experimental site of $327.7 \pm 0.26_{\text{stat}} \pm 9.56_{\text{syst}}$ muons/m²/day, where the systematic uncertainty is dominated by the top-side area calculation. This is slightly higher than that at the KIMS experimental site (Zhu, *et al.*, 2003), which is consistent with an expectation based on the surface geometry of the Y2L and an approximately 200 m horizontal distance between two sides. This rate is approximately 2.8×10^{-5} times the muon rate of the ground laboratory measurement. The muon rates measured during a three-month period were very stable as shown in Fig. IV.8.

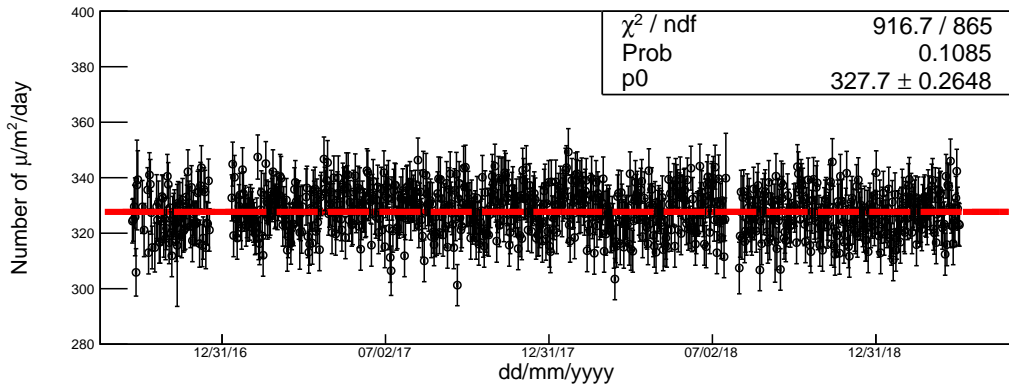


Figure IV.8: Measurement of the muon flux at the COSINE-100 detector over a 2 years and 3 months period.

IV.3.1 Muon in crystal-events

Muons are estimated to be 3,200 muons/day that tagged by muon detector. But, muon passing through the crystal detector are expected at a rate of tens of muons/day, deposit high energy in the crystal, and induce scintillation waveform with a pulse shape similar to that of gamma events. These characteristics combine to form the muon tag. Muons in crystal are identified by their waveform height and their characteristic pulse shape. When muon passed the crystal, it will deposit high energy in muon detector and liquid scintillator. Requirement of coincidence between three detectors can be used to select muon events.

Muons are separated from alphas using Pulse Shape Discrimination (PSD). Muons and gammas exhibit a similar pulse shape, while the alpha pulse shapes have a faster decay time. PSD allows the complete rejection of alphas from the muon event selection, with their PSD distributions characterized by non-overlapping normal distributions. In this study, the mean time (MT) weighted by the charge of the signal is used as a PSD parameter can be written as

$$MT = \frac{\sum A_i t_i}{\sum A_i} - t_0 \quad (\text{IV.2})$$

where A_i is charge of the i th cluster, t_i is the time of the i th cluster and t_0 is the time of the first cluster. Although the PMTs are nonlinear at high light output, alpha induced events inside the crystal can be identified by the mean time of the signal. Figure IV.9 shows a scatter plot of the energy versus mean time for events in the high energy region because of the faster decay times of alpha induced signals. Because of the nonlinearity of high energy signals,

alpha particles from different nuclides cannot be distinguished event by event by their measured energies. Here, alphas can be easily rejected by using mean time weighted selection.

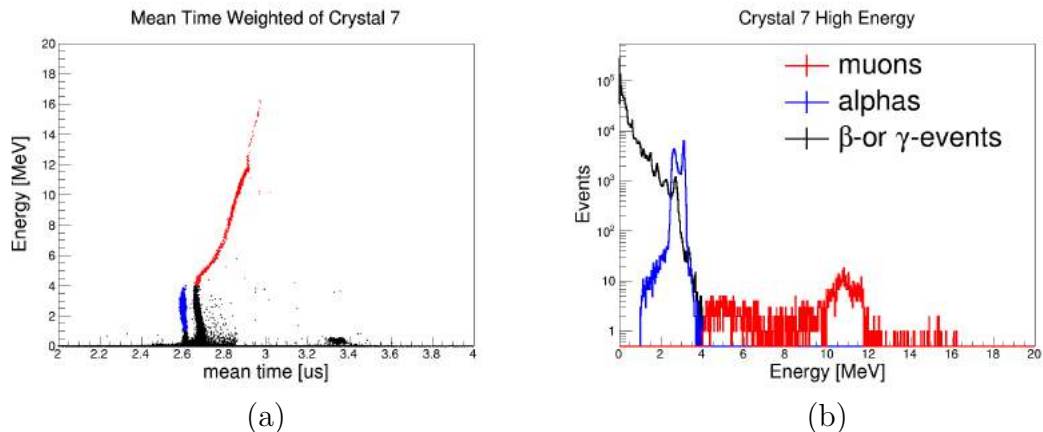


Figure IV.9: (a) Mean time distribution of high energy events. Left-blue island represents to alpha events while top-red island classified as muon events, (b) The energy spectrum of crystal 7 at high energy, with muons overlaid in red. Energy is defined as the integrated charge in the waveform

Muons energy depositions appear above 4 MeV in crystal 7, as shown in Fig. IV.9. Here, there is a nonlinearity in the high energy due to saturated the readout channel or the PMT. All energy spectra from PMTs are saturated over the muon region, rendering the gamma calibration meaningless in this regime. Since, the count of muons is more needed for understanding of phosphorescence after direct muons.

IV.3.2 DAQ Saturation and Deadtime

Cosmic ray muon can induce low energy phosphorescence events in the crystals and these events can mimic with WIMP signal with a confined modulation signature. One can see in Fig IV.10, there are large number of coincident events right after the muon events hit at the crystal. We have rejected all the events within 30 ms from a muon hit in plastic scintillator. We recorded about 125 muons per hour tagged in plastic scintillator, and it gives approximately 0.1 % deadtime in the detector. This of 30 ms muon veto rejection is used for event selection of crystal events to prevent large number of accidental phosphorescence-events induced by direct muons. Event selections for crystal events are not discussed in this report.

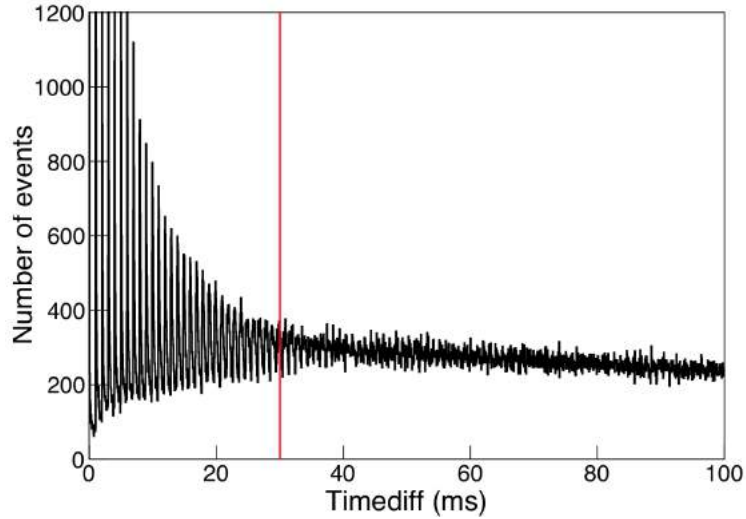


Figure IV.10: Time difference distribution between crystal trigger time and a muon signal from plastic scintillator. The events within 30 ms from a muon hit are removed in crystal event selections.

IV.4 Annual Modulation Analysis of Muon and Temperature

IV.4.1 Muon Modulation

Only muons with high energy (greater than energy threshold E_{thr}) can be detected by the COSINE-100 detector which is mostly from decay of charge pions (π^\pm), with a small fraction from the decay of kaons (K^\pm). Muons with the lowest energies are stopped during traverse before reaching the detectors. Variations of air temperature which is increase during summer and lowers the average gas density. The less dense medium allows a longer mean free path of the mesons and increases the fraction of mesons. The muon modulation observed with configuration of Top-Bottom side coincidence which considers the small of solid angle from incoming muons. This analysis is based on 2 years and 3 months of good physics data. The following formula is generally used to relate the muon intensity variations to the atmosphere temperature fluctuations (Gaisser, 2012 and Grashorn *et al.*, 2010):

$$I_\mu(t) = I_\mu^0 + \delta I_\mu \cos\left(\frac{2\pi}{T}(t - t_0)\right) \quad (\text{IV.3})$$

An average intensity of muons at Top-Bottom $I_\mu^{\text{Top-Bottom}}$ is about to be $550.92 \pm 0.87_{\text{stat.}} \times \text{day}^{-1}$ with fixed period (T) of 365.25 days. A modulation amplitude of $\delta I_\mu = 2.82 \pm 1.30 \times \text{day}^{-1}$, corresponding to $(0.51 \pm 0.24) \%$ and

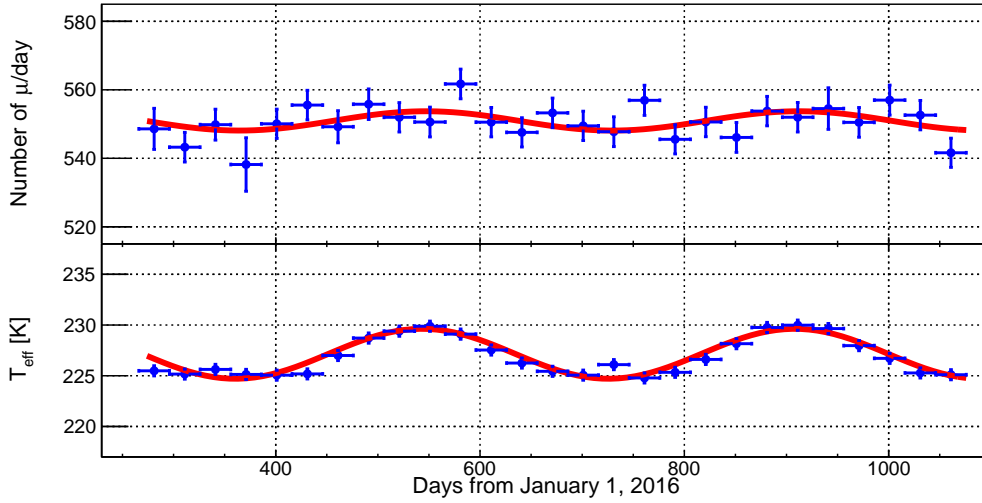


Figure IV.11: The data are shown in monthly bins. Upper plot: cosmic muon modulation observed by COSINE-100 as a function of time. Lower plot: effective temperature, T_{eff} , computed using eq. IV.5 and averaging over the four daily measurements. Monthly binning is used in both panels. The curves show the sinusoidal fit to the data.

a phase of $t_0 = (182 \pm 25)$ days, corresponding to a maximum on the 30th of June, the χ^2/NDF is 24.03/24.0.

IV.4.2 Atmospheric model and effective atmospheric temperature

The temperature data was obtained from the European Center for Medium-range Weather Forecasts (ECMWF) which exploits different types of observations (e.g. surface, satellite, and upper air sounding) at many locations around the planet, and uses a global atmospheric model to interpolate data. The location used: y2l. Atmospheric temperature is provided by the model at 37 discrete pressure levels in the [1-1000] hPa range ($1 \text{ hPa} = 1.019 \text{ g/cm}^2$, four times a day at 00.00 h, 06.00 h, 12.00 h, and 18.00 h²). Based on this data set, T_{eff} was calculated using eq. IV.5 four times a day. The four results were averaged, and the variance of the four values was used to estimate the uncertainty in the mean. E_{thr} is the minimum energy required for a muon to reach the considered underground site and θ is the angle between the muon and the vertical direction and $E_{\text{thr}} = 0.785 \pm 0.14 \text{ TeV}$ based on simulation, extracted from numerical methods assuming a flat overburden. An increase of the temperature results in a decrease of the air density and in a higher mean free path of (π^\pm and K^\pm), with an increase of single muon flux $\Delta I_\mu(t)$, related

²ECMWF ERA-interim daily data.

| Parameter | Value | Unit |
|----------------|-------------------------|-------------------|
| A_π^1 | 1 | – |
| A_K^1 | $0.38 \times r_{K/\pi}$ | – |
| $r_{K/\pi}$ | 0.149 ± 0.060 | – |
| B_π^1 | 1.460 ± 0.007 | – |
| B_K^1 | 1.740 ± 0.028 | – |
| ϵ_π | 114 ± 3 | GeV |
| ϵ_K | 851 ± 14 | GeV |
| γ | 1.7 ± 0.1 | – |
| Λ_N | 120 | g/cm ² |
| Λ_π | 180 | g/cm ² |
| Λ_K | 160 | g/cm ² |

Table IV.3: Input parameters with associated errors for the calculation of the atmospheric effective temperature T_{eff} .

to the temperature variation ΔT , given by:

$$\Delta I_\mu(t) = \int_0^\infty dX W(X) \Delta T(X, t) \quad (\text{IV.4})$$

where the integral extend over the atmospheric depth and $W(X)$ reflects the altitude dependence of the mesons production and their decays into muons that can be observed underground. The atmospheric can be described by many layers with a continuous distribution of temperature and pressure. A possible parametrization considers the atmosphere as an isothermal body with an effective temperature, T_{eff} , obtained from a weighted average over atmospheric depth:

$$T_{\text{eff}}(t) = \frac{\sum_{n=0}^N \Delta X_n T(X_n) (W_\pi(X_n) + W_K(X_n))}{\sum_{n=0}^N \Delta X_n (W_\pi(X_n) + W_K(X_n))} \quad (\text{IV.5})$$

where the approximation may be done considering that the temperature is measured at discrete atmospheric levels, X_n .

where ΔX_n is the difference between two adjunct pressure levels, $T(X_n)$ the corresponding temperature at X_n pressure level and $W_{\pi,K}$ the weighting functions of the contributions of pions and kaons to the altitude dependence of the muon production, given by the following expression:

$$W_{\pi,K}(X) \simeq \frac{(1 - X/\Lambda'_{\pi,K})^2 e^{-X/\Lambda_{\pi,K}} A_{\pi,K}^1}{\gamma + (\gamma + 1)B_{\pi,K}^1 K_{\pi,K}(X) (\langle E_{\text{thr}} \cos\theta \rangle / \epsilon_{\pi,K})^2} \quad (\text{IV.6})$$

where:

$$K_{\pi,K}(X) = \frac{(1 - X/\Lambda'_{\pi,K})^2}{(1 - e^{-X/\Lambda'_{\pi,K}})\Lambda'_{\pi,K}/X} \quad (\text{IV.7})$$

the approximation reflects the fact that the temperature is measured at discrete atmospheric levels X_n (not equally spaced).

In these equations $A_{\pi,K}^1$ includes the amount of inclusive meson production in the forward fragmentation region, masses of mesons and muons, and muon spectral index. $B_{\pi,K}^1$ corresponds to the relative atmospheric attenuation of mesons. The critical energies are given by $\epsilon_{\pi,K}$ while the muon spectral index is given by γ . Finally, Λ_N , Λ_π , and Λ_K represent the attenuation lengths for the cosmic ray primaries, pions, and kaons respectively. with $1/\Lambda'_{\pi,K} \equiv 1/\Lambda_N - 1/\Lambda_{\pi,K}$.

We may also define the effective temperature coefficient, α_T , which quantifies the correlation effect that is discussed in section.

$$\alpha_T = \frac{T_{\text{teff}}^0}{I_\mu^0} \int_0^\infty dX W(X) \quad (\text{IV.8})$$

such that eq. () may be written :

$$\frac{\Delta I_\mu}{I_\mu^0} = \alpha_T \frac{\Delta T_{\text{eff}}}{T_{\text{eff}}^0} \quad (\text{IV.9})$$

Figure IV.11 (lower panel) shows the monthly values of T_{eff} for the two year and three months period considered. A simple average gives $T_{\text{eff}}^0 = 220.99$ K, while the fit with a function to eq. return $T_{\text{eff}}^0 = (22.1 \pm 12)$ K.

IV.4.3 Correlation between muon and temperature

Figure shows the correlation between fluctuations in the atmosphere temperature and the cosmic muon flux.

We perform a linear regression accounting for error bars on both axes using a numerical minimization method. As a result we obtain $\alpha_T = 0.815 \pm 0.097_{\text{stat}}$

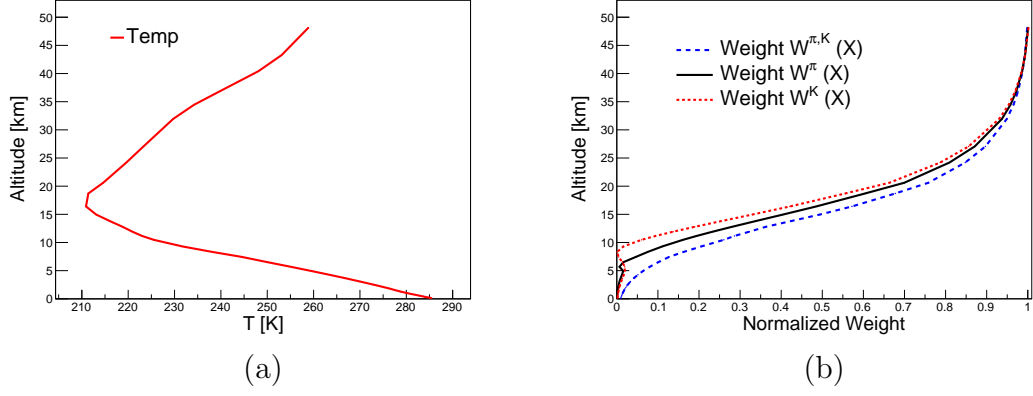


Figure IV.12: (a) an average temperature (solid red line), (b) normalized weight $W(X)$ (blue dashed line) as a function of pressure levels computed with pion (π) and kaon (K) contributions.

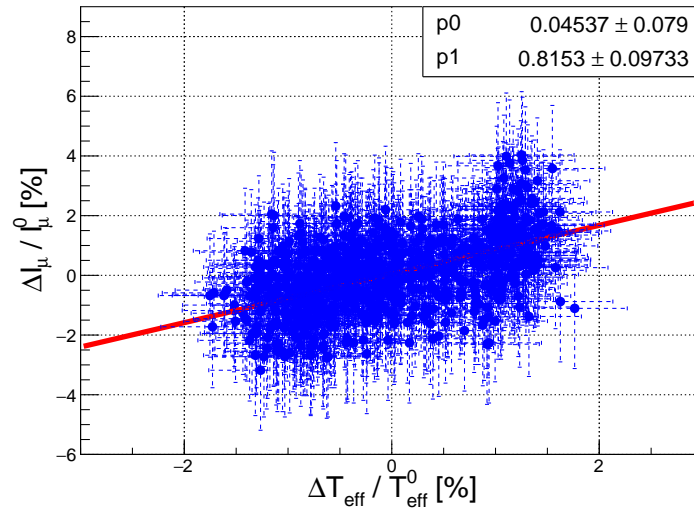


Figure IV.13: $\Delta I_{\mu} / I_{\mu}^0$ vs $\Delta T_{\text{eff}} / T_{\text{eff}}^0$ for each day in figure for a total of 774 days.

with $\chi^2/\text{NDF} = 1144/1164$. This result is consistent and features smaller errors when compared.

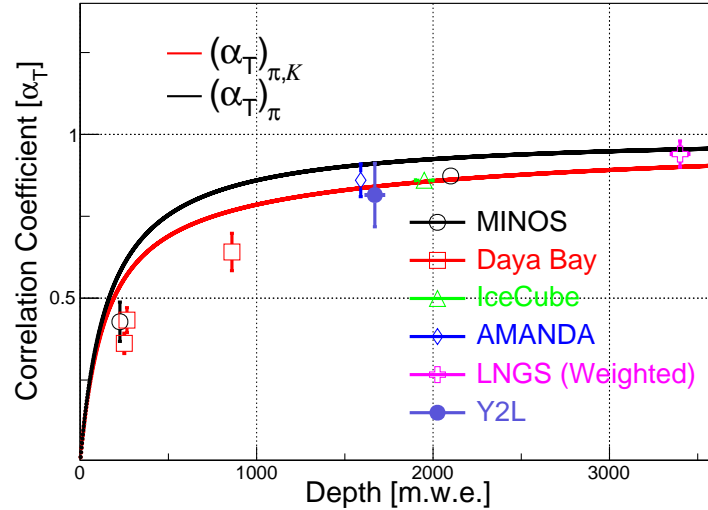


Figure IV.14: Measured values for the effective temperature coefficient, α_T , at varying site depths. The results from this analysis (in blue) as well as those from different experiments are presented. The red line is the value predicted including muon production by pions and kaons. The black line account for one production of pion (π) mechanism only.

Fig. IV.14 shows the measured value for α_T . This is because the air-density-independent contribution to the muon signal originating from mesons which have interacted before decaying in progressively left below threshold. At Y2L α_T is expected to be 0.815 ± 0.097 (considering muon production from both pions and kaons) in good agreement with the result from this analysis.

Table IV.4: Results of the muon and temperature modulation in other experiments

| Experiment | COSINE-100 | Borexino | GERDA | LVD | OPERA |
|-------------------------------|-----------------|-----------------|-----------------|-------------|-----------------|
| Location | Y2L - Korea | Hall C | Hall A | Hall A | Hall C |
| Time | 2016-2018 | 2007-2017 | 2010-2013 | 1992-2016 | 2008-2013 |
| Period | 365.25 | 366.3 ± 0.6 | 365.1 ± 0.1 | 365 | 365.25 |
| Phase of I_μ | 182 ± 25 | 174.8 ± 3.8 | 191 ± 4 | 187 ± 3 | 197 ± 5 |
| Amplitude of I_μ | 0.51 ± 0.24 | 1.36 ± 0.4 | 1.4 ± 0.1 | 1.5 | 1.55 ± 0.8 |
| Phase of T_{eff} | 178 ± 5 | 182.8 ± 0.2 | 186 ± 0.5 | 187 ± 3 | 188.8 ± 0.2 |
| Amplitude of T_{eff} | 1.08 ± 0.07 | 1.54 | 1.81 | 2.26 | 1.77 |

Chapter V Conclusions and Future Work

In this chapter, we present conclusion of the dissertation results and future work of the research. This dissertation has presented in particular the study of annual modulation analysis in crystal detectors.

V.1 Conclusions

COSINE-100 is a direct dark matter searches based on an array of ultra-low background Sodium Iodide NaI(Tl) crystal detectors located at A5 tunnel Yangyang Underground Laboratory (Y2L) in South Korea. COSINE-100 is independently to confirm or refute DAMA's long standing annual modulation signature of signal-like events in nuclear recoil events of dark matter interactions. The first data taking has been started in September 2016 with ongoing reaches 2 years of physics phenomena. The eight NaI(Tl) crystal detector of total mass 106 kg mass encapsulated immersed into 2 tons of liquid scintillator. Outside shielding is consist of several layers of lead brick and plastic scintillator to prevent external radioactivity. The COSINE-100 equipped with cosmic-rays muon panels to tag and study the muon-induced background and liquid scintillator veto to tag ^{40}K induced events as well as other internal coincidence events and external backgrounds provide 70% tagging efficiency for internal ^{40}K . The number of control and monitoring systems are in place that collect and record physics data as well as the environment condition on site.

The sensitivity of an experiment is limited by background level, muons and muon-induced particles. Muon is a mandatory to count and well understood in the crystal data. It can produce an accidental events that can affect the physics analysis. When a muon hit the plastic scintillator, the DAQ will tag an event and internal trigger cross another channel to get any sign of event with the integration width of 192 ns for all the M64ADC modules. Integrated charge trigger threshold has been set up to 4,000 ADC counts to select muon-like events by removing γ -background events from outside. The DAQ system has been performed to capture events in M64ADC modules and save to the storage system. The muon selection criteria has been developed to identify muons which passed all of detector components in COSINE-100. A coincidence and threshold is used to remove low energy background and it will remain muon-like events in high energy region and the threshold is set to be different for each side detector. To get better efficiency in selecting muons, a time difference cut has been developed to reduce fake-events in signal re-

gion. The muon coincident signal should be in close time-range of the gap. The time correlation observed for the muon candidate events, a signal range of $-100\text{ns} \leq \Delta T \leq T-115\text{ns}$. Considering the background distribution, the background contamination in the signal region is calculated to be 0.3%. Muon candidate events are fitted with the expected signal shape, Landau distributions, together with an exponential background component. Furthermore, the muon selection efficiency was estimated to be $99.9 \pm 0.1\%$ when the charge threshold cuts are applied. A similar muon selection technique is applied for all pairs of different sides to tag muon candidate events.

The muon events in the crystal detectors were studied. Muon events were found with direct or prompt energy deposition $\geq 4\text{MeV}$. A cut for muon veto time was defined to reject the phosphorescence effect after first muon. A mean of muon rate of $I_{\mu}^0 = 327.7 \pm 0.26_{(\text{stat.})} \pm 9.56_{(\text{syst.})}$ muons/m²/day was found. The seasonal modulation of the flux of high energetic cosmic muons is confirmed with an amplitude of $(0.51 \pm 0.24)\%$ and a phase of $(182 \pm 25)\text{d}$ corresponding to a maximum on the 30st of June. Using the atmospheric temperature data, we studied the correlation between muon and temperature modulation with a positive correlation. With an effective coefficient $\alpha_T = 0.815 \pm 0.097$. This result represents the most precise study of the muon flux modulation for the site and is in good agreement with expectations.

V.2 Future Work for COSINE-200

The hunt for dark matter is currently a lively field of astroparticle research. Muon is one of the main background in underground experiment around the world. Muon induced events will also show the evidence of possibility an events in region of interest at 2-6 keV low energy in rare event search. It is also interesting to know in COSINE100, with more than of 3200 muons are tagged by muon detector. After first muon hit in the crystals, it produces a thousands events at low energy which is may not be rejected by DAMA event selection. At least 3 years of stable operation will provide enough data to study the annual modulation and test DAMA's annual modulation signature. Next to COSINE phase II, COSINE has planned to grow 200 kg of crystals with approximately 1 dru in the 2-10 keV region of interest. Understanding the background is mandatory to the goal achievable of 1 keV threshold. The growing facility of Sodium Iodide has been started at IBS headquarter in Daejeon, South Korea. Mass production will be started at end of 2019 and roughly can operate at early 2021. Another Sodium Iodide experiment named ANAIS, has requested to join

the accumulated data. It can improve our understanding of background and perform the annual modulation analysis. The result is important to reproduce or reject DAMA annual modulation signature.

REFERENCES

===== CoGeNT Collaboration =====

Aalseth, C.E., Barbeau, P.S., Colaresi, J., Collar, J.I., Diaz Leon, J., Fast, J.E., Fields, N., Hossbach, T.W., Keillor, M.E., Kephart, J.D., Knecht, A., Marino, M.G., Miley, H.S., Miller, M.L., Orrell, J.L., Radford, D.C., Wilkerson, J.F., and Yocum, K.M. (2011): Search for an annual modulation in a p-type point contact germanium dark matter detector, *Physical Review Letter*, **107**, 141301.

Aalseth, C.E., Barbeau, P.S., Colaresi, J., Collar, J.I., Diaz Leon, J., Fast, F.E., Fields, N.E., Hossbach, T.W., Knecht, A., Kos, M.S., Marino, M.G., Miley, H.S., Miller, M.L., Orrell, J.L., and Yocum, K.M. (2013): CoGeNT: a search for low-mass dark matter using p-type point contact germanium detectors, *Physical Review D*, **88**, 012002.

===== XMASS Collaboration =====

Abe, K., Hiraide, K., Ichimura, K., Kishimoto, Y., Kobayashi, K., Kobayashi, M., Moriyama, S., Nakahata, M., Norita, T., Ogawa, H., Sekiya, H., Takachio, O., Takeda, A., Yamashita, M., Yang, B.S., Kim, N.Y., Kim, Y.D., Tasaka, S., Fushimi, K., Liu, J., Martens, K., Suzuki, Y., Xu, B.D., Fujita, R., Hosokawa, K., Miuchi, K., Onishi, Y., Oka, N., Takeuchi, Y., Kim, Y.H., Lee, J.S., Lee, K.B., Lee, M.K., Fukuda, Y., Itow, Y., Kegasa, R., Kobayashi, K., Masuda, K., Takiya, H., Nishijima, K., Nakamura, S. (2016): Direct dark matter search by annual modulation in XMASS-I (XMASS Collaboration), *Physics Letter B*, **759**, 272-276.

===== COSINE Collaboration =====

Adhikari, P., Adhikari, G., Choi, S., Ha, C., Hahn, I.S., Jeon, E.J., Joo, H.W., Kang, W.G., Kim, H.J., Kim, H.O., Kim, K.W., Kim, N.Y., Kim, S.K., Kim, Y.D., Kim, Y.H., Lee, H.S., Lee, J.H., Lee, M.H., Leonard, D.S., Li, J., Oh, S.Y., Olsen, S.L., Park, H.K., Park, K.S., So, J.H., and Yoon, Y.S. (2016): Understanding internal backgrounds in NaI(Tl) crystals toward a 200kg array for the KIMS-NaI experiment (COSINE Collaboration), *The European Physical Journal C*, **76**, 185.

Adhikari, G., Adhikari, P., Ha, C., Jeon, E.J., Kim, N.Y., Kim, Y.D., Kong, S.Y., Lee, H.S., Oh, S.Y., Park, J.S., and Park, K.S. (2017): Understanding NaI(Tl) crystal background for dark matter searches (COSINE Collaboration), *The European Physical Journal C*, **77**, 437.

Adhikari, G., Adhikari P., Barbosa de Souza, E., Carlin, N., Choi, S., Choi, W.Q., Djamal, M., Ezeribe, A.C., Ha, C., Hahn, I.S., Hubbard, A.J.F., Jeon, E.J., Jo, H.J., Joo, H.W., Kang, W., Kang, W.G., Kauer, M., Kim, B.H., Kim, H., Kim, H.J., Kim, K.W., Kim, M.C., Kim, N.Y., Kim, S.K., Kim, Y.D., Kim, Y.H., Kudryavtsev, V.A., Lee, H.S., Lee, J., Lee, J.Y., Lee, M.H., Leonard, D.S., Lim, K.E., Lynch, W.A., Maruyama, R.H., Mouton, F., Olsen, S.L., Park, H.K., Park, H.S., Park, J.S., Park, K.S., Pettus, W., Pierpoint, Z.P., Prihtiadi, H., Ra, S., Rogers, F.R., Rott, C., Scarff, A., Spooner,

N.J.C., Thompson, W.G., Yang, L., and Yong, S.H. (2018): Initial performance of the COSINE-100 experiment (COSINE Collaboration), *The European Physical Journal C*, **78**, 107.

===== SuperCDMS Collaboration =====

Agnese, R., Anderson, A.J., Asai, M., Balakishiyeva, D., Basu Thakur, R., Bauer, D.A., Billard, J., Borgland, A., Bowles, M.A., Brandt, D., Brink, P.L., Bunker, R., Cabrera, B., Caldwell, D.O., Cerdeno, D.G., Chagani, H., Cooley, J., Cornell, B., Crewdson, C.H., Cushman, P., Daal, M., Di Stefano, P.C.F., Doughty, T., Esteban, L., Fallows, S., Figueroa-Feliciano, E., Godfrey, G.L., Golwala, S.R., Hall, J., Harris, H.R., Hertel, S.A., Hofer, T., Holmgren, D., Hsu, L., Huber, M.E., Jastram, A., Kamaev, O., Kara, B., Kelsey, M.H., Kennedy, A., Kiveni, M., Koch, K., Loer, B., Lopez Asamar, E., Mahapatra, R., Mandic, V., Martinez, C., McCarthy, K.A., Mirabol-fathi, N., Moffatt, R.A., Moore, D.C., Nadeau, P., Nelson, R.H., Page, K., Partridge, R., Pepin, M., Phipps, A., Prasad, K, Pyle, M., Qiu, H., Rau, W., Redl, P., Reisetter, A., Ricci, Y., Saab, T., Sadoulet, B., Sander, J., Schneck, K., Schnee, R.W., Scorza, S., Serfass, B., Shank, B., Speller, D., Villano, A.N., Welliver, B., Wright, D.H., Yellin, S., Yen, J.J., Young, B.A., and Zhang, J. (2014): Search for low-mass weakly interacting massive particles using voltage-assisted calorimetric ionization detection in the SuperCDMS experiment (SuperCDMS Collaboration), *Physical Review Letter*, **112**, 041302.

Agnese, R., Anderson, A.J., Asai, M., Balakishiyeva, D., Basu Thakur, R., Bauer, D.A., Billard, J., Borgland, A., Bowles, M.A., Brandt, D., Brink, P.L., Bunker, R., Cabrera, B., Caldwell, D.O., Cerdeno, D.G., Chagani, H., Cooley, J., Cornell, B., Crewdson, C.H., Cushman, P., Daal, M., Di Stefano, P.C.F., Doughty, T., Esteban, L., Fallows, S., Figueroa-Feliciano, E., Godfrey, G.L., Golwala, S.R., Hall, J., Harris, H.R., Hertel, S.A., Hofer, T., Holmgren, D., Hsu, L., Huber, M.E., Jastram, A., Kamaev, O., Kara, B., Kelsey, M.H., Kennedy, A., Kiveni, M., Koch, K., Loer, B., Lopez Asamar, E., Mahapatra, R., Mandic, V., Martinez, C., McCarthy, K.A., Mirabol-fathi, N., Moffatt, R.A., Moore, D.C., Nadeau, P., Nelson, R.H., Page, K., Partridge, R., Pepin, M., Phipps, A., Prasad, K, Pyle, M., Qiu, H., Rau, W., Redl, P., Reisetter, A., Ricci, Y., Saab, T., Sadoulet, B., Sander, J., Schneck, K., Schnee, R.W., Scorza, S., Serfass, B., Shank, B., Speller, D., Villano, A.N., Welliver, B., Wright, D.H., Yellin, S., Yen, J.J., Young, B.A., and Zhang, J. (2014): Search for low-mass weakly interacting massive particles with SuperCDMS (SuperCDMS Collaboration), *Physical Review Letter*, **112**, 241302.

Agnese, R., Anderson, A.J., Aramaki, T., Asai, M., Baker, W., Balakishiyeva, D., Barker, D., Basu Thakur, R., Bauer, D.A., Billard, J., Borgland, A., Bowles, M.A., Brink, P.L., Bunker, R., Cabrera, B., Caldwell, D.O., Calkins, R., Cerdeno, D.G., Chagani, H., Chen, Y., Cooley, J., Cornell, B., Cushman, P., Daal, M., Di Stefano, P.C.F., Doughty, T., Esteban, L., Fal-

lows, S., Figueroa-Feliciano, E., Ghaith, M., Godfrey, G.L., Golwala, S.R., Hall, J., Harris, H.R., Hofer, T., Holmgren, D., Hsu, L., Huber, M.E., Jardin, D., Jastram, A., Kamaev, O., Kara, B., Kelsey, M.H., Kennedy, A., Leder, A., Loer, B., Lopez Asamar, E., Lukens, P., Mahapatra, R., Mandic, V., Mast, N., Mirabolfathi, N., Moffatt, R.A., Morales Mendoza, J.D., Oser, S.M., Page, K., Page, W.A., Partridge, R., Pepin, M., Phipps, A., Prasad, K., Pyle, M., Qiu, H., Rau, W., Redl, P., Reisetter, A., Ricci, Y., Roberts, A., Rogers, H.E., Saab, T., Sadoulet, B., Sander, J., Schneck, K., Schnee, R.W., Scorza, S., Serfass, B., Shank, B., Speller, D., Toback, D., Underwood, R., Upadhyayula, S., Villano, A.N., Welliver, B., Wilson, J.S., Wright, D.H., Yellin, S., Yen, J.J., Young, B.A., and Zhang, J. (2016): New results from the search for low-mass weakly interacting massive particles with the CDMS low ionization threshold experiment (SuperCDMS Collaboration), *Physical Review Letter*, **116**, 071301.

===== LUX Collaboration =====

Akerib, D.S., Alsum, S., Araújo, H.M., Bai, X., Bailey, A.J., Balajthy, J., Beltrame, P., Bernard, E.P., Bernstein, A., Biesiadzinski, T.P., Boulton, E.M., Bramante, R., Brás, P., Byram, D., Cahn, S.B., Carmona-Benitez, M.C., Chan, C., Chiller, A.A., Chiller, C., Currie, A., Cutter, J.E., Davison, T.J.R., Dobi, A., Dobson, J.E.Y., Druszkiewicz, E., Edwards, B.N., Faham, C.H., Fiorucci, S., Gaitskell, R.J., Gehman, V.M., Ghag, C., Gibson, K.R., Gilchriese, M.G.D., Hall, C.R., Hanhardt, M., Haselschwardt, S.J., Hertel, S.A., Hogan, D.P., Horn, M., Huang, D.Q., Ignarra, C.M., Ihm, M., Jacobsen, R.G., Ji, W., Kamdin, K., Kazkaz, K., Khaitan, D., Knoche, R., Larsen, N.A., Lee, C., Lenardo, B.G., Lesko, K.T., Lindote, A., Lopes, M.I., Manalaysay, A., Mannino, R.L., Marzioni, M.F., McKinsey, D.N., Mei, D.-M., Mock, J., Moongweluwan, M., Morad, J.A., Murphy, A.St.J., Nehrkorn, C., Nelson, H.N., Neves, F., O’Sullivan, K., Oliver-Mallory, K.C., Palladino, K.J., Pease, E.K., Phelps, P., Stephenson, S., Sumner, T.J., Szydagis, M., Taylor, D.J., Taylor, W.C., Tennyson, B.P., Terman, P.A., Tiedt, D.R., To, W.H., Tripathi, M., Tvrznikova, L., Uvarov, S., Verbus, J.R., Webb, R.C., White, J.T., Whitis, T.J., Witherell, M.S., Wolfs, F.L.H., Xu, J., Yazdani, K., Young, S.K., and Zhang, C. (2017): Results from a search for dark matter in the complete LUX exposure (LUX Collaboration), *Physical Review Letter*, **118**, 021303.

Akerib, D.S., Araujo, H.M., Bai, X., Bailey, A.J., Balajthy, J., Bernard, E., Bernstein, A., Bradley, A., Byram, D., Cahn, S.B., Carmona-Benitez, M.C., Chan, C., Chapman, J.J., Chiller, A.A., Chiller, C., Coffey, T., Currie, A., de Viveiros, L., Dobi, A., Dobson, J., Druszkiewicz, E., Edwards, B., Gehman, V.M., Ghag, C., Gibson, K.R., Gilchriese, M.G.D., Hall, C., Hertel, S.A., Horn, M., Huang, D.Q., Ihm, M., Jacobsen, R.G., Kazkaz, K., Knoche, R., Larsen, N.A., Lee, C., Lindote, A., Lopes, M.I., Malling, D.C., Mannino, R., McKinsey, D.N., Mei, D.-M., Mock, J., Moongweluwan, M., Morad, J., Murphy, A.St.J., Nehrkorn, C., Nelson, H., Neves, F., Ott, R.A.,

Pangilinan, M., Parker, P.D., Pease, E.K., Pech, K., Phelps, P., Reichhart, L., Shutt, T., Silva, C., Solovov, V.N., Sorensen, P., O'Sullivan, K., Sumner, T.J., Szydagis, M., Taylor, D., Tennyson, B., Tiedt, D.R., Tripathi, M., Uvarov, S., Verbus, J.R., Walsh, N., Webb, R., White, J.T., Witherell, M.S., Wolfs, F.L.H., Woords, M., Zhang, C. (2015): Radiogenic and muon-induced backgrounds in the LUX dark matter detector (LUX Collaboration), *Astroparticle Physics*, **62**, 33-46.

===== ANAIS Collaboration =====

Amare, J., Cebrian, S., Cuesta, C., Garcia, E., Ginestra, C., Martinez, M., Olivan, M.A., Ortigoza, Y., Ortiz de Solorzano, A., Pobes, C., Puimedon, J., Sarsa, M.L., Villar, J.A., Villar, P. (2014): Preliminary results of ANAIS-25, *Nuclear Instruments and Methods in Physics Research A*, **742**, 187-190.

Amare, J., Cebrian, S., Cuesta, C., Garcia, E., Martinez, M., Olivan, M.A., Ortigoza, Y., Ortiz de Solorzano, A., Pobes, C., Puimedon, J., Sarsa, M.L., Villar, J.A., and Villar, P. (2016): Status of the ANAIS dark matter project at the Canfrac Underground Laboratory, *J. Phys. Conf. Series*, **718**, 042052.

===== CRESST Collaboration =====

Angloher, G., Bauer, M., Bavykina, I., Bento, A., Bucci, C., Ciemniak, C., Deuter, G., von Feilitzsch, F., Hauff, D., Huff, P., Isaila, C., Jochum, J., Kiefer, M., Kimmerle, M., Lanfranchi, J.-C., Petricca, F., Pfister, S., Potzel, W., Probst, F., Reindl, F., Roth, S., Rottler, S., Sailer, C., Schaffner, K., Schmalzer, J., Scholl, S., Seidel, W., Sivers, M.v., Stodolsky, L., Strandhagen, C., Straub, R., Tanzke, A., Usherov, I., Wawaoczny, S., Willers, M., Zoller, A. (2012): Results from 730kg days of the CRESST-II dark matter search, *The European Physical Journal C*, **72**, 1971.

Angloher, G., Bento, A., Bucci, C., Canonica, L., Erb, A., von Feilitzsch, F., Ferreira Iachellini, N., Gorla, P., Gutlein, A., Hauff, D., Huff, P., Jochum, J., Kiefer, M., Kister, C., Kluck, H., Kraus, H., Lanfranchi, J.-C., Loebell, L., Munster, A., Petricca, F., Potzel, W., Probst, F., Reindl, F., Roth, S., Rottler, S., Sailer, C., Schaffner, K., Schieck, J., Schmalzer, J., Scholl, S., Seidel, W., Sivers, M.v., Stodolsky, L., Strandhagen, C., Straub, R., Tanzke, A., Uffinger, M., Ulrich, A., Usherov, I., Wawaoczny, S., Willers, M., Wustrich, M., Zoller, A. (2014): Results on low mass WIMPs using an upgraded CRESST-II detector, *The European Physical Journal C*, **74**, 3184.

===== XENON Collaboration =====

Aprile, E., Alfonsi, M., Arisaka, K., Arneodo, F., Balan, C., Baudis, L., Bauermeister, B., Behrens, A., Beltrame, P., Bokeloh, K., Brown, E., Bruno, G., Budnik, R., Cardoso, J.M.R., Chen, W.-T., Choi, B., Cline, D., Colijn, A.P., Contreras, H., Cussonneau, J.P., Decowski, M.P., Duchovni, E., Fattori, S., Ferella, A.D., Fulgione, W., Gao, F., Garbini, M., Ghag, C., Giboni, K.-L., Goetzke, L.W., Grignon, C., Gross, E., Hampel, W., Kaether, F., Kish, A., Lamblin, J., Landsman, H., Lang, R.F., Calloch, M.Le, Levy, C., Lim, K.E., Lin, Q., Lindemann, S., Lindner, M., Lopes, J.A.M., Lung, K., Mar-

rodán Undagoitia, T., Massoli, F.V., Melgarejo Fernandez, A.J., Meng, Y., Molinario, A., Nativ, E., Ni, K., Oberlack, U., Orrigo, S.E.A., Pantic, E., Persiani, R., Plante, G., Priel, N., Rizzo, A., Rosendahl, S., dos Santos, J.M.F., Sartorelli, G., Schreiner, J., Schumann, M., Scotto Lavina, L., Scovell, P.R., Selvi, M., Shagin, P., Simgen, H., Teymourian, A., Thers, D., Vitells, O., Wang, H., Weber, M., and Weinheimer, C. (2012): Dark matter results from 225 live days of XENON100 data (XENON Collaboration), *Physical Review Letter*, **109**, 181301.

Aprile, E., Aalbers, J., Agostini, F., Alfonsi, M., Amaro, F.D., Anthony, M., Arneodo, F., Barrow, P., Baudis, L., Bauermeister, B., Benabderrahmane, M.L., Berger, T., Breur, P.A., Brown, A., Brown, A., Brown, E., Bruenner, S., Bruno, G., Budnik, R., Bütikofer, L., Calvén, J., Cardoso, J.M.R., Cervantes, M., Cichon, D., Coderre, D., Colijn, A.P., Conrad, J., Cussonneau, J.P., Decowski, M.P., de Perio, P., Di Gangi, P., Di Giovanni, A., Diglio, S., Eurin, G., Fei, J., Ferella, A.D., Fieguth, A., Fulgione, W., Gallo Rosso, A., Galloway, M., Gao, F., Garbini, M., Gardner, R., Geis, C., Goetzke, L.W., Grandi, L., Greene, Z., Grignon, C., Hasterok, C., Hogenbirk, E., Howlett, J., Itay, R., Kaminsky, B., Kazama, S., Kessler, G., Kish, A., Landsman, H., Lang, R.F., Lellouch, D., Levinson, L., Lin, Q., Lindemann, S., Lindner, M., Lombardi, F., Lopes, J.A.M., Manfredini, A., Maris, I., Marrodán Undagoitia, T., Masbou, J., Massoli, F.V., Masson, D., Mayani, D., Messina, M., Micheneau, K., Molinario, A., Morå, K., Murra, M., Nagonama, J., Ni, K., Oberlack, U., Pakarha, P., Pelssers, B., Persiani, R., Piastra, F., Pienaar, J., Pizzella, V., Piro, M.-C., Plante, G., Priel, N., Rauch, L., Reichard, S., Reuter, C., Riedel, B., Rizzo, A., Rosendahl, S., Rupp, N., Saldanha, R., dos Santos, J.M.F., Sartorelli, G., Scheibelhut, M., Schindler, S., Schreiner, J., Schumann, M., Scotto Lavina, L., Selvi, M., Shagin, P., Shockley, E., Silva, M., Simgen, H., Sivers, M.v., Stein, A., Thapa, S., Thers, D., Tiseni, A., Trincherro, G., Tunnell, C., Vargas, M., Upole, N., Wang, H., Wang, Z., Wei, Y., Weinheimer, C., Wulf, J., Ye, J., Zhang, Y., and Zhu, T. (2017): First dark matter search results from the XENON1T experiment (XENON Collaboration), *Physical Review Letter*, **119**, 181301.

Aprile, E., Aalbers, J., Agostini, F., Alfonsi, M., Amaro, F.D., Anthony, M., Arneodo, F., Barrow, P., Baudis, L., Bauermeister, B., Benabderrahmane, M.L., Berger, T., Breur, P.A., Brown, A., Brown, A., Brown, E., Bruenner, S., Bruno, G., Budnik, R., Bütikofer, L., Calvén, J., Cardoso, J.M.R., Cervantes, M., Cichon, D., Coderre, D., Colijn, A.P., Conrad, J., Cussonneau, J.P., Decowski, M.P., de Perio, P., Di Gangi, P., Di Giovanni, A., Diglio, S., Eurin, G., Fei, J., Ferella, A.D., Fieguth, A., Fulgione, W., Gallo Rosso, A., Galloway, M., Gao, F., Garbini, M., Geis, C., Goetzke, L.W., Greene, Z., Grignon, C., Hasterok, C., Hogenbirk, E., Itay, R., Kaminsky, B., Kessler, G., Kish, A., Landsman, H., Lang, R.F., Lellouch, D., Levinson, L., Lin, Q., Lindemann, S., Lindner, M., Lombardi, F., Lopes, J.A.M., Manfredini, A., Maris, I., Marrodán Undagoitia, T., Masbou, J., Massoli, F.V., Masson,

- D., Mayani, D., Messina, M., Micheneau, K., Miguez, B., Molinario, A., Murra, M., Nagonama, J., Ni, K., Oberlack, U., Pakarha, P., Pelssers, B., Persiani, R., Piastra, F., Pienaar, J., Pizzella, V., Piro, M.-C., Plante, G., Priel, N., Rauch, L., Reichard, S., Reuter, C., Rizzo, A., Rosendahl, S., Rupp, N., dos Santos, J.M.F., Sartorelli, G., Scheibelhut, M., Schindler, S., Schreiner, J., Schumann, M., Scotto Lavina, L., Selvi, M., Shagin, P., Shockley, E., Silva, M., Simgen, H., Sivers, M.v., Stein, A., Thers, D., Tiseni, A., Trincherro, G., Tunnell, C., Wang, H., Wei, Y., Weinheimer, C., Wulf, J., Ye, J., and Zhang, Y. (2017): Search for electronic recoil event rate modulation with 4 years of XENON100 data (XENON Collaboration), *Physical Review Letter*, **118**, 101101.
- Barbosa de Souza, E., Cherwinka, J., Cole, A., Ezeribe, A.C., Grant, D., Halzen, F., Heeger, K.M., Hsu, L., Hubbard, A.J.F., Jo, H.J., Karle, A., Kauer, M., Kudryavtsev, V.A., Lim, K.E., Macdonald, C., Maruyama, R.H., Mouton, F., Paling, S.M., Pettus, W., Pierpoint, Z.P., Reilly, B.N., Robinson, M., Rogers, F.R., Sandstrom, P., Scarff, A., Spooner, N.J.C., Telfer, S., and Yang, L. (2017): First search for a dark matter annual modulation signal with NaI(Tl) in the Southern Hemisphere by DM-Ice17 (DM-Ice Collaboration), *Physical Review D*, **95**, 032006.
- Barker, D. and Mei, D.-M. (2012): Germanium detector response to nuclear recoils in searching for dark matter, *Astroparticle Physics*, **38**, 1-6.
- Bellini, G., Benziger, J., Bick, D., Bonfini, G., Bravo, D., Buizza Avanzini, M., Caccianiga, B., Cadonati, L., Calaprice, F., Carraro, C., Cavalcante, P., Chavarria, A., Chepurinov, A., D'Angelo, D., Davini, S., Derbin, A., Etenko, A., von Feilitzsch, F., Kemenko, F., Franco, D., Galbiati, C., Gazzana, S., Ghiano, C., Giammarchi, M., Goeger-Neff, M., Goretti, A., Grandi, L., Guardincerri, E., Hagner, C., Hardy, S., Aldo Ianni, Andrea Ianni, Korablev, D., Korga, G., Koshio, Y., Kryn, D., Laubenstein, M., Lewke, T., Litvinovich, E., Loer, B., Lombardi, F., Lombardi, P., Ludhova, L., Machulin, I., Manecki, S., Maneschg, W., Manuzio, G., Meindl, Q., Meroni, E., Miramonti, L., Misiaszek, M., Montanari, D., Mosteiro, P., Muratova, V., Oberauer, L., Obolensky, M., Ortica, F., Otis, K., Pallavicini, M., Papp, L., Perasso, L., Perasso, S., Pocar, A., Raghavan, R.S., Ranucci, G., Razeto, A., Re, A., Romani, A., Sabelnikov, A., Saldanha, R., Salvo, C., Schönert, S., Simgen, H., Skorokhvatov, M., Smirnov, O., Sotnikov, A., Sukhotin, S., Suvorov, Y., Tartaglia, R., Testera, G., Vignaudi, D., Vogelhaar, R.B., Winter, J., Wojcik, M., Wright, A., Wurm, M., Xu, J., Zaimidoroga, O., Zavatarelli, S., and Zuzel, G. (2012): Cosmic-muon flux and annual modulation in Borexino at 3800m water-equivalent depth (BOREXINO Collaboration), *Journal of Cosmological and Astroparticle Physics*, **05**, 015.
- Bergstrom, L. (2009): Dark matter candidates, *New Journal Physics*, **11**, 105006.
===== DAMA/LIBRA Collaboration =====

- Bernabei, R., Belli, P., Bussolotti, A., Cappella, F., Cerulli, R., Dai, C.J., d'Angelo, A., He, H.L., Incicchitti, A., Kuang, H.H., Ma, J.M., Mattei, A., Montecchia, F., Nozzoli, F., Prosperi, D., Sheng, X.D., and Ye, Z.P. (2008): The DAMA/LIBRA apparatus (DAMA Collaboration), *Nuclear Instruments and Methods in Physics Research Section A: Accelerators, Spectrometers, Detector and Associated Equipment*, **592**, 297-315.
- Bernabei, R., Belli, P., Cerulli, R., Montecchia, F., Amato, M., Ignestib, G., Incicchitti, A., Prosperi, D., Dai, C.J., He, H.L., Kuang, H.H., and Ma, J.C. (2000): Search for WIMP annual modulation signature: results from DAMA/NaI-3 and DAMA/NaI-4 and the global combined analysis (DAMA Collaboration), *Physics Letter B*, **480**, 23-31.
- Bernabei, R., Belli, P., Cappella, F., Cerulli, R., Dai, C.J., d'Angelo, A., He, H.L., Incicchitti, A., Kuang, H.H., Ma, X.H., Montecchia, F., Nozzoli, F., Prosperi, D., Sheng, X.D., Wang, R.G., Ye, Z.P. (2010): New results from DAMA/LIBRA (DAMA Collaboration), *The European Physical Journal C*, **67**, 39-49.
- Bernabei, R., Belli, P., Cappella, F., Caracciolo, V., Castellano, S., Cerulli, R., Dai, C.J., d'Angelo, S., Di Marco, A., He, H.L., Incicchitti, A., Kuang, H.H., Ma, X.H., Montecchia, F., Prosperi, D., Sheng, X.D., Wang, R.G., Ye, Z.P. (2013): Final model independent result of DAMA/LIBRA-phase I (DAMA Collaboration), *The European Physical Journal C*, **73**, 2648.
- Bernabei, R., Belli, P., Di Marco, A., Montecchia, F., d'Angelo, A., Incicchitti, A., Cappella, F., Caracciolo, V., Cerulli, R., Dai, C.J., He, H.L., Kuang, H.H., Ma, X.H., Sheng, X.D., Wang, R.G., and Ye, Z.P. (2014): New results and perspectives of DAMA/LIBRA (DAMA Collaboration), *European Physical Journal Web of Conferences*, **70**, 00043.
- Bertone, G., Hooper, D., and Silk, J. (2005): Particle dark matter : evidence, candidates and constrains, *Phys. Rep.*, **405**, 279.
- Billard, J., and Figueroa-Feliciano, E. (2014): Implication of neutrino backgrounds on the reach of next generation dark matter direct detection experiments, *Physical Review D*, **89**, 023524.
- Bugaev, E.V., Misaki, A., Naumov, V.A., Sinegovskaya, T.S., Sinegovsky, S.I., and Takahashi, N. (1998): Atmospheric muon flux at sea level, underground, and underwater, *Physical Review D*, **58**, 054001.
- ===== DM-Ice17 Collaboration =====
- Cherwinka, J., Grant, D., Halzen, F., Heeger, K.M., Hsu, L., Hubbard, A.J.F., Karle, A., Kauer, M., Kudryavtsev, V.A., Macdonald, C., Maruyama, R.H., Paling, S., Pettus, W., Pierpoint, Z.P., Reilly, B.N., Robinson, M., Sandstrom, P., Spooner, N.J.C., Telfer, S., and Yang, L. (2014): First data from DM-Ice17 (DM-Ice Collaboration), *Physical Review D*, **90**, 092005.
- Cherwinka, J., Grant, D., Halzen, F., Heeger, K.M., Hsu, L., Hubbard, A.J.F., Karle, A., Kauer, M., Kudryavtsev, V.A., Lim, K.E., Macdonald, C., Maruyama, R.H., Paling, S.M., Pettus, W., Pierpoint, Z.P., Reilly, B.N., Robinson, M., Sandstrom, P., Spooner, N.J.C., Telfer, S., and Yang, L. (2016): Mea-

- surement of muon annual modulation and muon-induced phosphorescence in NaI(Tl) crystals with DM-Ice17 (DM-Ice Collaboration), *Physical Review D*, **93**, 042001.
- Clowe, D., Gonzalez, A., and Markevitch, M. (2004): Weak-lensing mass reconstruction of the interacting cluster 1E 0657-558: Direct evidence for the existence of dark matter, *The Astrophysical Journal*, **604**, 596-603.
- Clowe, D., Bradac, M., Gonzalez, A.H., Markevitch, M., Randall, S.W., Jones, C., and Zaritsky, D. (2006): A direct empirical proof of the existence of dark matter, *The Astrophysical Journal Letters*, **648**, L109-L113.
- Cui, X., Abdukerim, A., Chen, W., Chen, X., Chen, Y., Dong, B., Fang, D., Fu, C., Giboni, K., Giuliani, F., Gu, L., Gu, Y., Guo, X., Guo, Z., Han, K., He, C., Huang, D., He, S., Huang, X., Huang, Z., Ji, X., Ju, Y., Li, S., Li, Y., Lin, H., Liu, H., Liu, J., Ma, J., Mao, Y., Ni, K., Ning, J., Ren, X., Shi, F., Tan, A., Wang, C., Wang, H., Wang, M., Wang, Q., Wang, S., Wang, X., Wang, X., Wu, Q., Wu, S., Xiao, M., Xie, P., Yan, B., Yang, Y., Yue, J., Zhang, D., Zhang, H., Zhang, T., Zhang, T., Zhao, L., Zhou, J., Zhou, N., and Zhou, X. (2017): Dark matter results from 54-ton-day exposure of PandaX-II experiment (PandaX Collaboration), *Physical Review Letter*, **119**, 181302.
- Cushman, P., Galbiati, C., McKinsey, D.N., Robertson, H., and Tait, T.M.P. (2013): Working grup report: WIMP dark matter direct detection, *arXiv: 1310.8327v2*.
- Davis, J.H. (2014): Fitting the annual modulation in DAMA with neutrons from muons and neutrinos, *Physical Review Letter*, **113**, 081302.
- Drukier, A.K., Freese, K., and Spergel, D.N. (1986): Detecting cold dark-matter candidates, *Physical Review D*, **33**, 3495-3508.
- Freese, K., Lisanti, M., and Savage, C. (2013): Annual modulation of dark matter: A review, *Review of Modern Physics*, **85**, 1561-1581.
- Fushimi, K., Ejiri, H., Hazama, R., Ikea, H., Imagawa, K., Inoue, K., Kanzaki, G., Kozlov, A., Orito, R., Shima, T., Takemoto, Y., Teraoka, Y., Umehara, S., Yasuda, K., Yoshida, S. (2016): Dark matter search project PICO-LON, *Journal of Physics Conference Series*, **718**, 042022.
- Gaisser, T. (1990): Cosmic rays and particle physics, *Cambridge University Press*, 69-81.
- Goodman, M.W. and Witten, E. (1985): Detectability of certain dark-matter candidates, *Physical Review D*, **31**, 3059-3063.
- Huterer, D. (2010): Weak lensing, dark matter, and dark energy, *General Relativity and Gravitation*, **42**, 2177-2195.
- Jarosik, N., Bennet, C.L., Dunkley, J., Gold, B., Greason, M.R., Halpern, M., Hill, R.S., Hinshaw, G., Kogut, A., Komatsu, E., Larson, D., Limon, M., Meyer, S.S., Nolte, M.R., Odegard, N., Pagel, L., Smith, K.M., Spergel, D.N., Tucker, G.S., Weiland, J.L., Wollack, E., Wright, E.L. (2011): Seven-year Wilkinson Microwave anisotropy probe (WMAP*) Observations: Sky Maps, Systematic Errors, and Basic Results, *The Astrophysical Journal Supplement Series*, **192:14**, 15.

- Jeon, E.J., and Kim, Y.D. (2016): A simulation-based study of the neutron backgrounds for NaI dark matter experiments, *Astroparticle Physics*, **73**, 28-33.
- Jungman, G., Kamionkowski, M., and Griest, K. (1996): Supersymmetric dark matter, *Physical Reports*, **267**, 195.
- Kim, S.C., Bhang, H., Choi, J.H., Kang, W.G., Kim, B.H., Kim, H.J., Kim, K.W., Kim, S.K., Kim, Y.D., Lee, J., Lee, J.H., Lee, J.K., Lee, M.J., Lee, S.J., Li, J., Li, J., Li, X.R., Li, Y.J., Myung, S.S., Olsen, S.L., Ryu, S., Seong, I.S., So, J.H., and Yue, Q. (2012): New limits on interactions between weakly interacting massive particles and nucleons obtained with CsI(Tl) crystal detectors (KIMS Collaboration), *Physical Review Letter*, **108**, 181301.
- Kim, K.W., Kang, W.G., Oh, S.Y., Adhikari, P., So, J.H., Kim, N.Y., Lee, H.S., Choi, S., Hahn, I.S., Jeon, E.J., Joo, H.W., Kim, B.H., Kim, H.J., Kim, Y.D., Kim, Y.H., Lee, J.K., Leonard, D.S., Li, J., Olsen, S.L., and Park, H.S. (2015): Tests on NaI(Tl) crystals for WIMP search at Yangyang underground laboratory (KIMS Collaboration), *Astroparticle Physics*, **62**, 249-257.
- Klinger, J., and Kudryavtsev, V.A. (2015): Muon-induced neutrons do not explain the DAMA data, *Physical Review Letter*, **114**, 151301.
- Larson, D., Dunkley, J., Hinshaw, G., Komatsu, E., Nolte, M.R., Bennett, C.L., Gold, B., Halpern, M., Hill, R.S., Jarosik, N., Kogut, A., Limon, M., Meyer, S.S., Odegard, N., Page, L., Smith, K.M., Spergel, D.N., Tucker, G.S., Weiland, J.L., Wollack, E., and Wright, E.L. (2011): Seven-year wilkinson microwave anisotropy probe (WMAP*) observations: power spectra and WMAP-derived parameters, *The Astroparticle Journal Supplement Series*, **192**, 16.
- Lee, B.W., and Weinberg, S. (1977): Cosmological lower bound on heavy-Neutrino masses, *Physical Review Letter*, **39**, 165-168.
- Malgin, A.S. (2015): Seasonal modulations of the underground cosmic-ray muon energy, *Journal of Experimental and Theoretical Physics*, **121**, 212-216.
- Mao, Y.-Y., Strigari, L.E., and Wechsler, R.H. (2014): Connecting direct dark matter detection experiments to cosmologically motivated halo models, *Physical Review D*, **89**, 063513.
- Nygren, D. (2012): A testable conventional hypothesis for the DAMA-LIBRA annual modulation, *ArXiv:1102.0815*.
- Plante, G., Aprile, E., Budnik, R., Choi, B., Giboni, K.-L., Goetzke, L.W., Lang, R.F., Lim, K.E., and Melgarejo Fernandez, A.J. (2011): New measurement of the scintillation of low-energy nuclear recoils in liquid xenon, *Physical Review C*, **84**, 045805.
- Persic, M., Salucci, P., and Stel, F. (1996): The universal rotation curve of spiral galaxies - I. The dark matter connection, *Mon. Not. R. Astron. Soc.*, **281**, 27-47.
- Savage, C., Freese, K., Gondolo, P., and Spolyar, D. (2009): Compatibility of DAMA/LIBRA dark matter detection with other searches, *Journal of Cosmology and Astroparticle Physics*, **09**, 036.

- Schmidt, B., Armengaud, E., Augier, C., Benoit, A., Bergé, L., Bergmann, T., Blümer, J., Bres, G., Broniatowski, A., Brudanin, V., Censier, B., Chapellier, M., Charlieux, F., Collin, S., Coulter, P., Cox, G.A., Crauste, O., Dommage, J., Dumoulin, L., Eitel, K., Filosofov, D., Fourches, N., Garde, G., Gascon, J., Gerbier, G., Gros, M., Hehn, L., Henry, S., Hervé, S., Heuermann, G., Juillard, A., Kluck, H., Kozlov, V.Y., Kleifges, M., Kraus, H., Kudryavtsev, V.A., Loaiza, P., Marnieros, S., Menshikov, A., Navick, X.-F., Nieder, H., Nones, C., Olivieri, E., Pari, P., Paul, B., Robinson, M., Rodenas, H., Rozov, S., Sanglard, V., Siebenborn, B., Tcherniakhovski, D., Torrentó-Coello, A.S., Vagneron, L., Walker, R.J., Weber, M., Yakushev, E., Zhang, W. (2013): Muon-induced background in the EDELWEISS dark matter search (EDELWEISS Collaboration), *Astroparticle Physics*, **44**, 28-39.
- Tan, A., Xiao, M., Cui, X., Chen, X., Chen, Y., Fang, D., Fu, C., Giboni, K., Giuliani, F., Gong, H., Guo, X., Han, K., Hu, S., Huang, X., Ji, X., Ju, Y., Lei, S., Li, S., Li, X., Li, X., Liang, H., Lin, Q., Liu, H., Liu, J., Lorenzon, W., Ma, J., Mao, Y., Ni, K., Ren, X., Schubnell, M., Shen, M., Shi, F., Wang, H., Wang, J., Wang, M., Wang, Q., Wang, S., Wang, X., Wang, Z., Wu, S., Xiao, X., Xie, P., Yan, B., Yang, Y., Yue, J., Zeng, X., Zhang, H., Zhang, H., Zhang, H., Zhang, T., Zhao, L., Zhou, J., Zhou, N., and Zhou, X. (2016): Dark matter results from first 98.7 days of data from the PandaX-II experiment (PandaX Collaboration), *Physical Review Letter*, **117**, 121303.
- Undagoitia, T.M., and Rauch, L. (2016): Dark matter direct-detection experiments, *Journal of Physics G: Nuclear and Particle Physics*, **43**, 013001.
- Xu, J., Calaprice, F., Froborg, F., Shields, E., Suerfu, B. (2015): SABRE - a test of DAMA with high-purity NaI(Tl) crystals, *AIP Conf. Proc.*, **1672**, 040001.
- Yue, Q., Zhao, W., Kang, K.J., Cheng, J.P., Li, Y.J., Lin, S.T., Chang, J.P., Chen, N., Chen, Q.H., Chen, Y.H., Chuang, Y.C., Deng, Z., Du, Q., Gong, H., Hao, X.Q., He, H.J., He, Q.J., Huang, H.X., Huang, T.R., Jiang, H., Li, H.B., Li, J.M., Li, J., Li, J., Li, X., Li, X.Y., Li, Y.L., Liao, H.Y., Lin, F.K., Liu, S.K., Lu, L.C., Ma, H., Mao, S.J., Qin, J.Q., Ren, J., Ruan, X.C., Shen, M.B., Singh, L., Singh, M.K., Soma, A.K., Su, J., Tang, C.J., Tseng, C.H., Wang, J.M., Wang, L., Wang, Q., Wong, H.T., Wu, S.Y., WU, Y.C., Wu, Y.C., Xianyu, Z.Z., Xiao, R.Q., Xing, H.Y., Xu, F.Z., Xu, Y., Xu, X.J., Xue, T., Yang, L.T., Yang, S.W., Yi, N., Yu, C.X., Yu, H., Yu, X.Z., Zeng, X.H., Zeng, Z., Zhang, L., Zhang, Y.H., Zhao, M.G., Zhou, Z.Y., Zhu, J.J., Zhu, W.B., Zhu, X.Z., Zhu, Z.H. (2014): Limits on light weakly interacting massive particles from the CDEX-1 experiment with a p-type point-contact germanium detector at the China Jinping Underground Laboratory, *Physical Review D*, **90**, 091701(R).
- Zwicky, F. (1933): Die Rotverschiebung von extragalaktischen Nebeln, *Helv. Phys. Act.* **6**, 110.
- Zwicky, F. (1937): On the masses of nebulae and of clusters of nebulae, *ApJ* **86**, 217.

LIST OF PUBLICATIONS

International Journals

1. **Prihtiadi, H.** et al., (2018): Muon detector for the COSINE-100 experiment (COSINE Collaboration), *Journal of Instrumentation*, **13**, T02007. (**IF: 1.310**, Q1, Indexed by SCOPUS).
2. Adhikari, G. et al., (2018): Background model for the NaI(Tl) crystals in COSINE-100, *Nature*, **564**, 83-86. (**IF=41.57**, Q1, Indexed by SCOPUS).
3. Ha, C. et al., (2019): First direct search for Inelastic Boosted Dark Matter with COSINE-100, *Physical Review Letter*, **122**, 131802. (**IF=8.84**, Q1, Indexed by SCOPUS).
4. Adhikari, G. et al., (2018): Initial Performance of the COSINE-100 experiment, *The European Physical Journal C*, **78**, 107. (**IF=5.33**, Q1, Indexed by SCOPUS).
5. Adhikari, P. et al., (2018): Background model for the NaI(Tl) crystals in COSINE-100, in *The European Physical Journal C*, **78**, 490. (**IF=5.33**, Q1, Indexed by SCOPUS).
6. Adhikari, G. et al., (2018): The COSINE-100 Data Acquisition System, *Journal of Instrumentation*, **13**, P09006. (**IF:1.310**, Q1, Indexed by SCOPUS).
7. **Prihtiadi, H.**, Djamal, M. (2017): The realibility of wireless sensor network on pipeline monitoring system, *Journal of Mathematical and Fundamental Sciences*, **49**, 51-56. (**IF=0.4**, Q4, Indexed by SCOPUS).
8. Lee, J.Y. et al., (2016): A study of radioactive contamination of $^{40}\text{Ca}^{100}\text{MoO}_4$ crystals for the AMoRE experiment, *Journal of IEEE Transactions on Nuclear Science*, **63**, 543-547. (**IF=1.1**, Q3, Indexed by SCOPUS).
9. Adhikari, G. et al., (2018): Study of fast neutron detector for COSINE-100 experiment, *Journal of Instrumentation*, **78**, 490. (**IF=1.310**, Q1, Indexed by SCOPUS).
10. Adhikari, G. et al., (2019): Search for a dark matter-induced annual modulation signal in NaI(Tl) with the COSINE-100 experiment, submitted to *Physical Review Letter*. arXiv:1903.10098. (**IF=8.84**, Q1, Indexed by SCOPUS).
11. Adhikari, G. et al., (2019): DAMA/LIBRA-phase2 in WIMP effective model, submitted to *Journal of Cosmology and Astroparticle Physics*, 2019. arXiv:1904.00128.
12. **Prihtiadi, H.** et al., (2019): Modulations of the cosmic muon signal of COSINE-100 Experiment, prepare to be submitted to *Journal of Cosmology and Astroparticle Physics*, 2019.
13. V Alenkov, et al., (2019): First results from the AMoRE-Pilot Neutrinoless double beta decay experiment, submitted to *The European Physical Journal C*, 2019. arXiv:1903.09483.

International Conference Proceedings

1. **Prihtiadi, H.**, Azwar, A., and Djamal, M. (2016): A simple method to determine leakage location in water distribution based on pressure profiles, AIP Conf. Proc. 1719, 030045.
2. **Prihtiadi, H.**, and Djamal, M. (2017): High sensitivity spring coil as displacement sensor for slope stability monitoring, *Proceeding of International Conference on Intelligent Systems and Image Processing*, **4**, 312-316, doi: 10.12792/icisip2016.055.
3. **Prihtiadi, H.** (2017): Muon detector and muon flux measurement at Yangyang underground laboratory for the COSINE-100 experiment, Proceeding of the 35th International Cosmic Ray Conference, Busan, South Korea, pos.sissa.it/301/883.
4. **Prihtiadi, H.** (2018): Muon and muon-induced phosphorescence events in the COSINE-100 dark matter searches, accepted.

Talks

1. **Prihtiadi, H.**, The plastic scintillator cosmic-ray muon detector of The KIMS NaI-experiment, **The Korean Physics Society (KPS) Spring Meeting 2016**, Daejeon, South Korea, Apr. 2016.
2. **Prihtiadi, H.**, Performance test of muon detectors for AMoRE experiment, **The Korean Physics Society (KPS) Fall Meeting 2016**, Gwangju, South Korea, Oct. 2016.
3. **Prihtiadi, H.**, A study of muon flux measurement in the COSINE dark matter experiment, **The Korean Physics Society (KPS) Fall Meeting 2016**, Gwangju, South Korea, Oct. 2016.
4. **Prihtiadi, H.**, Analysis performance test of muon detectors for AMoRE Neutrinoless Double Beta Decay Experiment, **The Korean Physics Society (KPS) Spring Meeting 2017**, Daejeon, South Korea, Apr. 2017.
5. **Prihtiadi, H.**, Performance of muon detectors for AMoRE 0vBB Neutrinoless Double Beta Decay Experiment, **The 7th BK21Plus Workshop for Young Physicists Kyungpook National University**, Namwon, South Korea, Jul. 2017.
6. **Prihtiadi, H.**, Muon detector and muon flux measurement at Yangyang underground laboratory for the COSINE-100 experiment, **The 35th International Cosmic Ray Conference**, Busan, South Korea, Jul. 2017.
7. **Prihtiadi, H.**, The COSINE-100 dark matter experiment, **The 10th Conference of Indonesian Students Association in South Korea**, Daejeon, South Korea, Jul. 2017.
8. **Prihtiadi, H.**, Muon rate and study of phosphorescence events on NaI(Tl), The Korean Physics Society (KPS) Spring Meeting 2018, Daejeon, South Korea, Apr. 2018.
9. **Prihtiadi, H.**, Muon and muon-induced phosphorescence events in the COSINE-100 Dark Matter Searches, ICHEP 2018, Seoul, South Korea.

LIST OF COSINE MEMBER

Institut Teknologi Bandung (ITB)

Hafizh Prihtiadi, Mitra Djamal

Center for Underground Physics, Institute for Basic Science (CUP-IBS)

Woon Gu Kang, Chang Hyon Ha, Eunju Jeon, Hyounggyu Kim, KyungWon Kim,
Nam Young Kim, Yeongduk Kim, Yong-Hamb Kim, Young Ju Ko, Hyun
Su Lee*, Moo Hyun Lee, Jaison Lee, Douglas Leonard, Sejin Ra, Stephen
Lars Olsen, Kangsoon Park, Keon Ah Shin

Ewha Womans University

In Sik Hahn

University of Illinois at Urbana-Champaign

Liang Yang

Korea Research Institute of Standards and Science (KRISS)

Hyeonso Park

Korea University

Hyang Kyu Park

Kyungpook National University (KNU)

Gwang Soo Kim, Hongjoo Kim, Jooyoung Lee

University of São Paulo

Nelson Carlin, Ricardo L. C. Pitta

University of Science and Technology (UST)

Byungju Park, (Hyun Su Lee)

Sejong University

Govinda Adhikari, Pushparaj Adhikari, (Yeongduk Kim)

Seoul National University (SNU)

Seonho Choi, Hanwool Joo, Sun Kee Kim

University of Sheffield

Anthony C. Ezeribe, Vitaly Kudryavtsev, Warren A. Lynch, Frederic Mouton ,
Andrew Scarff, Neil J.C. Spooner

Sungkyunkwan University (SKKU)
Woosik Kang, Carsten Rott, Gyun Ho Yu

University of Wisconsin-Madison
Matthew Kauer

Yale University
Estella Barbosa de Souza, Jay Hyun Jo, Reina H. Maruyama*, William G.
Thompson